



# Modeling of Microwave Absorption Mechanisms in Metallic Powders

Dissertation

zur

Erlangung des akademischen Grades

Doktor-Ingenieur (Dr.-Ing.)

der Fakultät für Informatik und Elektrotechnik  
der Universität Rostock

Rostock, 2013

vorgelegt von

**Tomasz Galek**, geb. am 25. Juli 1980 in Stalowa Wola



**Gutacher:**

1. Gutacher: Prof. Dr. rer. nat. habil. Ursula van Rienen  
Fakultät für Informatik und Elektrotechnik,  
Universität Rostock
2. Gutacher: Prof. Dr. rer. nat. habil. Eberhard Burkel  
Mathematisch-Naturwissenschaftlichen Fakultät,  
Universität Rostock
3. Gutacher: Prof. Darin T. Zimmerman, Ph.D.  
Physics Faculty,  
Pennsylvania State University

**Datum der Einreichung:** 02. November 2012

**Datum der Verteidigung:** 01. März 2013



*Human beings make life so interesting. Do you know that in a universe so full of wonders they have managed to invent boredom? Quite astonishing...*

Terry Pratchett, Hogfather



# Abstract

Application of microwave heating in ceramic powder processing was studied since early 1970's. However the microwave processing in powder metallurgy has only been under focus since the pioneering work of Roy and coworkers in 1999. After the discovery that metallic powders do not reflect microwaves like bulk metallic objects, but absorb and heat up in microwave fields quite effectively, there has been growing interest in this topic. Similarly to the calculation of effective properties of complicated structures of metamaterials the combination of the electromagnetic simulations using the Finite Integration Technique (FIT) technique and the extraction of effective properties can be used with success in the field of material science. The model of metallic powder consists of periodically arranged spherical conductive particles. The choice of copper as a representative of metals was due to availability of experimental data. The effective properties of the copper powders were simulated using FIT technique, which gives a general overview of the sample properties by way of scattering parameters. The frequency dependent scattering parameters yield information on effective electromagnetic properties of the investigated material or mixture. By adopting a mathematical formulation from an experimental reflection/transmission-free space measurement method, one can extract the effective dielectric permittivity and the effective magnetic permeability from the scattering parameters. A numerical procedure has been developed in order to automatically extract the effective electromagnetic properties from the scattering parameters. The extraction procedure has been validated on known materials. The simulation results are compared to the experimental data allowing studying and understanding the basic mechanisms of microwave absorption as well as the sintering of metallic powders. The heating behavior of copper powders in either the electric or the magnetic field is similar however it is driven by different mechanisms. During sintering in the electric field the microfocusing effect plays an important role. The electric field is much stronger in the contact zones between the particles leading to tremendous dielectric losses in the native oxide layer covering the copper particles. During sintering in the magnetic field the conductive particles are heated by induced eddy currents. The absorption of the magnetic component depends on the conductivity and the particle size. The simulations over a wide range of frequency show a resonant behavior in the effective magnetic permeability of copper powders. The simulations of microwave heating in the separated magnetic field of copper powders with different particle sizes are in a very good agreement with the experimentally measured initial heating rates of copper compacts. It has been found out that the effective magnetic permeability has a diamagnetic behavior and the resonance frequency depends on the particle size and the conductivity of the material.





# Zusammenfassung

Die Anwendung des Mikrowellenheizens im Verarbeitungsprozess von keramischen Pulvern wird seit den frühen 1970er Jahren untersucht. Allerdings stand der Prozess zur Verarbeitung von metallischen Pulvern erst seit 1999 aufgrund dieser Pionierarbeit von Roy im Fokus. Nachdem entdeckt wurde, dass metallische Pulver Mikrowellen nicht wie metallische Festkörper reflektieren, sondern effektiv absorbieren und sich im Mikrowellenfeld erhitzen, wuchs das Interesse an dem Themengebiet. Ebenso wie die Berechnungen der effektiven Eigenschaften der komplizierten Strukturen der Metamaterialien kann auch die Kombination der elektromagnetischen Simulation mit finiter Intergrationstechnik und der Extraktion der effektiven Eigenschaften erfolgreich in den Materialwissenschaften genutzt werden. Das Simulationsmodell der metallischen Pulver besteht aus periodisch angeordneten, sphärischen, leitenden Partikeln. Die Wahl von Kupfer als repräsentatives Material geschah aufgrund der Verfügbarkeit von experimentellen Daten. Die effektiven Eigenschaften des Kupferpulvers wurden mit der FIT Technik simuliert, welche einen allgemeinen Überblick über die Probeneigenschaften in Form von Streuparametern geben. Die frequenzabhängigen Streuparameter geben Aufschluss über die effektiven elektromagnetischen Eigenschaften des untersuchten Materials oder Materialkombinationen. Durch die Adaptierung einer mathematischen Struktur von experimentellen Reflektions/Transmissionsmessungen ist es möglich, die effektive dielektrische Permittivität und die effektive magnetische Permeabilität aus den Streuparametern zu extrahieren. Es wurde eine numerische Prozedur entwickelt, die die effektiven elektromagnetischen Eigenschaften automatisch aus den Streuparametern automatisch extrahiert. Diese Prozedur wurde dann anhand bekannter Materialien validiert. Die Simulationsergebnisse wurden mit experimentellen Daten verglichen, was es erlaubt, die grundlegenden Mechanismen der Mikrowellenabsorption als auch den Sinterprozess von metallischen Pulvern zu studieren und zu verstehen. Die Simulationen über ein weites Frequenzspektrum zeigten ein resonantes Verhalten in der effektiven magnetischen Permeabilität des Kupferpulvers. Die Simulationen des Mikrowellenheizens im separierten Magnetfeld des Kupferpulvers mit verschiedenen Partikelgrößen sind in guter Übereinstimmung mit den experimentell bestimmten anfänglichen Heizraten der Kupferpresslinge. Es konnte herausgefunden werden, dass die effektive magnetische Permeabilität ein diamagnetisches Verhalten aufweist und dass die Resonanzfrequenz von der Partikelgröße und der Leitfähigkeit des jeweiligen Materials abhängt.



# Contents

<b>Abstract</b>	<b>vii</b>
<b>Zusammenfassung</b>	<b>ix</b>
<b>Table of contents</b>	<b>xi</b>
<b>1 Introduction</b>	<b>1</b>
1.1 Microwave Heating . . . . .	1
1.2 Sintering . . . . .	7
1.3 Maxwell's Equations . . . . .	9
1.4 Finite Integration Technique . . . . .	13
1.4.1 Maxwell's Grid Equations . . . . .	14
1.4.2 Time Domain Formulation . . . . .	15
1.4.3 Frequency Domain Formulation . . . . .	16
1.4.4 Boundary Conditions . . . . .	17
1.5 General Electromagnetic Properties of Materials . . . . .	18
<b>2 Extraction of Effective Properties</b>	<b>23</b>
2.1 Techniques for Material Characterization . . . . .	23
2.2 Transmission/Reflection Free Space Method . . . . .	25
2.3 Limitations of the Extraction Method . . . . .	33
<b>3 Metallic Powders</b>	<b>37</b>
3.1 Microwave Sintering of Metallic Powders . . . . .	37
3.2 Theory of Microwave Sintering of Powdered Metals . . . . .	42
3.2.1 Microwave Heating in Separated Electric and Magnetic Fields	43
3.2.2 Effective Medium Approach . . . . .	46
3.2.3 Interparticle Neck Growth . . . . .	50
3.3 Modeling of Copper Powders . . . . .	52
3.4 Mechanisms of Dielectric Losses . . . . .	53

3.5	Mechanisms of Magnetic Losses . . . . .	60
3.6	Microwave Heating in the Magnetic Field . . . . .	63
3.7	Resonance Frequency Dependence . . . . .	65
<b>4</b>	<b>Summary</b>	<b>69</b>
	<b>Appendix</b>	<b>71</b>
	Extraction of the Effective Properties - Script Listing . . . . .	71
	<b>Bibliography</b>	<b>79</b>
	<b>Index</b>	<b>91</b>
	<b>Acknowledgments</b>	<b>93</b>
	<b>List of Contributions</b>	<b>95</b>
	<b>Erklärung</b>	<b>97</b>

# Chapter 1

## Introduction

### 1.1 Microwave Heating

The rapid development of microwave technology came during World War II with the urgent need to improve radar detection of enemy aircraft and submarines and the invention of high power cavity magnetron. Rapid advances made in the research and development of microwave radar and associated technologies emerged during the war. Additionally, the important milestones in the development of microwave technology over the last century are summarized in an review article by Sobol and Tomiyasu [1]. The microwave oven was developed after W.W.II, the engineer who is best known for birthing the idea of using microwaves to prepare food was Percy Spencer, of the Raytheon Company, located in Waltham Massachusetts. One of the subject matter experts on this topic is John Osepchuk, who worked at Raytheon during the 60s, 70s and 80s. His review papers on the topic give extensive overview on the history and the engineering behind microwave heating [2, 3]. Much work was underway in the latter days of W.W.II by companies looking for industrial heating applications of microwaves, including diathermy, and industrial heating of products such as inks, glue, and tires.

Since their rapid development during World War II, microwaves have been expanded to numerous applications in addition to radar and communication. Microwaves are being used for their ability to heat materials. The most common application of microwave heating is the domestic microwave oven, where it is used to heat and cook various food. In industry, microwave heating has been applied to tempering frozen meat, processing of potato chips, vulcanization of rubber or simply heating of liquids [4, 5, 6]. Microwave processing systems usually consist of a microwave source, for generation of microwaves, an applicator to deliver the power to the material and a control system for the monitoring and regulation of

power to the material. The most common type of microwave generator used is the magnetron. Microwave applicators include multimode, where multiple modes are sustained simultaneously inside the cavity, and single mode, where only a single mode is sustained. The heating of materials is controlled by variations in the power and duration of microwave radiation on the materials. The use of microwaves for the processing of organic materials and inorganic materials, such as polymers, ceramic and minerals has been widely reported [7, 8, 9, 10, 11, 12].

Microwaves are extensively used in satellite communication for the transmission of signals and information because of their ability to penetrate Earth's atmosphere with minimum losses. The high frequency of microwaves provides a greater bandwidth capability so that more information can be transmitted within the bandwidth. For example, when using an AM radio signal with carrier frequency of 1000 kHz to transmit audio information contained over a bandwidth of 40 kHz, it will take up 4% of the carrier, while the use of a 10 GHz microwave signal with a 10% bandwidth system can provide a bandwidth of 1 GHz that will allow transfer of more information such as AM and FM radio signals, shortwave radio, broadcast television, telephone calls and computer digital data simultaneously. The short wavelength of microwaves allows high-gain antennas with narrow bandwidth to be constructed for use in radar applications, since antenna gain is proportional to the square of the operating frequency. Information from spacecraft is transmitted at microwave frequencies and received by huge antennas on Earth. Microwave technologies have revolutionized the communication and transfer of information in the modern world. Examples include telecommunication, digital data transfer, wireless local area networks, navigation, power transmission, radar detection, etc. New applications for microwaves are still being developed. Worth mentioning are systems for electronic warfare like deceptive jamming, i.e. emission of microwave signals to attempt to camouflage the presence of targets or to mislead the enemy by the transmission of false information by altering the original signal. Nonlethal weaponry is being developed, that includes electromagnetic pulse (EMP) devices and active denial systems (ADS). EMP systems create a short and intense electromagnetic pulse which generates a transient surge of thousands of volts capable of disabling electronic devices within range. ADS is being tested by US military as a nonlethal riot control weapon. ADS consists of a huge directional array antenna that operates at 95 GHz mounted on a vehicle, that emits nonionizing electromagnetic beam of energy that penetrates approximately 0.5 mm into human skin tissue, where nerve receptors are concentrated. Within seconds, the beam will heat the exposed skin tissue to a level where intolerable pain is experienced.

Microwaves are used in medical applications for their ability to create intense heat and as a power source in medical equipment for radiology treatment. In radiation therapy, microwaves are used as a power source to accelerate electrons to high energy in medical linear accelerators and the electrons are then directed to collide with a metal target. Upon impact, electrons are displaced from the atomic shells of the target metal and X-rays are emitted. The high energy X-rays are used in cancer treatment to destroy the cancer cells. Microwaves can be also used in hyperthermia treatment of cancer by raising the temperature of the cancerous tissue and cause necrosis. This treatment exposes the body tissue to high temperatures up to 44 °C, with minimal injury to the surrounding healthy tissue. Cancerous regions are usually characterized by regions of low oxygen content in tissue and low pH due to insufficient blood flow, which makes the cancer cells particularly sensitive to temperatures between 40 and 44 °C. During hyperthermia treatment, the reduced blood flow in tumor tissue causes it to heat more easily than normal tissue. The effect of the heat causes damage and death to the cancer cells, probably due to protein denaturation observed at temperatures higher than 40 °C leading to alterations in the cell molecular structure and enzyme complexes. Hyperthermia treatment is frequently used in combination with either radiotherapy or chemotherapy [13].

A futuristic application of microwaves called the Solar Power System (SPS) was proposed in 1968 [14]. SPS was the theoretical concept of solar powerplants orbiting in space around the Earth, collecting solar power by means of photovoltaic arrays or heat engine, and transmitting it to earth with microwaves or laser beams. Such a system would introduce several advantages over current methods of generating power from sun, like omitting weather and atmospheric effects, higher collection rate and longer collection periods. Currently the design and implementation of the SPS is still theoretical and faces few hurdles. The system components need to be delivered to the orbits and with current state of art rockets it is not feasible. Also the impact of microwave beaming the power to Earth's surface on atmosphere and biosphere is discussed.

It has long been known that materials may be heated with the use of high frequency electromagnetic waves. The heating effect arises from the interaction of the electric field component of the wave with charged particles in the material. Two major effects are responsible for the heating which results from this interaction. If the charged particles are free to travel through the material, electrons or ions, a current will be induced which will travel in phase with the field. If, on the other hand, the charged particles are bound within regions of the material, the electric

field component will cause them to move until opposing forces balance the electric force. The result is a dipolar polarization in the material. Conduction and dipolar polarization may both give rise to heating under microwave irradiation.

The inability of partially bound charges to follow the rapid changes in a high frequency electric field gives rise to one mechanism of microwave heating. The total polarization  $a_t$  of the material arising from the displacement of charges may be expressed as the sum of a number of components

$$a_t = a_e + a_a + a_d, \quad (1.1)$$

where  $a_e$  results from the displacement of electron charges in relation to the nuclei in a material, and  $a_a$  from the displacement of nuclei relative to one another in materials with unequal charge distributions. Polarization of both  $a_e$  and  $a_a$  operates on timescales which are very much smaller than that required for microwave frequency field reversals, and therefore follow microwave frequency fields almost exactly. As such, they do not contribute to the microwave heating effect. The  $a_d$  results from the reorientation of polar molecules or other permanent dipoles in the material. As the timescale for its operation is of the order of those associated with microwaves, this is the most important of the polarization phenomena in relation to microwave heating.

The complex dielectric constant  $\varepsilon$  completely describes the dielectric properties of homogeneous materials and is expressed as the sum of real and complex dielectric constants  $\varepsilon = \varepsilon' - i\varepsilon''$ . The real part of  $\varepsilon$  represents the ability of a material to be polarized by an external electric field. At very high and very low frequencies, and with static fields,  $\varepsilon'$  represents the total dielectric constant of the material. Where electromagnetic energy is converted to heat by the material,  $\varepsilon''$  is non-zero, and quantifies the degree to which the electromagnetic energy is converted to heat.

A further quantity, the loss angle  $\delta$ , is also commonly used in the literature, and is more usually given in the form of its tangent. It is related to the complex dielectric constant by expression  $\tan \delta = \varepsilon''/\varepsilon'$ . The angle  $\delta$  is the phase difference between the electric field and the polarization of the material. Magnetic polarization may also contribute to the heating effect observed in materials where magnetic properties exist, and a similar expressions for the complex permeability of such materials may be formulated. For any material, both the real and complex dielectric constants will vary with frequency.

Dipole rotation is the phenomenon responsible for the majority of microwave



heating effects observed in solvent systems. In substances such as water, the different electronegativities of individual atoms results in the existence of a permanent electric dipole on the molecule. The dipole is sensitive to external electric fields, and will attempt to align with them by rotation, the energy for this rotation being provided by the field. This realignment is rapid for a free molecule, but in liquids instantaneous alignment is prohibited by the presence of other molecules. A limit is therefore placed on the ability of the dipole to respond to a field, which affects the behavior of the molecule with different frequencies of electric field.

Under low frequency irradiation, the dipole may react by aligning itself in phase with the electric field. Whilst some energy is gained by the molecule by this behavior, and some is also lost in collisions, the overall heating effect is small. Under the influence of a high frequency electric field, on the other hand, the dipoles do not have sufficient time to respond to the field, and so do not rotate. As no motion is induced in the molecules, no energy transfer takes place, and therefore, no heating. Between these two extremes, at frequencies which are approximately those of the response times of the dipoles, is the microwave region. The microwave frequency is low enough that the dipoles have time to respond to the alternating field, and therefore to rotate, but high enough that the rotation does not precisely follow the field. As the dipole reorientates to align itself with the field, the field is already changing, and a phase difference exists between the orientation of the field and that of the dipole. This phase difference causes energy to be lost from the dipole in random collisions, and to give rise to dielectric heating.

Where a dielectric material is not homogeneous, but consists of inclusions of one dielectric in another, it is still possible to treat the material theoretically. If the dielectric properties and geometry of the inclusions are known, it is possible to arrive at expressions for the dielectric behavior of the bulk sample.

In addition to the dielectric and magnetic losses, many materials may also display conduction losses under microwave irradiation. The complex dielectric constant may be expressed to take account of these losses by including a separate conduction term. The importance of this term is displayed by a large number of systems. The addition of dissolved salts in water markedly affects the dielectric properties as conduction increases, and may become important enough to overwhelm the dielectric losses. On the other hand, the dielectric losses of the majority of solids arise predominantly from these conduction terms, and may be strongly affected by temperature. The conductivity of alumina, for example, increases with temperature as electrons are promoted into the conduction band from

the valence band leading to increases in the dielectric constants.

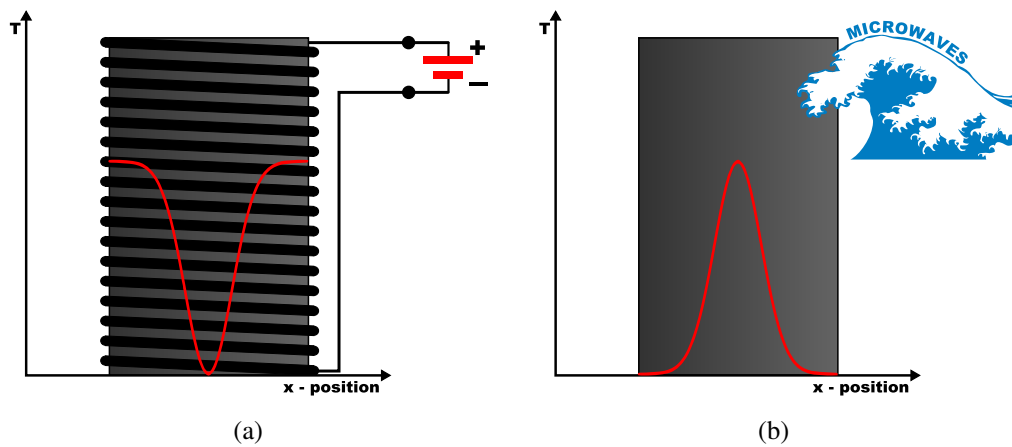


Figure 1.1: Comparison of a conventional (a) and a microwave (b) heating profiles in an example cylindrical object. In contrast to the conventional, resistive heating, microwave heating is a volumetric heating process. That means the sample is heated from the inside, rather than on the surface.

Microwave heating offers numerous advantages in productivity over conventional heating methods such as hot air, resistive heating, etc. Microwave energy penetrates to generate heat internally as well as at the surface of the treated material. Other methods apply heat only to the surface and temperature must be limited in order to avoid burning. Conventional processing time is slow due to thermal conductivity. Microwave energy overcomes those time and temperature limitations and produces a very high quality product even when the materials being processed are fairly thick. Some materials absorb microwaves readily, others do not, a characteristic used to advantage in the microwave process. Pharmaceuticals, for example, can be pasteurized within their packages without burning the packaging material. Most conventional heating systems, require appreciable amounts of time to effect temperature changes. Microwave power levels can be adjusted electronically in a fraction of a second, which makes microwave equipment readily adaptable to automated systems and to data logging programs and processes based on microwave heating and many industrial applications. The main benefits of exploiting microwave energy in thermally activated processes stem from the specificity of microwave energy absorption. In contrast to all other commonly used methods, microwaves allow volumetric heating of materials, as shown in figure 1.1. Microwave energy transforms into heat inside the material, which results, as a rule, in significant energy savings and reduction in process time.

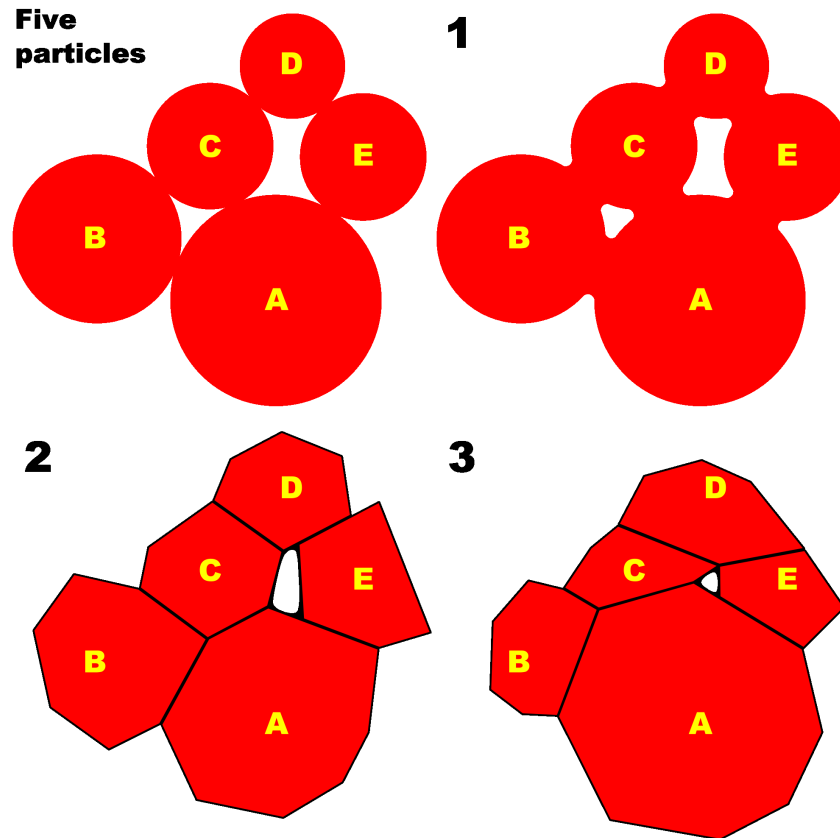


Figure 1.2: The three stages of the sintering process: 1. neck formation, 2. neck growth, 3. grain coarsening. The last stage of sintering process is usually unwanted. Special methods must be employed to avoid grain growth, and to produce materials with superior macro properties.

## 1.2 Sintering

Sintering, or to be more specific, solid state sintering is a method for solidification and densification of objects from powdered material by means of heating the material below melting point. Sintering is widely used in industry for manufacturing ceramic objects, as well as metallic ones; however, not to the same extent. Ceramic materials usually have very high melting point, much higher than metals, thus typical processing methods for metals like casting is not possible.

The main goal of sintering is to reduce the porosity and enhance macro-properties of sintered objects such as tensile strength, electrical conductivity or hardness. During the sintering process pores between powder particles become smaller as shown in figure 1.2. The first stage in sintering is formation of necks between particles. As heat is being applied necks grow, finally to create particular grains. Further heating leads to grain growth [15, 16]. Some grains grow at the expense of other grains. To obtain the desired macro-properties of the sintered

object, the heating process is performed in steps. The temperature is raised or lowered gradually in time and consists of firing plateaus. But these final stage sintering processes are always accompanied by rapid grain growth, which is usually not desirable. Special precautions and heating schedules must be used to suppress grain coarsening [17].

The driving force for densification is the change in free energy from the decrease in surface area and lowering of the surface free energy [18, 19, 20, 21]. Densification creates new but lower-energy solid-solid interfaces with a total decrease in free energy occurring on sintering of the powdered material. On a microscopic scale, material transfer is affected by the change in pressure and differences in free energy across the curved surface. If the size of the particle is small (or if the radius of curvature is large) these effects become very large in magnitude. The change in energy is much higher when the radius of curvature is less than a few  $\mu\text{m}$ , which is one of the main reasons why much ceramic technology is based on the use of fine-particle materials.

For properties such as strength and conductivity, the bond area in relation to the particle size is the determining factor. The variables that can be controlled for any given material are the temperature and the initial grain size, because the vapor pressure depends upon temperature.

The source of power for solid-state processes is the change in free- or chemical-potential energy between the neck and the surface of the particle. This energy creates a transfer of material through the fastest means possible; if transfer were to take place from the particle volume or the grain boundary between particles then there would be particle reduction and pore destruction. The pore elimination occurs faster for a sample with many pores of uniform size and higher porosity where the boundary diffusion distance is smaller.

The mechanism of forming interfaces between particles, or connecting particles during the first stage of sintering, can be described by a combination of following mechanisms: viscous flow, evaporation and condensation, volume diffusion and surface diffusion [22, 23], as shown in figure 1.3. Numerous chemical reactions or micro-structural changes in solids take place through solid state diffusion, i.e. the movement and transport of atoms in solid phases. The diffusion takes place because of the presence of defects in solids. Point defects, e.g. vacancies and interstitial ions, are responsible for lattice diffusion. Diffusion also takes place along line and surface defects which include grain boundaries, dislocations, inner and outer surfaces, etc. As diffusion along linear, planar and surface defects is generally faster than in the lattice, they are also termed high diffusivity or easy diffusion

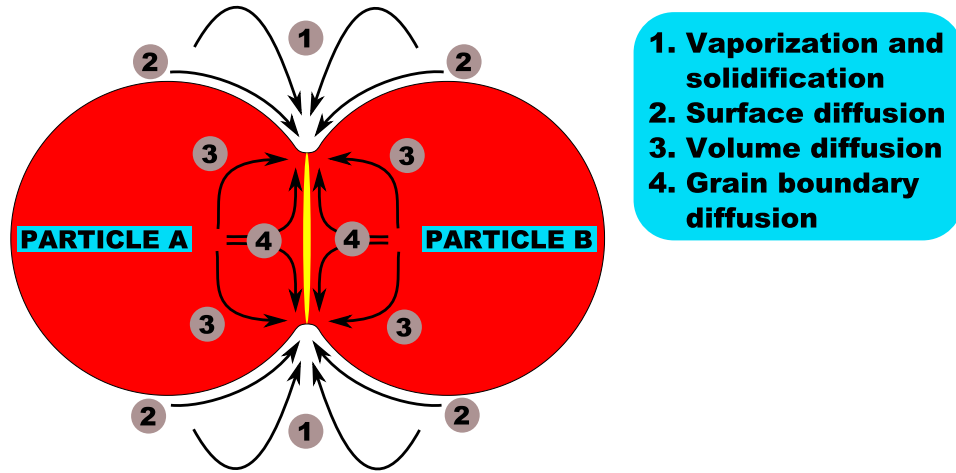


Figure 1.3: The main mechanisms of sintering. The temperature activated atomic transport processes like volume diffusion, surface diffusion and evaporation-condensation lead to decrease of surface free energy.

paths. The relative contribution of the different types of diffusion in materials are functions of the temperature, partial pressures or activities of the constituents of the compounds, the microstructure, grain size and porosity. Grain boundary and dislocation diffusion generally have smaller activation energies than lattice diffusion and as a result become increasingly important the lower the temperature in solids with a given microstructure.

Control of the temperature is very important to the sintering the process, since grain-boundary diffusion and volume diffusion rely heavily upon temperature, the size and distribution of particles of the material, the materials composition, and often the sintering environment have to be controlled.

### 1.3 Maxwell's Equations

Electromagnetic wave propagation is described by Maxwell's equations [24]. This set of partial differential equations relates the time and space rates of change of various field quantities at a point in space and time.

$$\nabla \times \mathbf{E}(\mathbf{r}, t) = -\frac{\partial}{\partial t} \mathbf{B}(\mathbf{r}, t), \quad (1.2)$$

$$\nabla \times \mathbf{H}(\mathbf{r}, t) = \frac{\partial}{\partial t} \mathbf{D}(\mathbf{r}, t) + \mathbf{J}(\mathbf{r}, t), \quad (1.3)$$

$$\nabla \cdot \mathbf{D}(\mathbf{r}, t) = \rho(\mathbf{r}, t), \quad (1.4)$$

$$\nabla \cdot \mathbf{B}(\mathbf{r}, t) = 0, \quad (1.5)$$

where  $\mathbf{E}$  is the electric field strength in V/m,  $\mathbf{H}$  the magnetic field strength in A/m,  $\mathbf{D}$  denotes electric induction or electric displacement in As/m<sup>2</sup>,  $\mathbf{B}$  magnetic induction or magnetic flux density in Vs/m<sup>2</sup>,  $\mathbf{r}$  is the position vector which defines a particular location in real space  $\mathbb{R}^3$  and  $t$  is the time. In the above equations  $\mathbf{J}$  is the electric current density in A/m<sup>2</sup> and  $\rho$  the electric charge density in C/m<sup>3</sup>. The relation between  $\mathbf{J}$  and  $\rho$  is the continuity equation

$$\nabla \cdot \mathbf{J}(\mathbf{r}, t) = -\frac{\partial}{\partial t} \rho(\mathbf{r}, t). \quad (1.6)$$

Furthermore, there are two more constitutive relations between the  $\mathbf{E}$  and  $\mathbf{H}$  field quantities, the  $\mathbf{D}$  and  $\mathbf{B}$  displacements, respectively,

$$\mathbf{D}(\mathbf{r}, t) = \varepsilon_0 \varepsilon \mathbf{E}(\mathbf{r}, t), \quad (1.7)$$

$$\mathbf{B}(\mathbf{r}, t) = \mu_0 \mu \mathbf{H}(\mathbf{r}, t). \quad (1.8)$$

Here  $\varepsilon_0 = 8.85 \cdot 10^{-12}$  F/m is the permittivity of free space,  $\mu_0 = 4\pi \cdot 10^{-7}$  H/m is the permeability of free space,  $\varepsilon = \varepsilon' - i\varepsilon''$  the complex permittivity of the material and  $\mu = \mu' - i\mu''$  the complex permeability of the material, and  $i^2 = -1$  is the imaginary unit. For conductive media, when an electric field  $\mathbf{E}$  is applied, the conduction current  $\mathbf{J}$  will flow, which is directly proportional to  $\mathbf{E}$ ,

$$\mathbf{J}(\mathbf{r}, t) = \sigma \mathbf{E}(\mathbf{r}, t), \quad (1.9)$$

where  $\sigma$  is the conductivity of the material in S/m. In case when the conduction current is not negligible, i.e. in lossy medium or a good conductor for that matter, it is convenient to write the conductivity of the material as a complex value  $\sigma = \sigma' - i\sigma''$ . The relation between the conductivity and the permittivity of the lossy material can be written as

$$\varepsilon = \varepsilon' - i \left( \varepsilon'' + \frac{\sigma}{\omega} \right), \quad (1.10)$$

where  $\omega$  is the angular frequency.

Maxwell's equations can also be written in integral form,

$$\oint_l \mathbf{E}(\mathbf{r}, t) \cdot d\mathbf{l} = -\frac{\partial}{\partial t} \int_S \mathbf{B}(\mathbf{r}, t) \cdot d\mathbf{S}, \quad (1.11)$$

$$\oint_l \mathbf{H}(\mathbf{r}, t) \cdot d\mathbf{l} = \frac{\partial}{\partial t} \int_S \mathbf{D}(\mathbf{r}, t) \cdot d\mathbf{S} + I(t), \quad (1.12)$$

$$\oint_S \mathbf{D}(\mathbf{r}, t) \cdot d\mathbf{S} = q, \quad (1.13)$$

$$\oint_S \mathbf{B}(\mathbf{r}, t) \cdot d\mathbf{S} = 0, \quad (1.14)$$

where  $l$  is a closed contour that forms the boundary of an open surface  $S$  and a volume  $V$  is surrounded by a closed surface  $S$ , as shown in figure 1.4,  $I$  is the total current flowing through the cross section  $S$  surrounded by closed curve  $l$ ,

$$I(t) = \int_S \mathbf{J}(\mathbf{r}, t) \cdot d\mathbf{S}, \quad (1.15)$$

$q$  the total electric charge contained in the volume  $V$  surrounded by the closed surface  $S$ ,

$$q = \int_V \rho \cdot dV. \quad (1.16)$$

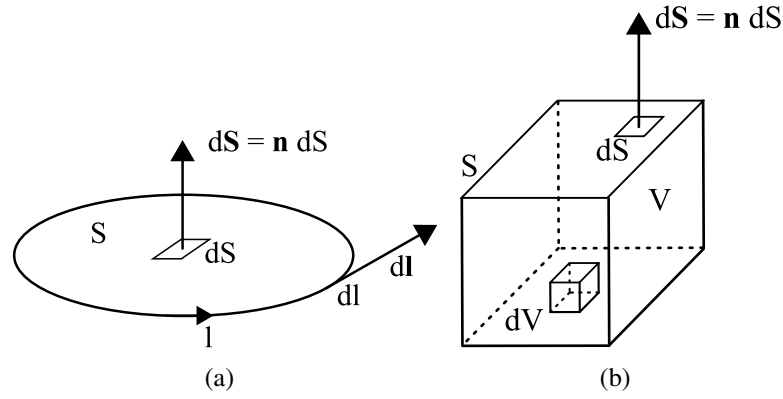


Figure 1.4: (a) A surface  $S$  surrounded by a closed curve  $l$  and (b) a volume  $V$  surrounded by a closed surface  $S$ .

Maxwell's equations, with steady-state sinusoidal field time dependence, can be rewritten by using the method of complex phasor notation. In the complex phasor notation the time derivative  $\partial/\partial t$  becomes  $i\omega$ , and Maxwell's equations in the differential phasor form can be written in the following manner

$$\nabla \times \mathbf{E}(\mathbf{r}) = -i\omega\mathbf{B}(\mathbf{r}), \quad (1.17)$$

$$\nabla \times \mathbf{H}(\mathbf{r}) = i\omega\mathbf{D}(\mathbf{r}) + \mathbf{J}(\mathbf{r}), \quad (1.18)$$

$$\nabla \cdot \mathbf{D}(\mathbf{r}) = \rho(\mathbf{r}), \quad (1.19)$$

$$\nabla \cdot \mathbf{B}(\mathbf{r}) = 0. \quad (1.20)$$

The complex permittivity and the complex permeability are also frequency dependent for dispersive materials:

$$\varepsilon(\omega) = \varepsilon'(\omega) - i\varepsilon''(\omega), \quad (1.21)$$

$$\mu(\omega) = \mu'(\omega) - i\mu''(\omega), \quad (1.22)$$

therefore, the constitutive relations 1.7 and 1.8 take the following complex forms:

$$\mathbf{D}(\mathbf{r}) = \left( \varepsilon'(\omega) - i\varepsilon''(\omega) \right) \mathbf{E}(\mathbf{r}), \quad (1.23)$$

$$\mathbf{B}(\mathbf{r}) = \left( \mu'(\omega) - i\mu''(\omega) \right) \mathbf{H}(\mathbf{r}). \quad (1.24)$$

In dispersive and conducting materials, energy dissipation occurs due to dielectric and magnetic losses and Joule heating. The quantities describing this behavior are the imaginary part of the permittivity  $\varepsilon''$ , the imaginary part of the permeability  $\mu''$  and the conductivity  $\sigma$ . Dielectric losses are mostly due to polarization dissipation. Similarly, in magnetic materials the mechanisms responsible for dissipation are magnetization dissipation and hysteresis losses. In conductive media, when electrical current flows through the material, the energy is dissipated due to Joule heating

$$Q = RI t, \quad (1.25)$$

where  $Q$  is the heat generated by a current flowing through a conductor,  $R$  the electrical resistance of the material, and  $t$  is the time over which the current flows. The electrical resistance is proportional to the inverse of the conductivity  $R \propto 1/\sigma$ ; thus, with increasing conductivity, the losses become smaller. The complex permittivity and permeability can also be expressed in polar form

$$\varepsilon = \varepsilon' - i\varepsilon'' = |\varepsilon|e^{-i\delta} = |\varepsilon|\cos\delta - i|\varepsilon|\sin\delta, \quad (1.26)$$

$$\mu = \mu' - i\mu'' = |\mu|e^{-i\theta} = |\mu|\cos\theta - i|\mu|\sin\theta, \quad (1.27)$$

where  $\delta$  is the dielectric loss angle and  $\theta$  the magnetic loss angle. The very useful quantities describing dissipation capabilities of the medium, dielectric  $\tan\delta$  and magnetic  $\tan\theta$  loss tangents, can be derived from the above equations

$$\tan\delta = \frac{\varepsilon''}{\varepsilon'}, \quad (1.28)$$



$$\tan \theta = \frac{\mu''}{\mu'}. \quad (1.29)$$

In similar fashion one can derive the loss tangent for a conductive material

$$\tan \delta = \frac{\omega \varepsilon'' + \sigma}{\omega \varepsilon'}, \quad (1.30)$$

where the loss tangent due to only the conductive losses is

$$\tan \delta = \frac{\sigma}{\omega \varepsilon'}. \quad (1.31)$$

An important relationship between the real part and the imaginary part of the frequency dependent complex permittivity is that one part is not independent of the other. The connection between the polarization and the electric field due to the causality principle indicates that the response of the matter to an excitation cannot precede the cause. The Kramers-Kronig equations relate the real part to the imaginary part of the frequency-dependent permittivity[25]

$$\varepsilon'(\omega) = 1 - \frac{1}{\pi} \mathcal{P} \int_{-\infty}^{\infty} \frac{\varepsilon''(\omega')}{\omega' - \omega} d\omega', \quad (1.32)$$

$$\varepsilon''(\omega) = \frac{1}{\pi} \mathcal{P} \int_{-\infty}^{\infty} \frac{\varepsilon'(\omega') - 1}{\omega' - \omega} d\omega', \quad (1.33)$$

where  $\mathcal{P}$  denotes the Cauchy principal value of the integral. Modified equations can be applied to the real part and the imaginary part of the frequency dependent complex permeability [26].

## 1.4 Finite Integration Technique

The Finite Integration Technique (FIT) is a discretization scheme of the integral form of Maxwells equations, in contrast to most numerical methods that make use of differential form of Maxwells equations. The FIT scheme was established by T. Weiland [27, 28] in 1977 and is implemented in general purpose electromagnetic simulation software package CST Microwave Studio (CST MWS) [29]. Throughout this work the CST MWS is used to perform full 3D electromagnetic high frequency simulations on models of ceramic and metallic mixtures. The analytical solution of Maxwells equations can be calculated only for a small number of electromagnetic problems that involve simple geometrical structures. All macroscopic electromagnetic phenomena occurring in practice can

be mathematically described with the set of Maxwell's equations. In most real-world cases the only option to solve Maxwell's equations is by using numerical methods. The resulting matrix equations of the discretized fields can be used for efficient numerical simulations on modern computers. In addition, the basic algebraic properties of this discrete electromagnetic field theory allow one to analytically and algebraically prove conservation properties with respect to energy and charge of the discrete formulation and gives an explanation of the stability properties of numerical formulations in the time and frequency domain. This finite volume-type discretization scheme for Maxwell's equations relies on the usage of integral balances and thus allows one to prove stability and conservation properties of the discrete fields even before starting with numerical calculations. In particular, such algebraic properties of the discrete formulation enable the development of stable numerical time-integration schemes or accurate eigenvalue solvers avoiding spurious modes.

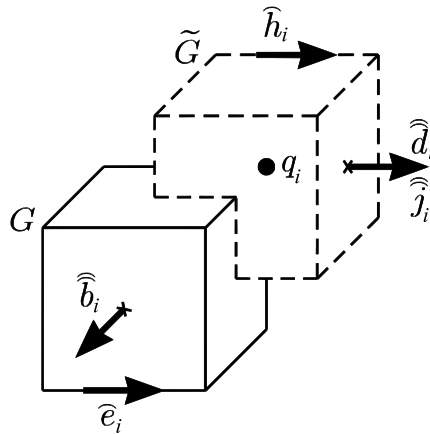


Figure 1.5: Primary (solid line) and secondary (dashed line) grids, with indicated integral variables

### 1.4.1 Maxwell's Grid Equations

In FIT, Maxwell's equations and the constitutive relations are mapped onto a dual grid system  $(G, \tilde{G})$  defining a finite computational domain. The primary grid  $G$  and the secondary grid  $\tilde{G}$  are orthogonal. The spatial discretization of Maxwell's equations is performed on these two orthogonal grid systems where degrees of freedom are introduced as integral values. The electric grid voltages  $\hat{e}_i$  and magnetic facet fluxes  $\hat{b}_i$  are allocated on the primary grid  $G$ , the magnetic grid voltages  $\hat{h}_i$ , the dielectric facet fluxes  $\hat{d}_i$ , electric grid current  $\hat{j}_i$  and electric grid charge  $q_i$  are defined on the secondary grid  $\tilde{G}$  as shown in figure 1.5. Using the

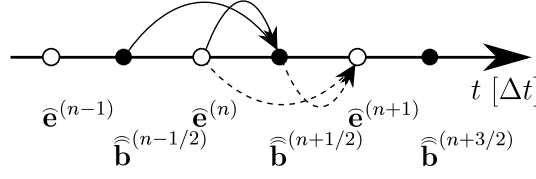


Figure 1.6: Leap-frog scheme

integral variables, Maxwell's equations are converted into a set of matrix-vector equations, referred to as Maxwell's Grid Equations (MGE)

$$\nabla \times \mathbf{E}(\mathbf{r}, t) = -\frac{d}{dt}\mathbf{B}(\mathbf{r}, t) \Leftrightarrow \mathbf{C}\hat{\mathbf{e}} = -\frac{d}{dt}\hat{\mathbf{b}}, \quad (1.34)$$

$$\nabla \times \mathbf{H}(\mathbf{r}, t) = \frac{\partial}{\partial t}\mathbf{D}(\mathbf{r}, t) + \mathbf{J}(\mathbf{r}, t) \Leftrightarrow \tilde{\mathbf{C}}\hat{\mathbf{h}} = \frac{\partial}{\partial t}\hat{\mathbf{d}} + \hat{\mathbf{j}}, \quad (1.35)$$

$$\nabla \cdot \mathbf{D}(\mathbf{r}, t) = \rho(\mathbf{r}, t) \Leftrightarrow \tilde{\mathbf{S}}\hat{\mathbf{d}} = \mathbf{q}, \quad (1.36)$$

$$\nabla \cdot \mathbf{B}(\mathbf{r}, t) = 0 \Leftrightarrow \mathbf{S}\hat{\mathbf{b}} = 0, \quad (1.37)$$

where sparse matrices  $\mathbf{C}$  and  $\tilde{\mathbf{C}}$  are the discretization of the curl operator ( $\nabla \times$ ), and matrices  $\mathbf{S}$  and  $\tilde{\mathbf{S}}$  are the discretization of the div operator ( $\nabla \cdot$ ) on the primary and secondary grid, respectively. The discrete equivalent of the constitutive relations and Ohm's law for non-bianisotropic media without permanent polarization or magnetization is based on diagonal material matrices ( $\mathbf{M}_\epsilon$ ,  $\mathbf{M}_\mu$ ,  $\mathbf{M}_\sigma$ )

$$\mathbf{D}(\mathbf{r}, t) = \epsilon_0\epsilon\mathbf{E}(\mathbf{r}, t) \Leftrightarrow \hat{\mathbf{d}} = \mathbf{M}_\epsilon\hat{\mathbf{e}}, \quad (1.38)$$

$$\mathbf{B}(\mathbf{r}, t) = \mu_0\mu\mathbf{H}(\mathbf{r}, t) \Leftrightarrow \hat{\mathbf{b}} = \mathbf{M}_\mu\hat{\mathbf{h}}, \quad (1.39)$$

$$\mathbf{J}(\mathbf{r}, t) = \sigma\mathbf{E}(\mathbf{r}, t) \Leftrightarrow \hat{\mathbf{j}} = \mathbf{M}_\sigma\hat{\mathbf{e}}. \quad (1.40)$$

The discrete constitutive relations are defining the necessary relations between voltages and fluxes. Their integral values have to be approximated over the grid edges and cell areas, respectively, and the resulting coefficients depend on the averaged material properties as well as on the spatial resolution of the grid, introducing a numerical error.

## 1.4.2 Time Domain Formulation

The time domain FIT solver is based on a method known as the leap-frog scheme [30], which calculates the values of  $\hat{\mathbf{e}}$  and  $\hat{\mathbf{b}}$  at time samples separated by half a time step  $\Delta t$ . Both types of unknowns are located alternately in time, thus the following

notation is used

$$\widehat{\mathbf{b}}((n + 1/2)\Delta t) = \widehat{\mathbf{b}}^{(n+1/2)}, \quad (1.41)$$

$$\widehat{\mathbf{e}}(n\Delta t) = \widehat{\mathbf{e}}^{(n)}. \quad (1.42)$$

For example, the magnetic flux  $\widehat{\mathbf{b}}$  at  $t = (n + 1)\Delta t$  is computed from the magnetic flux at the previous step  $t = n\Delta t$  and from the electric voltage  $\widehat{\mathbf{e}}$  at half time step before  $t = (n + 1/2)\Delta t$  as shown in figure 1.6. Substituting the time derivatives by central differences yields

$$\left(\frac{d}{dt}\widehat{\mathbf{b}}\right)^{(n)} = \frac{\widehat{\mathbf{b}}^{(n+1/2)} - \widehat{\mathbf{b}}^{(n-1/2)}}{\Delta t}, \quad (1.43)$$

$$\left(\frac{d}{dt}\widehat{\mathbf{e}}\right)^{(n+1/2)} = \frac{\widehat{\mathbf{e}}^{(n+1)} - \widehat{\mathbf{e}}^{(n)}}{\Delta t}, \quad (1.44)$$

and inserting into the two curl equations (1.34) and (1.35) one obtains the update formulation of the loss-free case

$$\widehat{\mathbf{b}}^{(n+1/2)} = \widehat{\mathbf{b}}^{(n-1/2)} - \Delta t \mathbf{C} \widehat{\mathbf{e}}^{(n)}, \quad (1.45)$$

$$\widehat{\mathbf{e}}^{(n+1)} = \widehat{\mathbf{e}}^{(n)} + \Delta t \mathbf{M}_\epsilon^{-1} \left( \widetilde{\mathbf{C}} \mathbf{M}_{\mu^{-1}} \widehat{\mathbf{b}}^{(n+1/2)} - \widehat{\mathbf{j}}^{(n+1/2)} \right). \quad (1.46)$$

Explicit time integration schemes are conditionally stable, the stability limit for the time step  $\Delta t$  is given by the Courant-Friedrichs-Levy criterion

$$\Delta t \leq \frac{\sqrt{\varepsilon\mu}}{\sqrt{\left(\frac{1}{\Delta x}\right)^2 + \left(\frac{1}{\Delta y}\right)^2 + \left(\frac{1}{\Delta z}\right)^2}}. \quad (1.47)$$

### 1.4.3 Frequency Domain Formulation

Similarly to the procedure applied to equations (1.17)-(1.20), by applying the phasor notation to MGE, one obtains discrete Maxwell's equations in frequency domain

$$\mathbf{C}\widehat{\mathbf{e}} = -i\omega\widehat{\mathbf{b}}, \quad (1.48)$$

$$\widetilde{\mathbf{C}}\widehat{\mathbf{h}} = i\omega\widehat{\mathbf{d}} + \widehat{\mathbf{j}}, \quad (1.49)$$

$$\widetilde{\mathbf{S}}\widehat{\mathbf{d}} = \mathbf{q}, \quad (1.50)$$

$$\mathbf{S}\widehat{\mathbf{b}} = 0. \quad (1.51)$$

Since the div equations (1.50) and (1.51) do not contain time derivatives, these equations remain unchanged.

By taking into account the material relations (1.38)-(1.40) and inserting the second curl MGE (1.49) into the first curl MGE (1.48), one can derive the discrete wave equation for the electric field in the frequency domain

$$\left( \tilde{\mathbf{C}}\mathbf{M}_{\mu^{-1}}\mathbf{C} - \omega^2\mathbf{M}_{\epsilon} \right) \hat{\mathbf{e}} = -i\omega\hat{\mathbf{j}}, \quad (1.52)$$

The above equation is also called curl-curl equation, due to the double application of the curl operator. In the special case of no excitation, i.e.  $\hat{\mathbf{j}} = 0$ , the curl-curl equation is equivalent to the eigenvalue equation of the system whose eigenvalues represent the resonance frequencies of the system, whereas the eigenvectors are corresponding electric field solutions (eigenmodes)

$$\left( \mathbf{M}_{\epsilon}^{-1}\tilde{\mathbf{C}}\mathbf{M}_{\mu^{-1}}\mathbf{C}\hat{\mathbf{e}} \right) = \omega^2\hat{\mathbf{e}}. \quad (1.53)$$

#### 1.4.4 Boundary Conditions

The numerical solution of MGE requires a finite computational domain. To limit the numerical space, proper boundary conditions are needed [31, 32, 33].

The electric and magnetic boundary conditions correspond to enclosing the computational domain with a perfect electric conductor or a perfect magnetic conductor, respectively. At electrically conducting walls the tangential components of  $\mathbf{E}$  and the normal components of  $\mathbf{B}$  vanish. The FIT implementation of the electric boundary condition relies on setting the columns and rows of the curl matrix  $\mathbf{C}$ , corresponding to tangential  $\hat{\mathbf{e}}$  and normal  $\hat{\mathbf{b}}$  at the boundary, to zero values. On the other hand, at magnetically conducting walls the tangential components of  $\hat{\mathbf{h}}$  and normal components of  $\hat{\mathbf{d}}$  vanish. The FIT implementation is based on the integration of Ampere's law over half of the tangentially oriented boundary facet, where the  $\hat{\mathbf{h}}$  tangential to the boundary is assumed to be zero. An alternative approach takes advantage of the integration over virtually extended dual grid boundary cells and the symmetry condition for tangential  $\hat{\mathbf{h}}$  at magnetic boundary.

The periodic boundary condition (PBC) connects two opposite boundaries with a defined phase shift and the calculation domain is simulated as periodically expanded in the given direction. In FIT, the boundary field components located on one side of the computational domain are replaced by the components located on the opposite side of the domain and multiplied by a complex phase factor  $e^{i\varphi}$  corresponding to the periodic direction of the structure.

The open boundary condition is based on a perfectly matched layer (PML) that absorbs electromagnetic (EM) waves traveling towards boundaries [34]. The

absorbing layers are characterized by electric and (virtual) magnetic conductivities, gradually increasing from zero at the interior interface to certain values at the outer side of the PML. The conductivities represent loss parameters and control the wave attenuation rate in the PML, according to a chosen profile. In order to minimize reflections, several layers are commonly used.

The waveguide port boundary condition is based on a quasi-infinite, homogeneous waveguide connected to the boundary of the structure. The ports are typically used to feed the structure with power and to absorb the returning power. The exchange of the EM energy between the structure and the outside space takes place through a discrete number of the orthonormal waveguide modes, obtained from the solution of a two-dimensional eigenvalue problem at the plane of the port. The modes are chosen according to their significant contribution to the field distribution in the waveguide. When a particular mode is not considered by the boundary operator, it undergoes total reflection from the boundary. This undesirable effect can be avoided, when an absorbing boundary operator is applied to the field distribution that remains after subtraction of all considered modes. Waveguide ports are commonly used for the simulation of scattering parameters.

## 1.5 General Electromagnetic Properties of Materials

Figure 1.7 qualitatively shows a typical behavior of the dielectric permittivity  $\varepsilon = \varepsilon' - i\varepsilon''$  as a function of frequency. The permittivity of a material is related to a variety of physical phenomena. Ionic conduction, dipolar relaxation, atomic polarization and electronic polarization are the main mechanisms that contribute to the permittivity of a dielectric material. In the low frequency range,  $\varepsilon''$  is dominated by the influence of ion conductivity. The variation of permittivity in the microwave range is caused mainly by dipolar relaxation, and the absorption peaks in the infrared region and beyond is due mainly to atomic and electronic polarizations.

Electronic and atomic polarization are similar; electronic polarization occurs in neutral atoms when an electric field displaces the nucleus with respect to the surrounding electrons and atomic polarization occurs when adjacent positive and negative ions stretch under an applied electric field. Actually, electronic and atomic polarizations are of similar nature. Figure 1.8 shows the Lorentzian type behavior of permittivity in the vicinity of the resonant frequency  $\omega_0$ . In the figure,  $A$  is the contribution of higher resonance to  $\varepsilon'$  at the present frequency range, and  $2B/\omega_0$  is the contribution of the present resonance to lower frequencies. For many dry

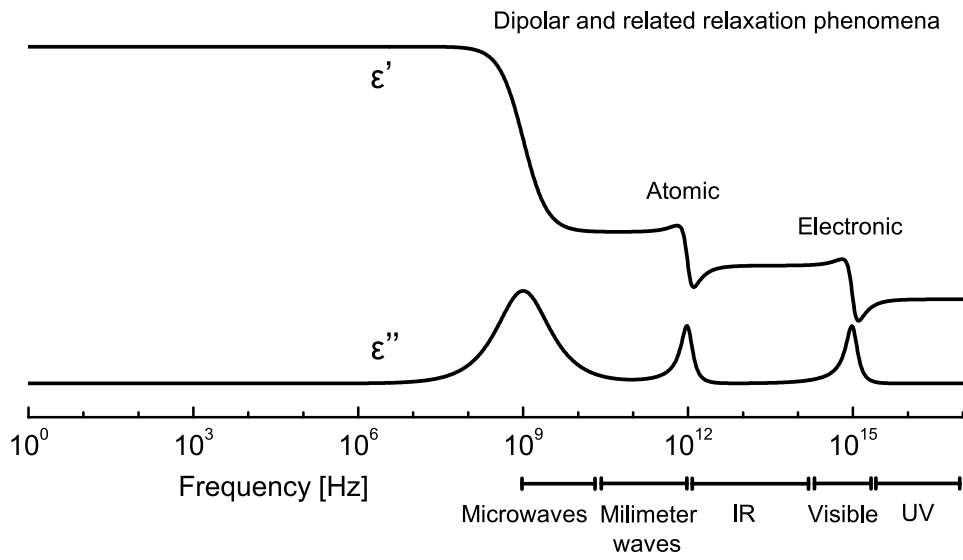


Figure 1.7: Dipolar relaxation, atomic polarization and electronic polarization are the main mechanisms that contribute to the permittivity of a dielectric material.

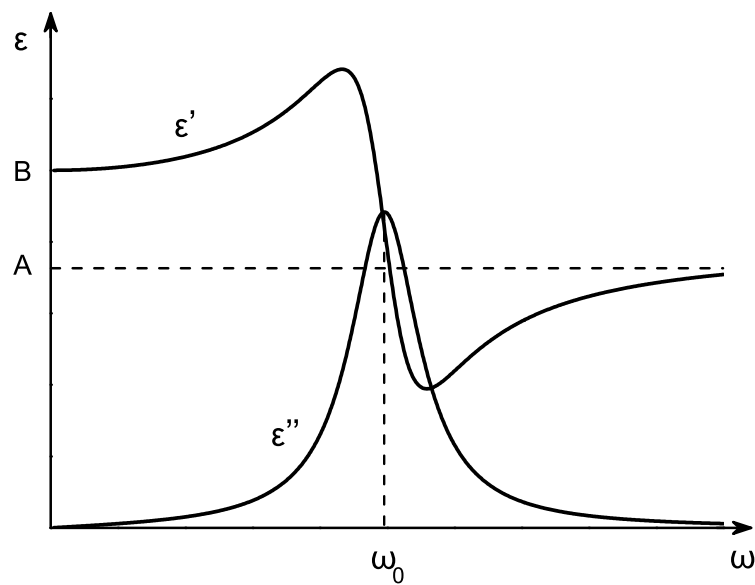


Figure 1.8: Lorentz distribution

solids these are dominant polarization mechanisms determining the permittivity at microwave frequencies, although the actual resonance occurs at a much higher frequency. If only these two polarizations are present the material are almost lossless at microwave frequencies. When an external electric field is applied to neutral atoms, the electron cloud of the atoms will be distorted, resulting in the electronic polarization. In a classical model, it is similar to a spring-mass resonant system. Owing to the small mass of the electron cloud, the resonant frequency of electronic polarization is at the infrared region or the visible light region. Usually, there are several different resonant frequencies corresponding to different electron orbits and other quantum-mechanical effects. For a material with  $s$  different oscillators, its permittivity is given by

$$\varepsilon = \sum_s \frac{(n_s e^2)/(m_s)}{\omega_s^2 - \omega^2 + i\omega^2 \alpha_s}, \quad (1.54)$$

where  $n_s$  is the number of electrons per volume with resonant frequency  $\omega_s$ ,  $e$  is the charge of electron,  $m_s$  is the effective mass of electron,  $\omega$  is the frequency, and  $\alpha_s$  is the damping factor. As microwave frequencies are far below the lowest resonant frequency of electronic polarization, the permittivity due to electronic polarization is almost independent of the frequency and temperature.

In spite of their different origins, various types of resonance at microwave and millimeter wave ranges can be described in a similar qualitative way. In most cases, the Debye equations can be applied, although they were first derived for a special case of dipolar relaxation. According to Debye theory, the complex permittivity of a dielectric can be expressed as

$$\varepsilon = \varepsilon_\infty + \frac{\varepsilon_0 - \varepsilon_\infty}{1 + i\gamma}, \quad (1.55)$$

with

$$\varepsilon_\infty = \lim_{\omega \rightarrow \infty} \varepsilon, \quad (1.56)$$

$$\varepsilon_0 = \lim_{\omega \rightarrow 0} \varepsilon, \quad (1.57)$$

$$\gamma = \omega\tau \frac{\varepsilon_0 + 2}{\varepsilon_\infty + 2}, \quad (1.58)$$

where  $\tau$  is the relaxation time and  $\omega$  is the frequency. Equation 1.55 indicates that the dielectric permittivity due to Debye relaxation is determined mainly by three parameters  $\varepsilon_\infty$ ,  $\varepsilon_0$  and  $\tau$ . At sufficiently high frequencies, as the period of the electric field  $\mathbf{E}$  is much smaller than the relaxation time of the permanent dipoles,



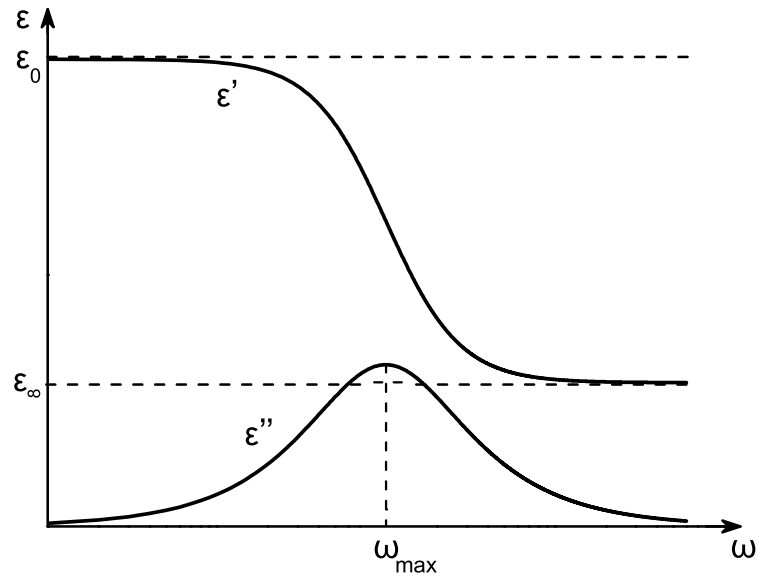


Figure 1.9: Debye distribution

the orientations of the dipoles are not influenced by electric field  $\mathbf{E}$  and remain random, so the permittivity at the infinite frequency  $\epsilon_\infty$  is a real number. As  $\epsilon_\infty$  is mainly due to electronic and atomic polarization, it is independent of the temperature. As at sufficiently low frequencies there is no phase difference between the polarization  $\mathbf{P}$  and electric field  $\mathbf{E}$ ,  $\epsilon_0$  is a real number. However, the static permittivity  $\epsilon_0$  decreases with increasing temperature because of the increasing disorder, and the relaxation time  $\tau$  is inversely proportional to the temperature as the collision rate increases at higher temperatures.



# Chapter 2

## Extraction of Effective Properties

### 2.1 Techniques for Material Characterization

The topic of microwave measurement techniques is a vastly studied subject and is still in development. For a few decades microwaves have been used to characterize materials, dozens of microwave material characterization methods exist. Extensive review papers compare and describe microwave measurement techniques, discussing their applicability for the measurement of specific material properties. Coaxial line reflection methods for measuring dielectric properties of biological materials at radio and microwave frequencies are reviewed in where methods are compared from the point of view of their relative uncertainties of measurement of lossy substances with high dielectric constant. Advantages and limitations of different methods and some practical recommendations are presented by Stuchly in [35]. Afsar *et al.* [36] summarize nearly 75 years of development in the techniques used to measure dielectric properties of materials over the frequency range 1 MHz to 1500 GHz. An introductory section summarizes the broad development trends and is followed by short sections which deal with developments at a more detailed level. The approaches described include time and frequency domain methods and reflection, transmission, and resonant methods. In [37], microwave measurements methods for characterization of polar liquids are extensively discussed. The requirements for dielectric measurements on polar liquids lie largely in two areas. First, there is scientific interest in revealing the structure of and interactions between the molecules. Second, polar liquids are widely used as dielectric reference and tissue equivalent materials for biomedical studies and for mobile telecommunications, health and safety related measurements. The review article by Sheen [38], provides a general comparison of the two most commonly used techniques for measurement of complex permittivity at microwave

frequencies: transmission/reflection and resonance. The transmission/reflection techniques are analyzed using distributed and lumped impedance models. The resonance techniques are analyzed using both dielectric and cavity resonance models. The analysis, combined with experimental results, enables us to illustrate the advantages and disadvantages of the various techniques and provide guidance on which techniques to use under particular circumstances.

The microwave methods for material characterization basically fall into two main groups, resonant methods and non-resonant methods. While resonant methods are effective to obtain magnetic and electric properties of a material at single frequency, non-resonant methods are usually broadband. The limitation of the resonant methods to single or very small frequency range, comes from the method itself. The resonant methods depend on an enclosure, where sample material is introduced. The resonance frequency depends on the size and shape of the resonance chamber, where discrete electromagnetic eigenmodes can be excited at the eigenfrequencies of the chamber.

The non-resonant methods are based on the fact that when an electromagnetic wave is propagating from one material to another reflection occurs at the interface between the two materials. For example when a wave propagates from vacuum to a material with different electric permittivity or magnetic permeability, part of the wave is reflected and the rest of the wave is transmitted through the material. The material properties can be deduced from the transmission/reflection characteristics. The amount of the reflected and transmitted wave depends on the relationship of the electric and magnetic properties of the two materials, more precisely on the impedance and the propagation constant.

Non-resonant methods can be divided into two types, reflection methods and transmission/reflection methods. In the reflection methods material properties are calculated from reflection characteristics of the sample, and in the transmission/reflection methods, both transmission through the sample and reflection from the interface are taken into account when calculating material properties. All non-resonant methods have in common the necessity to deliver electromagnetic energy to a sample, by means of transmission line. Both, experimental and numerical measurement data processing have been developed for different kinds of transmission lines such as, hollow-metallic and dielectric waveguides; coaxial-, strip-, and coplanar lines; as well as free space. Applications of these methods differ in the employable material range it can be applied to, extraction of effective properties algorithms and frequency ranges.

This chapter will focus on numerical adaptation of the free space method. This

method is usually experimentally realized by placing a sample material between two horn lens antennas, which are connected to a network analyzer. Availability of precision horn lens antennas has played an important role in making the free space method widely used. The free space method is non-destructive, contact-less and can be employed for a wide frequency range. In contrast to other measurement methods, the sample can have arbitrary shape and size. There are no restrictions, like for the example using metallic waveguides, where the sample must be machined so that it can fit inside the waveguide.

## 2.2 Transmission/Reflection Free Space Method

There are several methods for the extraction of effective material parameters for inhomogeneous mixtures. The most popular approach is the extraction from transmission and reflection characteristics of a sample. The method is based on free-space measurements of the complex permittivity and complex permeability popularized by Ghodgaonkar *et al.* [39], for measurements of dielectric properties of planar slabs of ceramic and composite materials in the frequency range of 14.5 to 17.5 GHz. The key components of the measurement system are a pair of spot-focusing horn lens antennas, a network analyzer, and a computer. Because of the far-field focusing ability of horn lens antennas, the free-space measurements can be made at microwave frequencies in a relatively compact and simple measurement setup [40].

The free space method has been chosen because it can be easily converted into a numerical problem, thus simulations and processing of results are straight forward. Secondly the free space method has been successfully employed in many cases and a vast number of publications on this topic exists. As one of the first, Varadan *et al.* [41], describes a free-space microwave measurements system used for the high-temperature measurement of dielectric constants and loss tangents of homogeneous materials and composite materials as well. Dielectric constants and loss tangents for fused quartz and boron nitride were calculated from the measured values of  $S_{21}$  in the 5.85 to 40 GHz frequency range, and in room to 850 °C temperature range, by using a high temperature furnace. Another interesting application can be found in [42], where a new method for simultaneous and independent determination of bulk density and moisture content in particulate materials by measurements of the relative complex permittivity is presented. The bulk density is determined, based on a representation in the complex plane of relative complex permittivity normalized to bulk density. In a work by Trablesi and Nelson [43], a system,

including a vector network analyser, horn/lens antennas, holder for grain and oilseed samples and a radiation absorbing enclosure was used for measurements and procedures to obtain reliable permittivity data for wheat, shelled corn and soybeans. Microwave attenuation and phase shift per unit sample thickness, each divided by the bulk density of the granular materials, and frequency and moisture content were calculated. The resulting permittivity components, dielectric constant and loss factor for wheat, corn and soybeans were obtained for reference at frequencies from 5 to 17 GHz at different densities and moisture levels.

The same theory underlies in the extraction of effective properties from simulation data and is used with great success to describe metamaterials and photonic crystals as homogeneous medium [44, 45, 46, 47, 48, 49, 50, 51, 52]. Metamaterials consist of a lattice of conducting, nonmagnetic elements that can be described by an effective magnetic permeability and an effective dielectric permittivity, both of which can exhibit values not found in naturally occurring materials, because the electromagnetic fields in conducting metamaterials can be localized to regions much smaller than the incident wavelength. Photonic crystals, on the other hand, are composed of periodic dielectric or metal-dielectric nanostructures that affect the propagation of electromagnetic waves in the same way as the periodic potential in a semiconductor crystal affects the electron motion by defining allowed and forbidden electronic energy bands. Essentially, photonic crystals are man made but also occurring in nature, nanostructures containing regularly repeating internal regions of high and low dielectric constant.

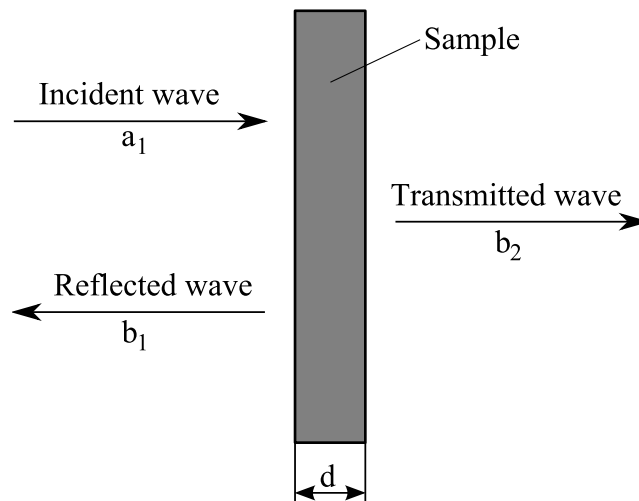


Figure 2.1: Schematic diagram of a slab, placed in free space, exposed to a linearly polarized plane wave normally incident on the sample.

Figure 2.1 shows a slab of a material of thickness  $d$  placed in free space. The

slab is irradiated with a plane wave incident normally on the slab. Such a setup with microwave ports on the left and right side, with a sample in between, can be considered as a two-port microwave network. The field amplitudes of the input and output waves at port 1 can be written as  $a_1$  and  $b_1$ , respectively, and those of input and output waves at port 2 as  $a_2$  and  $b_2$ , respectively. These parameters are either the complex field amplitudes of the electric field  $\mathbf{E}$  or the magnetic field  $\mathbf{H}$ .

The concept of a microwave network is developed from the transmission line theory, and is a powerful method in microwave engineering [53]. The microwave network method studies the responses of a given structure to external signals, and is complementary to the electromagnetic field theory that analyzes the field distribution inside the studied structures like waveguides, microstrips, etc. In the microwave network approach it is not necessary to know the distribution of electromagnetic fields inside the structure, the theory only describes how the structure reacts to external signals. Two sets of parameters are often used in network analysis. One set of parameters are voltage  $V$  and current  $I$ . The other set of parameters are complex valued amplitudes of the input wave  $a$  and the output wave  $b$ . Different network parameters are used for different sets of physical values. For example, impedance  $\mathbf{Z}$  and admittance  $\mathbf{Y}$  matrices are used to describe the relationship between voltage and current, while scattering  $\mathbf{S}$  and transmission  $\mathbf{T}$  matrices are used to describe the relationship between the input and output electromagnetic wave amplitudes.

The S-parameters are collected in the scattering matrix  $\mathbf{S}$ . S-parameters are used to describe the relationship between input waves  $\mathbf{a} = [a_1 \ a_2]^T$  and output waves  $\mathbf{b} = [b_1 \ b_2]^T$ . In case of a two-port network the output can be calculated in the following manner  $\mathbf{b} = \mathbf{S} \mathbf{a}$

$$\begin{bmatrix} b_1 \\ b_2 \end{bmatrix} = \begin{bmatrix} S_{11} & S_{12} \\ S_{21} & S_{22} \end{bmatrix} \begin{bmatrix} a_1 \\ a_2 \end{bmatrix}, \quad (2.1)$$

where  $S_{ij}$  are the S-parameters with indices denoting  $i$  the destination port and  $j$  the source port. Since in our case the structure is symmetric and the plane wave is excited only at port 1, only the two S-parameters  $S_{11}$  and  $S_{21}$  expressing the reflection and transmission characteristics, respectively are nonzero [53].

The S-parameters  $S_{11}$  and  $S_{21}$  for a given frequency  $f$  are related to the reflection  $R$  and transmission  $T$  coefficients, respectively [40]

$$S_{11} = \frac{R(1 - T^2)}{1 - R^2T^2} \quad (2.2)$$

$$S_{21} = \frac{T(1 - R^2)}{1 - R^2T^2}. \quad (2.3)$$

The reflection coefficient  $R$  at the boundary between free space and the slab can be expressed as

$$R = \frac{Z - 1}{Z + 1}. \quad (2.4)$$

The transmission coefficient  $T$  through a homogeneous slab is

$$T = e^{-\gamma d}. \quad (2.5)$$

In (2.4) and (2.5),  $Z$  and  $\gamma$  are the characteristic impedance and the propagation constant of the slab, respectively. The characteristic complex impedance  $Z$  and the complex propagation constant  $\gamma = \alpha + i\beta$ , where  $\alpha$  is the attenuation constant and  $\beta$  the phase constant, are related to the complex electric permittivity  $\varepsilon = \varepsilon' - i\varepsilon''$  and to the complex magnetic permeability  $\mu = \mu' - i\mu''$

$$\gamma = \gamma_0 \sqrt{\mu\varepsilon} \quad (2.6)$$

$$Z = \sqrt{\frac{\mu}{\varepsilon}}, \quad (2.7)$$

where  $\gamma_0 = i2\pi/\lambda_0$  is the propagation constant of free space, and  $\lambda_0$  the wavelength in free space. Rearranging (2.2) and (2.3) one obtains

$$R = K \pm \sqrt{K^2 - 1} \quad (2.8)$$

$$T = \frac{S_{11} + S_{21} - R}{1 - (S_{11} + S_{21})R}, \quad (2.9)$$

where

$$K = \frac{S_{11}^2 - S_{21}^2 + 1}{2S_{11}}. \quad (2.10)$$

In (2.8) the  $\pm$  sign is chosen such that it satisfies the requirement for a passive medium, i.e. the magnitude of the normalized reflection must not exceed one

$$|R| \leq 1. \quad (2.11)$$

Rearranging (2.4) and inserting (2.7) yields

$$\sqrt{\frac{\mu}{\varepsilon}} = \frac{1 + R}{1 - R}. \quad (2.12)$$



From (2.6) and (2.12) one obtains

$$\varepsilon = \frac{\gamma}{\gamma_0} \left( \frac{1-R}{1+R} \right) \quad (2.13)$$

$$\mu = \frac{\gamma}{\gamma_0} \left( \frac{1+R}{1-R} \right). \quad (2.14)$$

By inverting (2.5), the propagation constant can be written as

$$\gamma = \frac{\ln\left(\frac{1}{T}\right)}{d}. \quad (2.15)$$

The transmission parameter  $T$  is a complex number, giving multiple values for  $\gamma$ . One can define  $T$  as

$$T = |T| e^{i\phi}. \quad (2.16)$$

Then  $\gamma$  can be expressed as

$$\gamma = \frac{\left[ \ln\left(\frac{1}{|T|}\right) \right]}{d} + i \left( \frac{2\pi m - \phi}{d} \right), \quad (2.17)$$

where  $m = 0, 1, 2, \dots$  is an integer. By inserting the value for  $\gamma$  into (2.13) and (2.14) one obtains the effective complex permittivity  $\varepsilon$  and complex permeability  $\mu$  of the slab. The real part of  $\gamma$  is unique and single valued, contrary to the imaginary part of  $\gamma$  which can have multiple values. The major difficulty is the uncertainty in the change of phase of the transmitted field. In thick sample slabs or in highly dispersive materials the transmission phase advance can exceed  $2\pi m$ . This leads to an ambiguous result, with multiple branches of the frequency dependent complex functions for  $\varepsilon(f)$  and  $\mu(f)$ . When  $d$  is large enough, these branches can lie arbitrarily close to each another, making the selection of the correct branch difficult in the case of dispersive materials. For a plane wave the phase constant  $\beta$  is defined as

$$\beta = \frac{2\pi}{\lambda}, \quad (2.18)$$

where  $\lambda$  is the wavelength in the slab material. By comparing the expression for the phase constant  $\beta$  (2.18) and the imaginary part of the propagation constant  $\Im(\gamma)$  (2.17) one can obtain

$$\frac{d}{\lambda} = m - \frac{\phi}{2\pi}. \quad (2.19)$$

For  $m = 0$  and  $-2\pi < \phi < 0$ ,  $d/\lambda$  is between 0 and 1. If the slab thickness  $d$  is chosen such that it fulfills  $d < \lambda$ , then (2.13) and (2.14) will provide unique values

for  $\varepsilon(f)$  and  $\mu(f)$ , each.

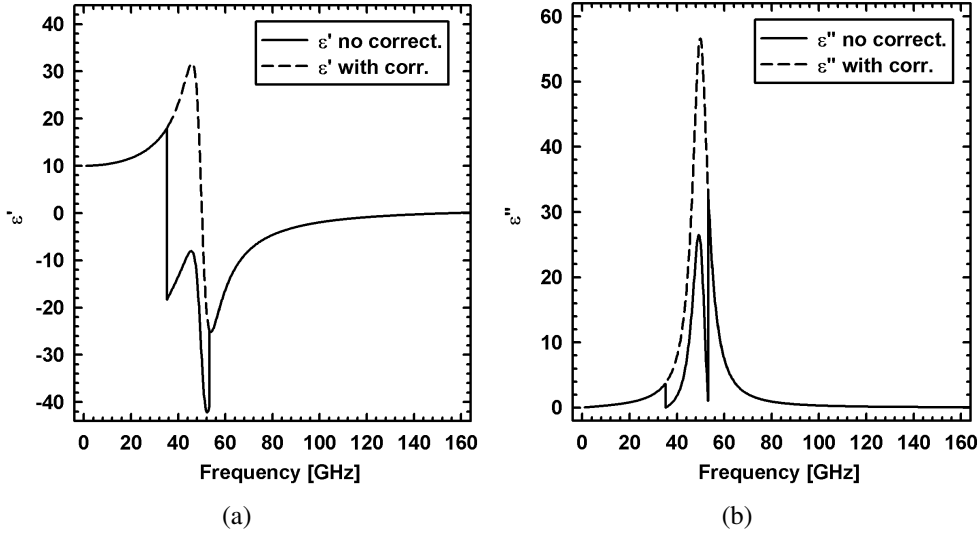


Figure 2.2: Example of a  $m$ -branch correction for the 2.2(a) real and 2.2(b) imaginary part of the dielectric permittivity. The non-corrected curve (solid line) is a result for  $m = 0$  in the whole frequency range, while the corrected curve (dashed line) is a result for  $m = 1$  modification in frequency range from 35.2 to 53.3 GHz.

As shown in figure 2.2 for an exemplary dielectric function, following the Lorentz distribution with the static permittivity  $\varepsilon_s = 10$ , the permittivity at infinity  $\varepsilon_\infty = 1$ , the resonance frequency  $f_0 = 50$  GHz and the damping frequency  $f_d = 50$  GHz, for a slab of thickness  $d = 1$  mm, the  $m$ -branch selection must be performed to obtain correct results. The procedure presented here can be done manually from within the extraction script described in (Appendix 4). The points at which the adjustment of the  $m$ -branch selection must be set, can be noticed by identifying sharp points of inflection in the real or imaginary part of the dielectric function, as can be seen in figure 2.2. After choosing the appropriate value for  $m$ , (2.17) must be recalculated, as well as, (2.13) and (2.14) to obtain correct values of the magnetic permeability and the dielectric permittivity. For the example shown in figure 2.2 the region between 35.2 and 53.3 GHz was recalculated with  $m = 1$ , and for the rest of the frequency range  $m = 0$  was set. In figure 2.3 the ratio of the slab thickness  $d$  to wavelength  $\lambda$  is shown, calculated according to

$$\lambda = \frac{c_0}{fn'}, \quad (2.20)$$

where  $n'$  is the real part of the refractive index  $n = \sqrt{\mu\varepsilon}$ . For the frequency region from 35.2 to 53.3 GHz the  $d/\lambda$  ratio is above 0.5, which is enough to trigger the

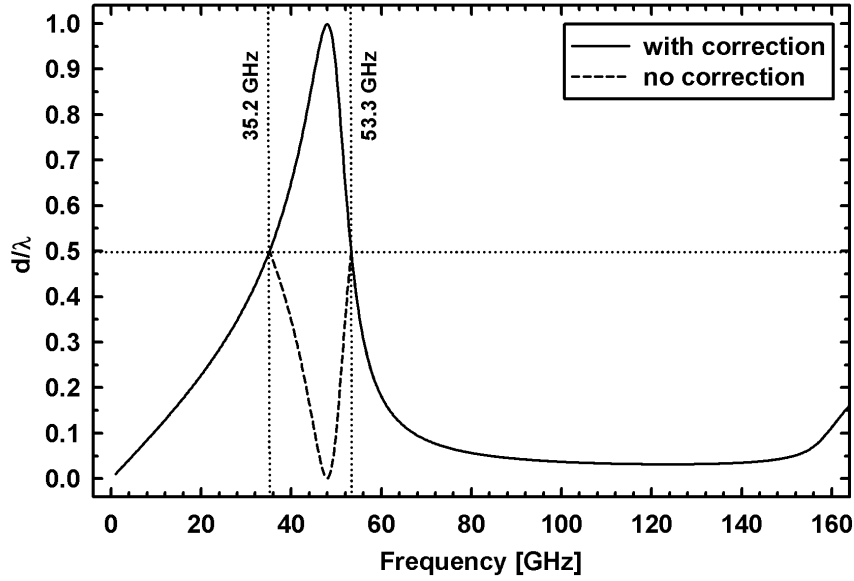


Figure 2.3: The  $d/\lambda$  ratio as a function of frequency for the example permittivity and permeability shown in figure 2.2. The non-corrected curve (dashed line) can be used as an indicator, to where the regions for different  $m$ -branches are located. After readjusting calculations, one obtains the corrected curve (solid line) for the  $d/\lambda$  ratio.

change in the  $m$ -branch and the solution for  $\varepsilon$  and  $\mu$ . The  $d/\lambda$  ratio can also be used to identify the  $m$ -branches and quickly re-adjust the calculations.

In 2007, it was proposed by Varadan and Ro [54] to employ the Kramers-Kronig relations in order to obtain a unique solution from the S-parameters results. The attenuation factor  $\alpha$  can be uniquely retrieved from measurement or simulation data by the requirement that the real part of the impedance cannot be negative. The constraints between the real and imaginary parts of the propagation constant, are contained in the Kramers-Kronig relations and employed to remove the ambiguity in finding. Measurement results have shown the efficacy of this approach in determining the effective properties of low-loss material and dispersive media described by a Lorentz or Drude model. The phase unwrapping process is automatically implemented in the Kramers-Kronig approach [54]. The method based on the Kramers-Kronig relations has been successfully employed for various dispersive materials and metamaterials [55, 56, 57, 58]. While the method is self-consistent, it was not used in this work, since it is more computationally expensive. Instead, the selection of the  $m$ -branch was done by a procedure using a simple peak detection of the first derivative of the imaginary part of the propagation constant

$$\frac{\partial}{\partial f} \Im(\gamma) d = \frac{\partial}{\partial f} \beta d. \quad (2.21)$$

The function  $\beta d$  can take values between  $-\pi$  and  $\pi$  only, thus sharp peaks can be detected at break points using first derivative with respect to frequency. After the detection of breaking points,  $\beta d$  is corrected iteratively in the intermediate intervals between the breaking points. This procedure has been found to be extremely fast and efficient to work with those materials presented in this work.

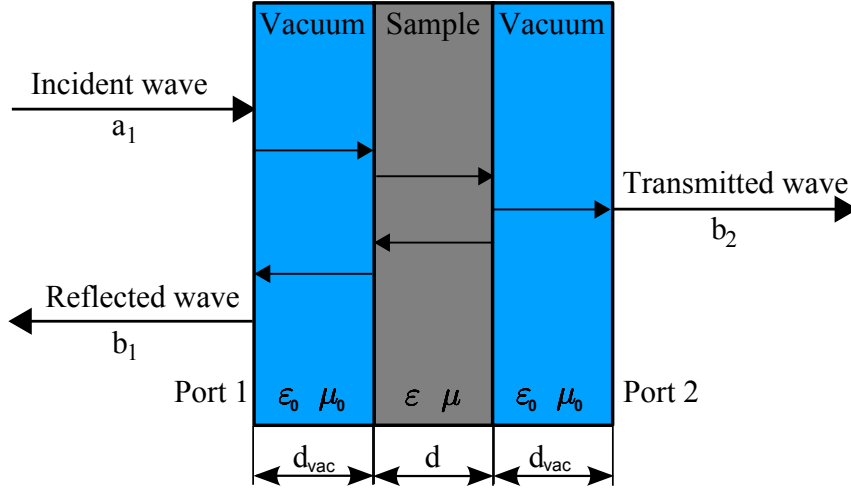


Figure 2.4: Schematic diagram of a slab with additional vacuum before in front and behind. The microwave ports are defined on vacuum rather than directly on the medium. To obtain viable results for such a system a phase correction must be applied, to take into account the phase shift due to the additional space  $d_{vac}$ .

In most cases it is necessary to add additional free space in front and behind the modeled domain as shown in figure 2.4. This is due to the fact that the port impedance is automatically set in CST MWS, to match the wave impedance of the material it is directly neighboring with. The wave impedance of the plane wave is defined as

$$Z_p = \sqrt{\frac{\mu\mu_0}{\varepsilon\varepsilon_0}}, \quad (2.22)$$

for a nonconducting medium; thus the resulting impedance is different for vacuum and the simulated material. If the ports are defined directly on the slab, the simulation will provide only  $S_{21}$ , while  $S_{11}$  would be vanishingly small over the whole frequency range. For a successful recovery of the complex magnetic and electric properties of the material, both parameters,  $S_{11}$  and  $S_{21}$  must be present. Defining additional free space in front and behind the slab ensures that the proper reflection/transmission characteristics will be obtained from the simulation. If additional free space is defined on both sides of the slab, one must also apply a phase correction to  $\angle S_{11}$  and  $\angle S_{21}$ . For the additional free space with thickness

$d_{vac}$ , in front and behind the slab, the phase shift  $\phi$  can be expressed by

$$\phi = 2d_{vac} \frac{2\pi f}{c_0}. \quad (2.23)$$

## 2.3 Limitations of the Extraction Method

The scheme presented above for the simulation and extraction of effective material parameters is affected by limitations, typical for every simulation method. Errors may occur due to disagreement between model and reality, as well as imprecisions in the simulation itself. In every discretization method the geometric details may not be represented accurately or may be even neglected. This can happen especially when the simulation model contains elements with small dimensions compared to the other elements or to the dimensions of the model. In most simulations the small elements of the model can not be neglected, which leads in most cases to a high number of mesh cells, thus to longer computation times.

Material properties are another essential aspect that may lead to simulation errors. Material properties like the magnetic permeability, the dielectric permittivity or the conductivity are usually not known for a broad frequency range. CST MWS, as well as most of the simulation and modeling software uses extrapolation of material properties to fill the gaps in the frequency range used for simulation. One must be very careful choosing the extrapolation method so that it will not give false results.

A crucial aspect of finite element modeling (FEM) and FIT simulations is the discretization of the simulated domain. The number of mesh cells is often the most significant limitation. On one hand, a very fine discretization is desired, to obtain results as close to reality as possible; on the other hand, one is always limited by the computational power. A large number of mesh cells requires lots of processing time; thus, a compromise is necessary between accuracy of the simulation and practical computing times. Most important in electromagnetic and wave propagation simulations is the adjustment of the size of the mesh according to the wavelength  $\lambda$  of the propagating wave. The default setting in CST MWS, is four mesh cells per  $\lambda$  for the frequency solver, using tetrahedral mesh, and ten mesh cells per  $\lambda$  for the time domain solver, using hexahedral mesh. The wavelength  $\lambda$  inside the material depends on its dielectric and magnetic properties as given in 2.20. Thus, modeling a system with large dimensions compared to  $\lambda$  inside the material leads to a mesh with a huge number of mesh cells.

Limitations in mesh generation may also be caused by specific physical

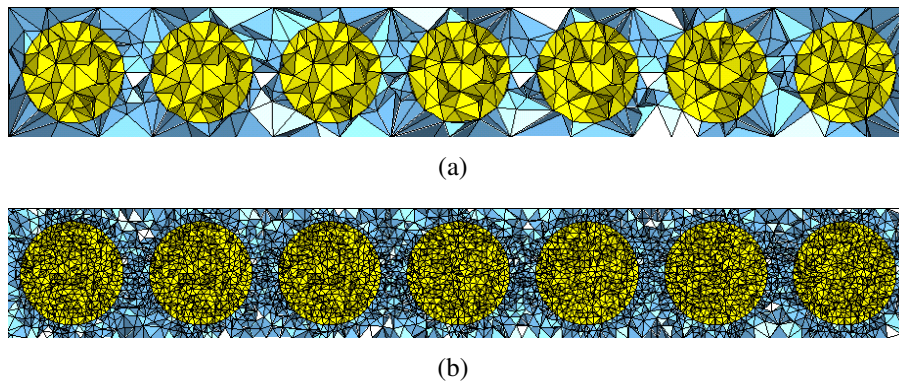


Figure 2.5: An example structure of seven copper particles. The mesh size in the first case 2.5(a) has been altered 2.5(b), through convergence study, to achieve a more realistic model. The very fine mesh is necessary in order to resolve eddy currents and to obtain correct results for the magnetic permeability as shown in figure 2.6.

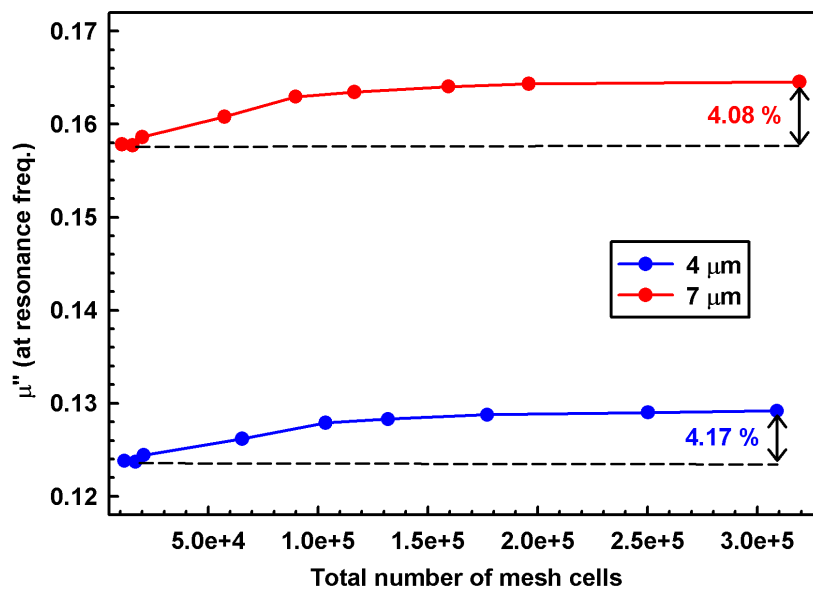


Figure 2.6: Dependence of the imaginary part of the permeability on the mesh size. An insufficient number of mesh cells does not resolve the eddy currents properly, which leads to a lower value of  $\mu''$  at the resonance frequency.

phenomena occurring in the modeled media. An example of this is eddy currents induced by high frequency alternating magnetic fields. Figure 2.6 shows the difference in the computed imaginary part of the magnetic permeability  $\mu''$  at the resonance frequency, for different mesh sizes. The computations were performed for models with copper particles. The sizes of the particles are 4  $\mu\text{m}$  and 7  $\mu\text{m}$  and the simulated unit cell contains seven particles in the direction of propagation of the plane wave, with periodic boundary conditions in the directions perpendicular to the propagation direction. The high number of mesh cells, shown in figure 2.5, is necessary in order to resolve eddy currents induced by the oscillating magnetic field. While they are non-magnetic under normal circumstances, the copper particles display diamagnetic properties under the influence of an alternating magnetic field. This problem is discussed in detail in Chapter 3. A convergence study with respect to  $\mu''$  as function of mesh resolution ensures good results.

As most of the simulations presented in this work were performed using the frequency domain solver in CST MWS, one more important issue should be discussed. Contrary to the time domain solver, where results in the frequency domain are obtained performing a Fourier transform on time domain results, the frequency domain results must be computed by the frequency domain solver one frequency at a time. Subsequently the results are interpolated to a representation with a desired number of frequency samples. That means that the number of actually computed frequency samples is always smaller than the representation of the results, which usually have a very high number of frequency samples. The quality of the representation of the computed results are subject to an interpolation error. The interpolation error can be monitored in CST MWS. Studying the convergence of the interpolation error in the S-parameters gives information on the maximal interpolation error for the computed frequency samples. In simulations presented in this work the interpolation error was kept under  $10^{-6}$  to ensure valid results.

Figure 2.7 shows typical results from a simulation where the interpolation error was too high: the solid lines represent the exemplary real and imaginary parts of the permittivity calculated using 200 frequency samples, keeping the maximum interpolation error around  $10^{-6}$ , which is in very good agreement with the correct permittivity function. In comparison, the dashed line shows the result of a simulation where only 33 frequency samples were calculated, and the maximum interpolation error is roughly  $10^{-3}$ .

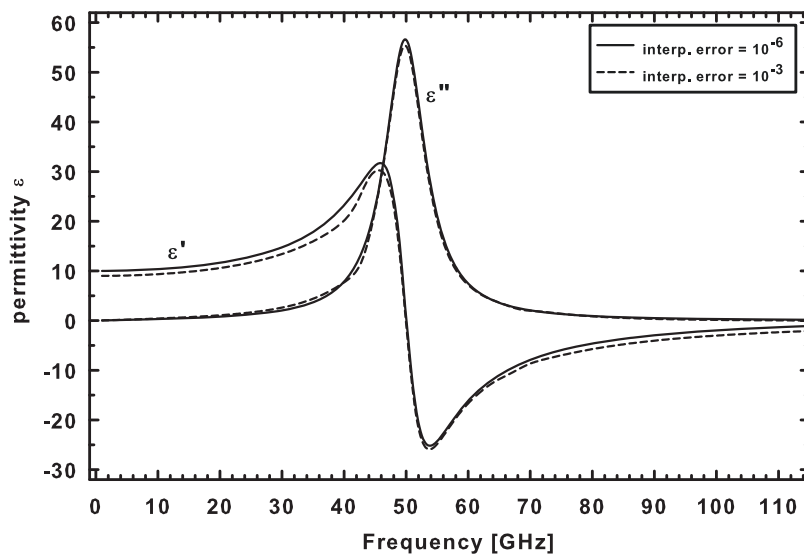


Figure 2.7: Comparison of the real and imaginary part of the permittivity, from simulations with interpolation error  $10^{-6}$  (solid lines), achieved with 200 frequency samples, and with interpolation error  $10^{-3}$  (dashed lines), being the result of using only 33 frequency samples. To ensure that the results are correct one must compute a sufficiently high number of frequency samples to keep the interpolation error under a value  $10^{-6}$ .



# Chapter 3

## Metallic Powders

### 3.1 Microwave Sintering of Metallic Powders

Microwave sintering of ceramic powders is a well established method in science and industry since few decades [59]. Microwave heating, in contrast to conventional heating, allows for volumetric heating of materials, which leads to time savings and reduced energy consumption. Additionally, high heating rates in metal carbide based materials used as microwave susceptors offer a combination of microwave and conventional heating to boost the processing of less absorbing materials like most of oxides and nitrides. Rapid and controllable heating and the use of fine powders lead to a smaller grain size and a more uniform grain size distribution which improves the mechanical properties of the sintered material. Much attention is given to the advantages of higher frequency millimetre wave processing, which include the enhanced absorption in many materials of industrial interest, improved distribution uniformity of temperature and electromagnetic energy density, and the possibility of surface treatment. Another interesting phenomenon is the microwave process rate enhancement, as well as the problem of the non-thermal microwave effect on mass transport in solids. Many researchers have observed an enhancement of the densification during microwave solid-phase sintering of ceramics. The densification rate at each temperature was demonstrated to be sensitive to the microwave power applied. The main advantages of microwave heating stem from direct energy deposition in the volume of a material. This eliminates the need for spending energy on heating the walls of the furnace or reactor, its massive components, and heat carriers. As a result, the use of microwave methods significantly reduces energy consumption, especially in high-temperature processes, since heat losses grow dramatically with an increase in the process temperature. The volumetric nature of energy deposition accelerates heating, which

reduces the time needed to complete a process. An idea of the energy-saving potential of microwave processing can be inferred from the results of a number of comparative studies in sintering. High rates of heating do not only lead to reductions in process time and energy consumption, many high-temperature processes include a sequence of various steps which replace each other with the rise of temperature. Such sequences occur in multistage thermally activated processes, in which separate stages are characterized by different values of the activation energy. Some of these stages may have a negative influence on the properties of the final product. In such cases rapid heating may be vital for reducing the role of undesired intermediate stages of the process. An example of such a multistage process is the sintering of ceramics. At different steps of sintering the diffusion processes of various natures, surface, grain boundary, and bulk diffusion, determine the mass transport [60].

Application of microwave energy for materials processing is emerging as a novel and innovative technology with many advantages over conventional processing, such as reduction in processing cycle time resulting into substantial energy and cost savings, providing finer microstructures leading to improved mechanical properties, and eco friendliness. Microwave energy is highly versatile in its application to numerous diverse fields such as communication, chemical reactions, rubber vulcanisation, drying, food processing and medical related fields. However, its application in ceramic processing and metallic materials has developed only in the last two decades. Most recent potential applications involve steel making, used tires recycling and alternative sources for energy recovery in oil shales and capped oil wells. Many specialty ceramics, composites, and metal powders have been successfully processed in microwave with improved properties. The selective heating feature of microwaves has led to effective brazing and joining of metal parts. Even bulk metals can be heated and melted in microwave field, under special circumstances, and the melt can be cast into useful products [61].

Until 1999, microwave processing of materials mostly was confined to ceramics, semimetals, inorganic and polymer materials. Now, it has been shown that all metallic materials in powder form do absorb microwaves at room temperature and can be very efficiently and effectively sintered providing better quality product. Recently microwave heating emerged as a powerful tool for processing of metallic powders. It was reported in 1999 by Roy *et al.* [62] that porous metal powder compacts heat when subjected to microwave irradiation in either electric or magnetic field despite the well known fact that microwaves do not penetrate bulk metals beyond skin depth and thus cannot heat metals in a microwave furnace. The results show that the porous metal powder compacts are materials

with both, effective dielectric and effective magnetic losses, corresponding to effective permittivity and effective permeability of the porous metal compacts. The microwave sintering of powdered metals was presented on the example Fe-Cu-C and Fe-Ni-C mixtures, heated in multimode, as well as in single mode microwave laboratory ovens. The reported microwave processing method offers finer microstructure and better properties in powdered-metal products at lower cost. The main reason why the microwave process yields better mechanical properties is that, especially in the case of powdered metals, it produces finer grain size, and the shape of the porosity is different from that generated during conventional heating. It was observed that microwave processed powdered metal samples had round edged pores, producing higher ductility and toughness. Also, compared to the conventional heating methods the microwave sintered samples have higher densities.

Since the pioneering work of Roy and coworkers on the microwave heating of metallic powders, there was a progressive effort on understanding and applications of the microwave sintering of powdered metals. In 2001 the same group responsible for the discovery of the microwave heating of metallic powders published an extensive paper about the influence of microwave sintering on microstructure of nickel and copper steels, extensively used for their high strength and excellent dimensional control [63]. The starting powder characteristics and the processing details of copper steel bar samples sintered in a conventional furnace and in an in laboratory modified commercial microwave oven has been covered at length. In this study, the sintering temperature used typically ranged between 1100 and 1300 °C, soaking time ranged from 5 to 20 min, and the atmosphere was controlled using flowing forming gas mixture of 95% N<sub>2</sub> + 5% H<sub>2</sub>. Microwave sintering resulted in higher sintered density, higher Rockwell hardness, and higher fracture strength as compared with conventional sintering. The improved mechanical properties of microwave sintered samples can be mainly attributed to the evolution of distinct porosity distribution, primarily consisting of small, rounded, and uniformly distributed pores as against large, angular and non-uniformly distributed pores observed in the case of conventional sintering.

In [64] the microwave and the conventional sintering of premixed and prealloyed Cu-12Sn bronze is studied. As compared to the conventional sintering, using microwave sintering the bronze samples were sintered in significantly less time. During conventional sintering, the premixed bronze compacts swelled at 775 and 830 °C, whereas no swelling occurred during microwave sintering of both premixed, as well as prealloyed compacts, pressed at 150 MPa. Hardness of the

premixed microwave samples is higher than for the corresponding conventionally sintered, premixed samples. Usually, the application of conventionally sintered premixed bronzes is restricted to making filters and bearings. However, the lack of swelling in premixed bronze, higher hardness during microwave sintering and uniform microstructure offer an opportunity of extending their use for structural applications as well. The high coalescence observed in microwave sintered bronze is attributed to the nonuniform microwave heating. In the case of prealloyed bronze, the degree of densification remains unaffected by varying porosity (green density) for both microwave, as well as conventional sintering. The premixed bronze samples show an increasing tendency to swell as the initial (green) porosity is reduced by increasing the compaction pressure. The microstructure in the case of microwave sintered samples was found to be more uniform.

In the work by Ariff *et al.* [65], pewter alloys made from tin, copper and antimony powders were sintered using microwave and conventional vacuum sintering. Three different compositions of the pewter alloy were used; 91Sn6Cu3Sb, 94Sn4Cu2Sb and 97Sn2Cu1Sb. The effect of densification and microstructure of the pewter alloys from varying sintering time and sintering mode were examined and compared. Samples in the conventional furnace were sintered for 60 and 120 min, while samples in the microwave furnace were sintered for 15 and 30 min. Samples sintered at longer sintering times resulted in higher density for both sintering methods. Microwave sintering produced samples with smaller grain size and better grain size uniformity than the conventionally sintered samples resulting in a better densification.

Supersolidus liquid phase sintering of Al-Mg-Si-Cu [66] and Al-Cu-Mg-Si-Sn [67] alloys is another example of how microwave assisted sintering can be used to obtain materials with superior properties in shorter time, compared to conventional sintering. These alloys, when exposed to intense heat, undergo a partial phase transition. In prealloyed condition, there is no second phase available for melt formation, the powder partially melts during sintering above the solidus temperature and this mode of sintering characteristics to prealloyed powder system is referred to as supersolidus liquid phase sintering. During subsequent heating, depending on the alloy composition, the formation of liquid phases at particular eutectic temperatures occurs. This liquid formation at intergranular regions results in particle fragmentation. Higher sintering temperature above solidus, lead to more liquid phase formation resulting in further compact densification.

In [68] microwave sintering of refractory metals like tungsten, molybdenum and rhenium, as well as W-Cu, W-Ni-Cu and W-Ni-Fe alloys is presented. Refractory

metals and alloys are well known for their very good mechanical properties which make them useful for wide range of high temperature applications. Due to the fact that these metals and alloys retain its strength at high temperatures there are limits in conventional sintering, like their long residence time which results in undesirable microstructural coarsening. The conventional sintering gets even more problematic if using submicron and nanometer precursor powder sizes. The study shows that in most cases, microwave sintering resulted in an overall reduction of sintering time of up to 80%. This sintering time reduction prevents grain growth substantially providing finer microstructure and as a result superior mechanical properties. Additionally, microwave sintering produced higher sintered densities, of as high as 98% of theoretical density, not achievable by conventional sintering.

Composite materials are well known for their tailored properties that are achieved by combining two or more materials to obtain the required macroscopic properties. The most distinctive feature of composites is that, while the individual constituents retain their properties, they combine to give properties which may not be found in any one of them alone. The article by Venkateswarlu *et al.* [69] reports on fabrication of Al-TiN composites by using microwaves. Al and TiN (10% - 30%) powders were selected as starting materials, mixed in a ball mill and sintered for various times. Results indicate that an optimum microwave sintering time of 2 min was essential and responsible for the improved densification and mechanical properties. The presence of TiN particles at grain boundaries plays a significant role in improving the densification and hardness values. Dry sliding wear results show the improved wear resistance of the Al-TiN composite due to the presence of TiN particles and the wear results are superior to the Al-TiN samples made by hot pressing technique.

Another work dealing with composite materials [70] is focused on aluminum and magnesium based nanocomposites processed using hybrid microwave sintering. Composites were prepared using blend compact - microwave sintering - extrusion methodology. Process evaluation revealed that microwave assisted sintering can lead to a reduction of 86% in sintering time and energy savings of 96% when compared to conventional sintering. Moreover, microwave assisted sintering of metal compacts in this study was carried out in air, in the absence of any protective atmosphere, without compromising the mechanical properties of the materials. To enhance the mechanical properties of aluminum and magnesium, three nanometre size reinforcements silicon carbide, alumina and copper have been added. As a result the aluminum and magnesium composites with improved hardness and failure strain were obtained. The biggest improvement although was in time and

the processing energy.

Annamalai *et al.* studied the effect of microwave heating mode on sintering of powdered ferrous Fe-Ni-C compacts [71]. The ferrous alloy compacts were sintered in a multimode microwave furnace of 2.45 GHz and 6 kW nominal power at 1120 °C for 60 min in forming gas. In general, it was observed that the microwave radiation generally enhances the properties of the sintered material when compared with conventionally sintered material.

Another interesting application of microwave heating is iron production from  $\text{Fe}_3\text{O}_4$  and graphite [72]. The chemical behavior of iron ore reduction was experimentally studied under electric and magnetic fields of microwaves. The microwave magnetic field rapidly heated the powdered ores so that the reduction of the ore to metal ions was completed. It was found that, first, the combined effect of thermal energy and a portion of the microwave magnetic field enhanced deoxidation and, secondly, the microwaves act as a dynamic catalyst at high temperatures. High frequency magnetic fields were found to enhance the antibonding character of oxygen.

All the above-mentioned studies, and many more, confirm that the microwave sintering of powdered metals offers various advantages. In most cases, compared to the conventional sintering, the microwave sintering is faster, thus more economic and energy saving. Microwave sintered metallic samples show higher density, finer microstructure, controllable grain size and more uniform distribution of pores. All of those properties have influence on macroscopic properties like Rockwell hardness, fracture strength, higher Young's modulus, etc. A particular advantage of the microwave sintering of metallic powders is a simpler fabrication process due to fewer steps, repetitiveness and a capability to produce nearly net-shaped objects.

## **3.2 Theory of Microwave Sintering of Powdered Metals**

The applicability of the microwave heating of metallic powders, as well as for materials processing in general, is under constant development [61, 73]. The need to develop a theoretical model to describe the interactions of microwaves with powdered metals has been pursued since the discovery of microwave sintering of metallic powders. Fundamentals of microwave heating of metals need to be analyzed considering the interaction of electric and magnetic fields with the metal surface. For example, a commonly observed tendency of better heating

of metal particles and films in the magnetic field needs to be explained. There are varieties of application fields of microwave heating of metals, in which microwave characteristics of rapid, internal and selective heating must be taken into consideration. The following section will attempt to summarize currently developed models and theories and present the validity to apply such models to real experimental results.

### 3.2.1 Microwave Heating in Separated Electric and Magnetic Fields

The same group responsible for the pioneering work on microwave heating and sintering of metallic powders, published in 2001 a paper dealing with microwave heating in single mode  $TE_{103}$  waveguide microwave furnace [74]. In the position of half of  $TE_{10}$  mode wavelength, at 2.45 GHz, from the shorted end of the waveguide, along the length of the cavity, the maximum electric  $E$  field is in the center of the cross section, where the magnetic  $H$  field is minimum, and the maximum magnetic field is near the wall, where the electric field is minimum. A quartz tube was introduced in these location to hold the sample and also to control the atmosphere. Small cylindrical samples, 5 mm in diameter and 3 mm thick, were placed inside at two different locations, the maximum electric field area where the magnetic field is minimum, and the maximum magnetic field area where the electric field is minimum, respectively. Sample temperatures were measured using an infrared pyrometer. Materials used for test heating in  $E$  and  $H$  fields were various metals, ceramics and metal-ceramic mixtures.

For a typical powdered metal sample, with composition of the powder Fe-2%Cu-0.8%C, the heating in the pure electric field did not lead to extensive rise of the temperature, with a maximum around 180 °C. After microwave heating the sample for 8 min some arcing occurred around the edge of the sample. In the magnetic field however the heating rate was much higher than 300 °C/min in the first two minutes, then it slowed down. The final temperature reading was 780 °C in 10 min time, and a quite uniform heating was observed. Two other compositions of pure metal powder compact samples, cobalt and copper were also tested in this study. The cobalt powder compact sample exhibited the same behavior during the microwave heating. There was little heating effect in the electric field but observed heating rates in the magnetic field were almost of an order higher. The microwave heating of the copper powder compact sample was different. The sample heated up very fast both in the electric and magnetic fields. For both cases the sample's

temperature rose to 700 °C in 1 to 2 min, then quickly dropped down to 500 °C and kept within that range during the continuous heating. For comparison, a pure solid copper bar with the same shape and size was put in the microwave cavity to check out the energy absorption and heating behavior. It was found that there is no temperature rise for the solid copper bar sample neither in the electric field nor in the magnetic field, even after being exposed in the microwave field for 10 min, the sample was still at room temperature.

Alumina is a typical ceramic material with excellent dielectric properties. This material usually has very low dielectric loss, and it is not easy to heat up by microwave, especially at lower temperatures. Since the dielectric loss of alumina increases with temperature, microwave heating of alumina becomes much more efficient at high temperature. In the experiment, the microwave heating of high purity alumina samples in the electric field went somewhat slowly in the beginning, then the heating rate increased up after the sample reached a temperature of 500 °C. But in the magnetic field, it could not be heated at all under the same microwave power for the same exposing time. In comparison, the pure tungsten carbide ceramic (WC) powder compact sample exhibited totally different heating behavior. The heating rate in the magnetic field was quite high, but very low in the electric field, and after 7 min heating, the temperature was only 180 °C and then there was some electrical discharge occurring around the sample.

Another two mixtures tested were, alumina mixed with powdered metal (Fe-2%Cu-0.8%C) and tungsten carbide (WC) mixed with pure cobalt powder. The WC-Co sample could only be efficiently heated up in the magnetic field, and the alumina-metal composite sample could be heated up in both electric and magnetic fields, however the heating effect was much faster in the magnetic field.

In subsequent study [75], radically different effects on materials by applying separated microwave electric and magnetic fields were reported. Various types of metals, oxides and composites were studied. From the results it was concluded that different materials have greatly different heating behaviors in the **E** and **H** microwave fields. In general, the high conductivity samples, such as powdered metal samples, can be much more efficiently heated up in the magnetic field. On the contrary, the pure ceramic samples, which are insulators with little or none conductivity, such as Al<sub>2</sub>O<sub>3</sub> and ZnO, showed much higher heating rates in the pure electric field. The structure of the materials plays important roles in the microwave-materials interaction. For example, the powdered compact copper sample absorbed lot of microwave energy in the microwave field, but the solid sample did not under the same condition. It was concluded that for the general theory of energy loss in



various materials when placed in a microwave field, it is no longer possible to ignore the effect of the magnetic component, especially for conductor and semiconductor materials. The contributions to the magnetic loss mechanism can be hysteresis, eddy currents, magnetic resonance, and domain wall oscillations. The induction of eddy currents was found to be a major factor, and hence ferromagnetism is an important variable for magnetic materials during microwave heating.

In a systematic study of microwave absorption and microstructure evolution of porous copper powder metal compacts [76], it has been shown that both **E** and **H** fields, have major influence on presintering and initial heating rates of copper powder compacts. Again, a single mode TE<sub>102</sub> microwave waveguide laboratory setup was used and samples were heated either in **E** or **H** fields. The initial heating behavior of green copper powder compacts in either field is characterized by a sharp rise in temperature that peaks and then relaxes to an equilibrium temperature. The initial heating temperature peak only occurs during the first heating of a green sample. Subsequent heating of the same sample, after cooling to room temperature, is characterized by a more gradual rise in temperature that asymptotically reaches equilibrium. It was also observed that the particle size of copper powders and the relative density of the compacts have an influence on initial heating rates. It was observed that compacts made from the same powder and same relative density heat more rapidly and to higher equilibrium temperature in the magnetic field compared to the electric field. An initial heating temperature peak is always apparent in the first microwave heating of a green, copper powder metal compact.

In one of the earlier studies [77] it was reported that the microwave heating in separate **E** and **H** fields, has not only an effect on heating rates and heating profiles of various material samples but also displays new effects, like oxide decrystallization. A similar single mode TE<sub>10</sub> microwave furnace setup was used to heat in electric and magnetic fields, oxide materials like Fe<sub>3</sub>O<sub>4</sub>, BaTiO<sub>3</sub>, CuO, MnO<sub>2</sub>, ZnFe<sub>2</sub>O<sub>4</sub>, BaFe<sub>12</sub>O<sub>19</sub>, CoFe<sub>2</sub>O<sub>4</sub>, FeFe<sub>2</sub>O<sub>4</sub> and NiFe<sub>2</sub>O<sub>4</sub>. The conclusions from this study are that many of these oxide undergo a phase transformation similar to glass transition, however without going through bulk liquid state, called decrystallization. It was speculated that the materials could undergo solid-melt phase transformation but only on a very local and nanoscale. It has been shown that magnetic field plays an important role in this process, and ferromagnetism has been ruled out as a requirement for decrystallization. Also a radical difference in microstructure of ferroic oxides exposed to electric or magnetic components of the microwave fields has been shown.

In more recent works [78, 79], the influence of the magnetic component of

microwaves on magnetic oxides is presented. Rapid heating and selective sintering of magnetic, metal-oxide particles by the microwave magnetic field is due to response of magnetization to microwaves, which originates from electron spins residing in the unfilled 3d shell. In magnetite ( $\text{Fe}_3\text{O}_4$ ), a nonresonant response causes a large change in the internal energy through the exchange interaction between spins. It persists above the Curie temperature because each electron spin is able to respond to the alternating magnetic field of microwaves even above the Curie temperature. Hematite ( $\text{Fe}_2\text{O}_3$ ), with weak spontaneous magnetization, was observed to heat much less when irradiated with microwaves.

These experimental studies of microwave heating of various materials, either in the magnetic or the electric field, provide first glimpses over the absorption mechanisms of the microwaves in powdered specimens. Ceramic materials usually heat up only in the electric field, even materials like alumina with very low dielectric losses at low temperature. However if ceramic materials, like magnetite for example, have magnetic properties, they can be heated in the magnetic field very effectively. Ceramic and metallic mixtures heat up in both, magnetic and electric fields, whereas the heating in the electric field is mainly due to dielectric losses in the ceramics, the magnetic losses are mainly due to induced eddy currents in non-ferromagnetic metallic particles. Purely metallic powders show some different behaviors. Some of the powders heat up in the electric field and some do not. It has been showed that metals that do not oxidize, i.e. there is no thin oxide layer on the powder particles, or have an oxide layer but with very low dielectric losses, do not heat in the electric field. On the other hand all metallic (conductive) powdered materials absorb microwaves very efficiently in the magnetic field due to induced eddy currents. Heating is even more rapid and efficient with ferromagnetic metals and it has also been shown that the powder particle size has an influence on absorption of the microwaves and the heating rate.

### 3.2.2 Effective Medium Approach

The first work attempting to explain microwave absorption in metallic powders was carried out by Luo *et al.* [80]. Microwave sintering of powdered metals has been successfully realized in single-mode cavities, as well as in multimode microwave systems. In the previous works, the experimental proof of the major role of magnetic field losses in metallic powders has been done in single-mode microwave cavities with small size samples. It is difficult to explain why the powdered metals can be sintered in multimode microwave systems because the electric field and the

magnetic field cannot be fixed in the systems. A model was developed based on classical electromagnetic theory, the magnetic induction in a metal at microwave frequencies is larger than the electric field and therefore the heating of powdered metals can be attributed to the result of eddy currents. A model assuming the shape of the oven as a cylinder and the powdered metal sample as a cylindrical rod placed symmetrically in the center of the oven was established and the field solution in different regions of this model was determined to obtain an equation for the absorbed power. Based on the equations, calculations showed that the attenuation coefficient of a mode in metallic powders decreases with increasing frequency if the mode is far from cutoff, however it can increase significantly with increasing frequency if the mode is near cutoff. The higher the mode order near cutoff, the larger the attenuation constant, indicating that the shape and the size of metallic powder compact sample has a direct effect on the microwave heating. Experimental verification was carried out to compare the heating rate of powdered Fe metal and Fe-Cr18-Ni10 alloy using a 30 GHz, 10 kW gyrotron system. With small discrepancies, the theoretical model was able to describe the early stages of microwave heating in cylindrical multimode cavity.

Another theoretical model by Rybakov *et al.* [81] considers the electrically conductive powder particles to be covered by insulating oxide layer using the effective medium approximation. The effective conductivity of the powder compact can differ significantly from the conductivity of the homogeneous solid material due to the presence of an oxide layer on the surface of each powder particle. The presence of the oxide layer or dielectric shells prevents the connectivity percolation between the particles and substantially increases the electromagnetic power dissipation in the powder compact. Using the effective medium approximation, the dielectric properties of the compact can be expressed in terms of the properties of the constituents by taking into consideration the density of the solid phase in the compact and assuming that each individual spherical powder particle in the compact is surrounded by a spherical dielectric layer. The presence of a very thin insulating layer between the conductive powder particles can decrease considerably the effective dielectric losses by several orders of magnitude while, at the same time, increase the real part of the dielectric permittivity. For example, as indicated by an oxidized silicon powdered sample, the real part of the effective permittivity can be increased, compared to the effective imaginary part of the effective permittivity (loss factor), with increasing thickness of the oxide layer. It was also reported that the efficiency of microwave heating of electrically conductive materials depends on the size of the samples and their position with respect to the peak positions of the  $\mathbf{E}$  and

H fields inside the single-mode waveguide microwave furnace. Experiments were performed on microwave heating of silicon, iron, and copper powder compacts. The results were found to be in a good agreement with the theoretical model. It was observed that conductive materials with dimensions approximately or slightly smaller than the skin depth, at a given frequency, heat up more efficiently at the maximum of the magnetic field due to induction heating, i.e. macro eddy currents that flow through the whole sample. Heating in the electric field was found to be more efficient for materials with moderate dielectric losses and materials with very low conductivity. The heating experiments were performed in a multimode cavity using a 24 GHz gyrotron with a peak power of 3 kW. The samples were prepared using silicon, iron and copper powders with 0.6, 30 and 20  $\mu\text{m}$  particle sizes respectively. Silicon powder was compacted into cylindrical samples of 11 mm in diameter and height, while iron and copper powders were pressed into spherical samples with a diameter of 5 mm. It was observed that the temperature at the center of the silicon sample is the highest and the temperature decreases away from the center, indicating the volumetric microwave heating of the silicon sample. On the other hand, it was observed in microwave heating of the spherical iron samples that the initial heating due to skin effect and macro eddy currents changes into volumetric heating at higher temperatures. There was no volumetric heating observed in the copper powder compact, and it was suggested that it is due to the fact, that iron powder is more oxidized, where the iron oxides take over the absorption of the microwaves at higher temperature.

Mishra *et al.* [82] developed a model to predict microwave heating behavior of metal-powder compacts by solving Maxwell's equations and the heat transfer equations simultaneously. A 2D finite difference time domain modeling technique was used to determine the electric and magnetic field distribution inside the cavity. The advantages of such simulations are due to incorporating of the temperature-dependent electromagnetic properties of the powder compact. Changes in the material properties, with increasing temperature, are updated after a defined amount of time, and allow one to predict heating profiles, as well as to modify the model more accordingly to fit the experimental results. The model was validated by comparing the predicted and experimental results of heating behavior of tin, copper and tungsten alloy samples. Some strict assumptions to the model were made to make it easier to simulate. Among most of the important assumptions made are: the powder particles size is much smaller than the wavelength of microwaves, the powder compact size is small enough to allow volumetric heating, coarsening of the powders during heating was neglected, the particles are perfect spheres

and there is no heat conduction between particles. It was observed that the predicted heating profiles were in quite good agreement with the experimental results. The discrepancy in the heating profiles was attributed to the fluctuations in the input power during the experiment, which was assumed to be constant in the simulations. An upper limit of the temperature achieved by the metal compacts during microwave heating was in perfect agreement for all the materials used for the experiment.

Another study dealing with the effective medium approximation, compares numerical predictions of the effective electromagnetic properties of powdered metals and heating profiles from previous studies with experimental data obtained for wide range of metals [83]. The most effectively heated powder was found to be iron because both eddy current loss and magnetic reversal loss mechanisms act in case of such a metal. Diamagnetic metals like Sn and Cu are heated better than paramagnetic Ti while Au is also only slightly heated. Cu and Ni based metallic powders are also moderately heated. Weak heating of Au powder, which is a noble metal, can be explained by the absence of the oxide layer on the particles, which allows eddy currents flowing through larger area compared to other metals, and screening is greater in such a case.

In a most recent paper by Kiley *et al.* [84], a systematic analysis of classical and contemporary models of complex permittivity of mixtures and the use of these models for determining effective permittivity of dielectric matrices with metal inclusions is discussed. Results from various mixture and core-shell mixture models are compared to experimental data for a titanium/stearic acid mixture and a boron nitride/graphite mixture, and for a tungsten/Teflon mixture. The comparison has shown that none of the models correctly predicts behavior beyond the percolation threshold, but below the percolation threshold, each of these models do an acceptable job of quantitatively predicting the effective complex permittivity of the considered mixtures and the heating profiles and behaviors of powdered metal compacts. The continuum approximation that is valid for dielectric mixtures is applicable only below the percolation threshold of the conductive phase. Some disagreement with the experimentally calculated values may also arise from the lessened validity of the cavity perturbation formalism for volume fractions above the percolation threshold.

As one can see, many attempts have been made to explain the heating behavior of the metallic powder compacts during exposure to the microwaves. The description of the effective electromagnetic properties of metallic powder compacts, based on dielectric and magnetic losses, and using the effective medium

approximation, is sufficient to explain the heating behaviors of the whole samples made from different types of metals. However these theories and experiments do not give insight into the microwave absorption mechanisms and complex interactions of microwaves with metallic particles on a micro scale. The calculations of an overall (effective) conductivity of metallic powder samples, give good predictions of heating behavior in an alternating magnetic field, where the main mechanism of the microwave absorption are macro eddy currents. It was noted that metals that do not oxidize, like silver, can only be heated by magnetic induction. The effective approximations of the dielectric properties and modeling of volumetric heating behaviors also works for most of the cases; however these effects can not be explained on the micro scale, or at least on the scale of the particle size.

### 3.2.3 Interparticle Neck Growth

The microstructure and material related aspects of microwave sintering cannot be neglected and give insight, to some extent, on the microwave absorption mechanisms in metallic powders. It was reported in 2004 by Veltl *et al.* [85] that the presence of a new microwave effect enhancing material transport between metallic powder particles during the microwave sintering of bronze powder and steel bearing balls in a multimode cavity. It was suggested that the high-frequency electric field acting between the particles generates plasma on a micro scale, which enhances mass transport into the contact areas, thus speeding up the presintering process. In conventional sintering, the particles have to be in contact with each other in order for diffusion to occur. In microwave sintering, as have been observed, particles can be sintered when in close proximity to each other, and physical contact between conductive particles is not required. It was concluded that the microwave field, the electric as well as the magnetic component, focuses at cracks in the materials, promoting mass transfer, and reducing porosity within the sintered materials [85].

In recent studies it has been confirmed that the microwaves play an important role during the early stages of sintering of copper [86, 87], nickel [88] and iron [89] powder compacts. Evidence of pure microwave effect on initial stage of sintering was found on fracture surface of sintered samples, as development of micro plasma discharges in porous material seems to enhance sintering process. The fracture surface of samples showed traces of plasma discharging, thus showing a clear effect of microwaves on sintering process. [87]. The initial stage of microwave sintering of nickel powder showed anomalous neck growth rate during isothermal soaking [88]. The evidences of formation of liquid phase during microwave sintering of

nickel powder have been revealed, that may support enhancement of mass transfer during microwave sintering process. The application of a classical sphere-to-sphere approach [89] showed the possibility of identifying the main diffusion mechanisms operating during the initial stage of microwave sintering of iron powder. It was found that microwave enhanced surface diffusion is the main sintering mechanism, which also promotes neck growth between conductive particles not observed during conventional sintering of powdered iron samples.

In [90], comparison between conventional, microwave and spark plasma sintering (SPS) of tungsten carbide (WC) is presented. In this work an emphasis was put on the use of the neck growth kinetics approach to determine the main mass transport mechanisms during different kinds of sintering of spherically shaped tungsten carbide powder. A detailed study of the neck growth mechanisms of tungsten carbide during the initial stage of sintering was carried out, and an analytical sphere-to-sphere model for the initial stage sintering of ceramics was successfully applied. It was found that the mass transport during SPS is substantially enhanced by applied stress and induction of eddy currents on the particle's surface and is governed by a combination of the mechanism of grain-boundary diffusion and power-law creep. During microwave sintering the mass transport is substantially enhanced by introduction of a small amount of a liquid phase and is governed by the mechanism of volume diffusion, which is followed by surface diffusion. Low values of the apparent activation energy for microwave and spark-plasma sintering have been obtained, and for the conventional sintering, all data collected indicate grain-boundary diffusion as the main sintering mechanism. Numerical simulation of neck growth revealed high values of the diffusion coefficient for microwave and spark plasma sintering, and for conventional sintering, the diffusion coefficients calculated are in good agreement with values for the diffusion of W and C in the WC system, validating the results for the microwave and the spark plasma sintering.

The microwave absorptions mechanism can not only be explained on the basis of macroscopic effects, like inductive heating of conductive samples or volumetric heating of samples with effective dielectric properties. To understand the microwave absorptions mechanism one has to include into a broader view of microwave effects on microscale or even nanoscale. The micro plasma discharges or local melting of the materials influence the effective properties of the compacted metallic powder samples, rapidly changing heating regimes and affecting macroscopic effects of the microwave heating.

### 3.3 Modeling of Copper Powders

There are numerous experimental studies of microwave heating of metallic powders. In the recent work of Ma *et al.* [76] microwave heating of copper powder compacts in either magnetic or electric field in a single mode  $TE_{102}$  cavity is studied together with measurements of magnetic and electric properties of metal compacts. The dependence of the conductivity of the sample as a function of heating time is also measured giving insight into mechanisms of presintering stage with characteristic high heating rates. This systematic work on heating and sintering of copper powder compacts contains measurement results that can be directly compared to the results obtained using numerical simulations. Thus the model of the copper powder was created to suit the initial conditions of the experiment, in order to make the model more physical feasible.

The model of metallic powder consists of periodically arranged spherical (for the sake of simplicity) particles in a cubic close packed (CCP) structure. The relative density of the CCP structure defined as a volume of non-overlapping spheres divided by the volume of the unit cell is  $\rho_r = 0.74$ . The CCP structure has been chosen due to its very close value of the relative density to the experimental value for copper compacts  $\rho_{r(exp)} = 0.76$  [76]. The structure is excited by a plane wave (TM<sub>00</sub> mode) with direction of propagation along the  $z$ -axis, the electric field (E) polarized in the  $x$ -direction and with the magnetic field (H) polarized in the  $y$ -direction as shown in figure 3.1. The ports are located at the  $\pm z$  limits of the mesh volume where open boundary conditions are used. A periodic boundary condition is applied at the  $\pm x$  and  $\pm y$  faces of the model structure. An auto meshing procedure with adaptive meshing is used in the CST MWS to create the tetrahedral mesh. The number of mesh cells varies between 100000 to 300000 depending on the model and the particle size. The numerical problem is solved by a frequency domain solver, for frequencies from 1 to 20 GHz.

The spherical particles are made of copper. The diameter of the particles varies from 100 nm to 25  $\mu\text{m}$ , while the distance between the neighboring particles is 5 nm. The assumption made during the creation of the model was that the particles do not make an electrical contact with each other. It was concluded in [85] that metallic particles can be sintered when in close proximity to each other, and physical contact between conductive particles is not required. This is the case in the initial stages of microwave sintering where there are electrical connections between particles and the sample behaves as a dielectric-conductive material mixture.

After the copper powder models are simulated in CST MWS, the obtained



scattering parameters  $S_{11}$  and  $S_{21}$  are used for the extraction of the effective electromagnetic properties as described in Chapter 2.

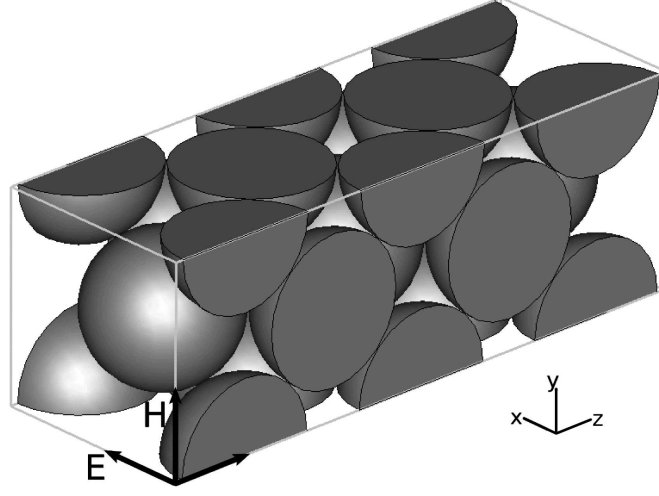


Figure 3.1: Model structure as used in the simulations with CST MWS. The arrows show the polarization of the magnetic (H) and electric field (E), and the direction of propagation. Ports are at the  $\pm z$ -limits and the periodic boundary condition is applied to  $\pm x$ - and  $\pm y$ -limits. In this example the model structure contains two unit cells of copper particles arranged in CCP structure

### 3.4 Mechanisms of Dielectric Losses

The simulations were conducted for copper spherical particles arranged in a *CCP* structure containing 8 unit cells, a number ascertained by convergence studies. The particles with the conductivity of bulk copper  $\sigma = 5.8 \times 10^7$  S/m are embedded in vacuum. The diameter of the particles used in the simulations is 3, 1, 0.5, 0.2 and 0.1  $\mu\text{m}$ . The simulations were performed for a wide frequency range from 1 to 20 GHz, and later the complex values for  $\varepsilon$  and  $\mu$  were extracted for a single frequency of 2.45 GHz. The penetration depth of the bulk copper is  $\delta = 1.34 \mu\text{m}$  at the frequency of 2.45 GHz. The penetration depth of the mixture can be calculated as an inverse of the attenuation constant  $\delta = 1/\alpha$  with

$$\alpha = \Re \left( i\omega \sqrt{\mu\varepsilon \left( 1 - \frac{i\sigma}{\omega\varepsilon} \right)} \right), \quad (3.1)$$

where  $\omega = 2\pi f$ .

The investigations were performed for two cases. In case 1, the distance between

the copper particles is 5 nm of free space. The particles can be considered as separated, non-interacting absorbers. Results for case 1 are presented in table 3.1. In

Table 3.1: Effective dielectric and magnetic properties of copper powders without an oxide layer

Particle diameter [ $\mu\text{m}$ ]	$\varepsilon'$	$\varepsilon''$	$\mu'$	$\mu''$	$\delta$ [m]
3	26.964	0.0006	0.9635	0.1596	0.046
1	28.117	0.0017	1.0065	0.0444	0.166
0.5	31.595	0.0019	1.0094	0.0235	0.297
0.2	32.397	0.0099	1.0048	0.0084	0.814
0.1	33.751	0.0076	1.0058	0.0078	0.864

case 2, particles are separated by a 5 nm thick oxide layer. The dielectric properties of the copper oxide were taken from [91] and are  $\varepsilon' = 9.483$  and  $\varepsilon'' = 0.9249$ . It has been reported by Ma *et al.* [76] that the assumption of the existence of a native oxide layer is realistic to some extent. The conductivity of cold pressed compacts made from 22  $\mu\text{m}$  copper powder was found to be  $10^4$  times greater than compacts made of 3  $\mu\text{m}$  powder [76]. It is coherent since larger particles are more likely to create electric contacts during pressing [76]. Results for case 2 are presented in

Table 3.2: Effective dielectric and magnetic properties of copper powders with a thin oxide layer

Particle diameter [ $\mu\text{m}$ ]	$\varepsilon'$	$\varepsilon''$	$\mu'$	$\mu''$	$\delta$ [m]
3	27.293	1.1019	0.9631	0.1604	0.037
1	28.476	1.4143	1.0021	0.0439	0.078
0.5	31.586	1.8553	1.0052	0.0219	0.086
0.2	33.341	2.2921	1.0076	0.0084	0.087
0.1	34.007	2.6253	1.0083	0.0061	0.084

table 3.2. In both cases an overall tendency is clear that with decreasing particle diameter the value of  $\varepsilon'$  is increasing. In case 1, the value of  $\varepsilon''$  is very low and within the error range. Thus, case 1 is not an appropriate model for the early stage of sintering in the electric field only. For case 2 the value of  $\varepsilon''$  increases with a decrease of the particle diameter. In both cases the real part of permeability is very close to 1, only for 3  $\mu\text{m}$  particles does the value of  $\mu'$  indicate that the mixture is diamagnetic. This effect is related to very high density eddy currents which are responsible for the magnetic losses. The value of  $\mu''$  follows the same pattern in both cases. The highest value of  $\mu''$  is found for 3  $\mu\text{m}$ . The penetration depth of

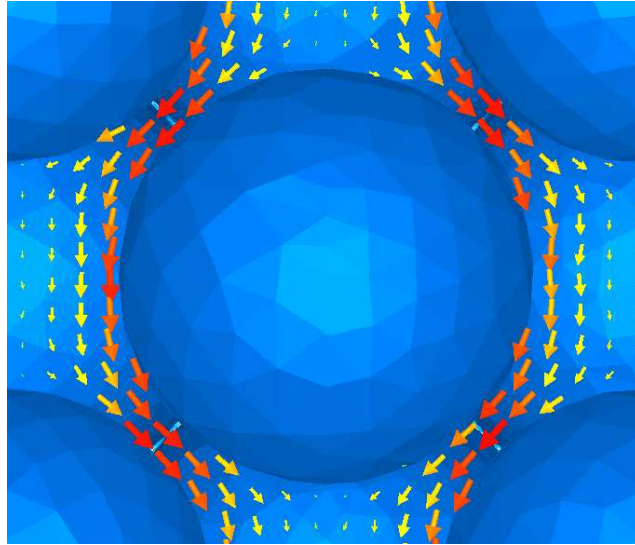


Figure 3.2: Cross-sectional plot of the power flow through the  $y$ -plane within the structure with  $2\ \mu\text{m}$  particles. Arrows indicate peak values of the Poynting vector

copper powders is in the range of few centimeters in case with oxide layer. It is also significantly larger compared to the penetration depth of the bulk copper  $\delta = 1.34\ \mu\text{m}$  at the frequency of 2.45 GHz. Worth denoting is the fact that even for a very small volume content of oxide layer in case 2, the electric losses are very high. Compared to the value of the imaginary part of permittivity  $\varepsilon'' = 0.9249$  for the bulk copper oxide, the electric absorption of the mixture is always higher [92]. One can understand this effect looking at the effective path of the electromagnetic wave in the mixture. Figure 3.2 shows a cross-sectional plot of the power flow for the structure with  $2\ \mu\text{m}$  particles. The power flow monitor in CST MWS stores the peak value of the Poynting vector  $\mathbf{S} = \mathbf{E} \times \mathbf{H}$ . The Poynting vector can be thought of as a representation of the energy flux and indicates the direction of propagation of an electromagnetic wave within the material.

Additionally to the longer effective path of the electromagnetic wave inside the mixture, the electric field which does not penetrate metallic particles is being squeezed between the particles as shown in figures 3.3, 3.4, 3.5 and 3.6. The effect is known as microfocusing of the electric field, responsible for an enhanced sintering of ceramic materials [93, 94, 85, 86, 87, 88, 89].

The local electric fields are disproportionately intense close to the particle's surface due to strong focusing. Also, the electric field is much stronger in the interparticle contact zones and form spherical neck contacts [95, 93, 96, 85, 86, 87, 88, 89].

Simulations show that the peak value of the microfocused electric field is  $10^3$

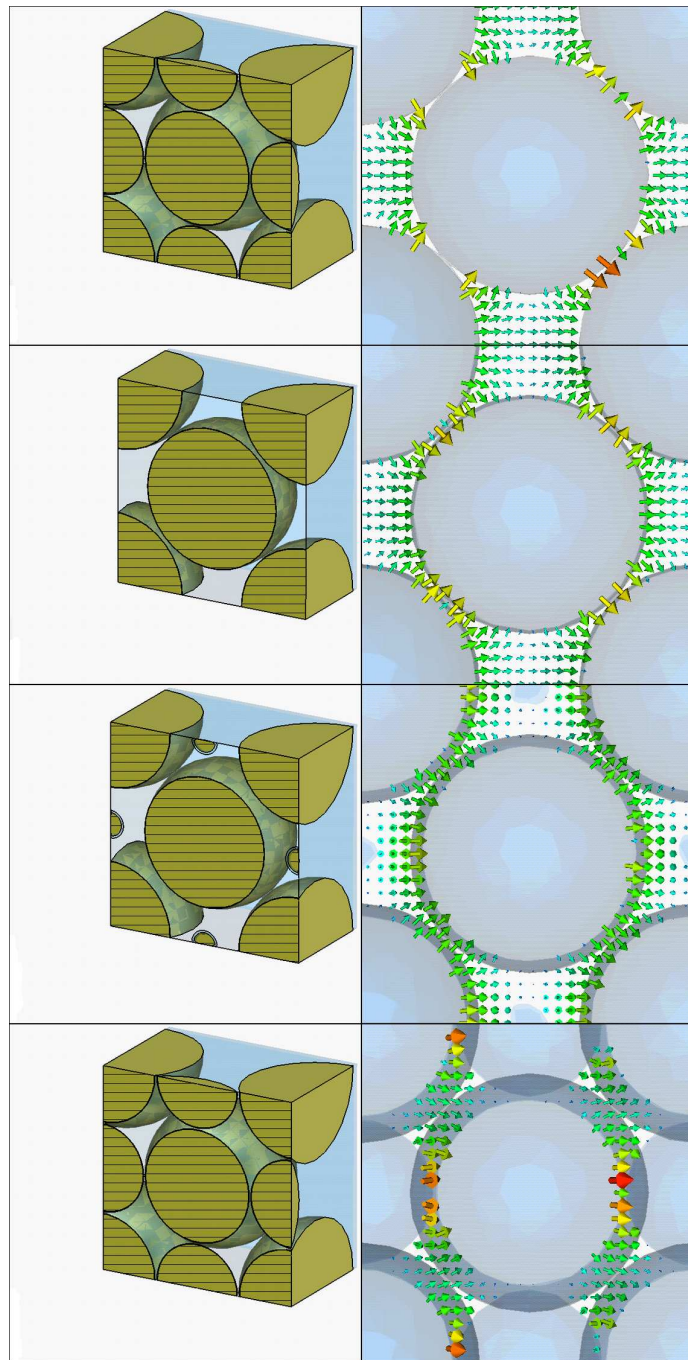


Figure 3.3: Cross-sectional plot through the  $z$ -planes of the model structure with 2  $\mu\text{m}$  particles at different locations. Arrows indicate the strength of the electric field, logarithmic scales was used and red color indicates the strongest electric field, while yellow and green color represent moderate and weak electric field strength, respectively.

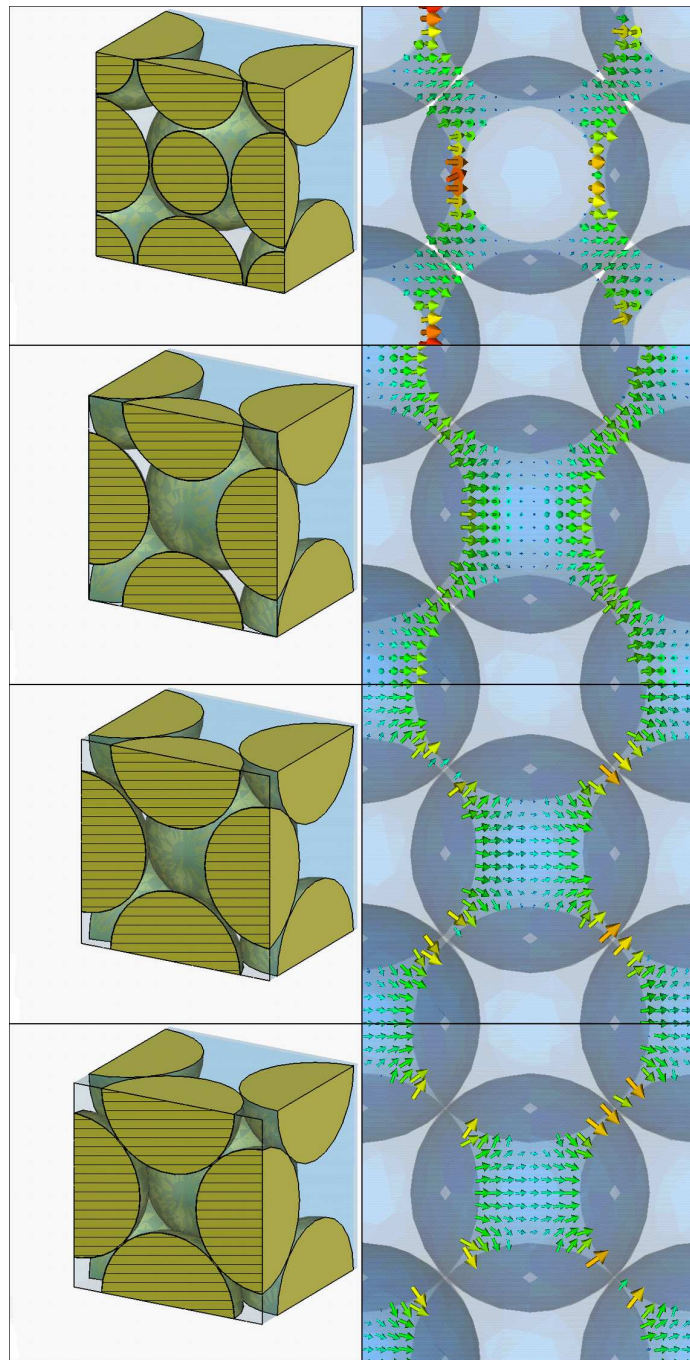


Figure 3.4: Cross-sectional plot through the  $z$ -planes of the model structure with  $2\ \mu\text{m}$  particles at different locations. Arrows indicate the strength of the electric field, logarithmic scales was used and red color indicates the strongest electric field, while yellow and green color represent moderate and weak electric field strength, respectively.



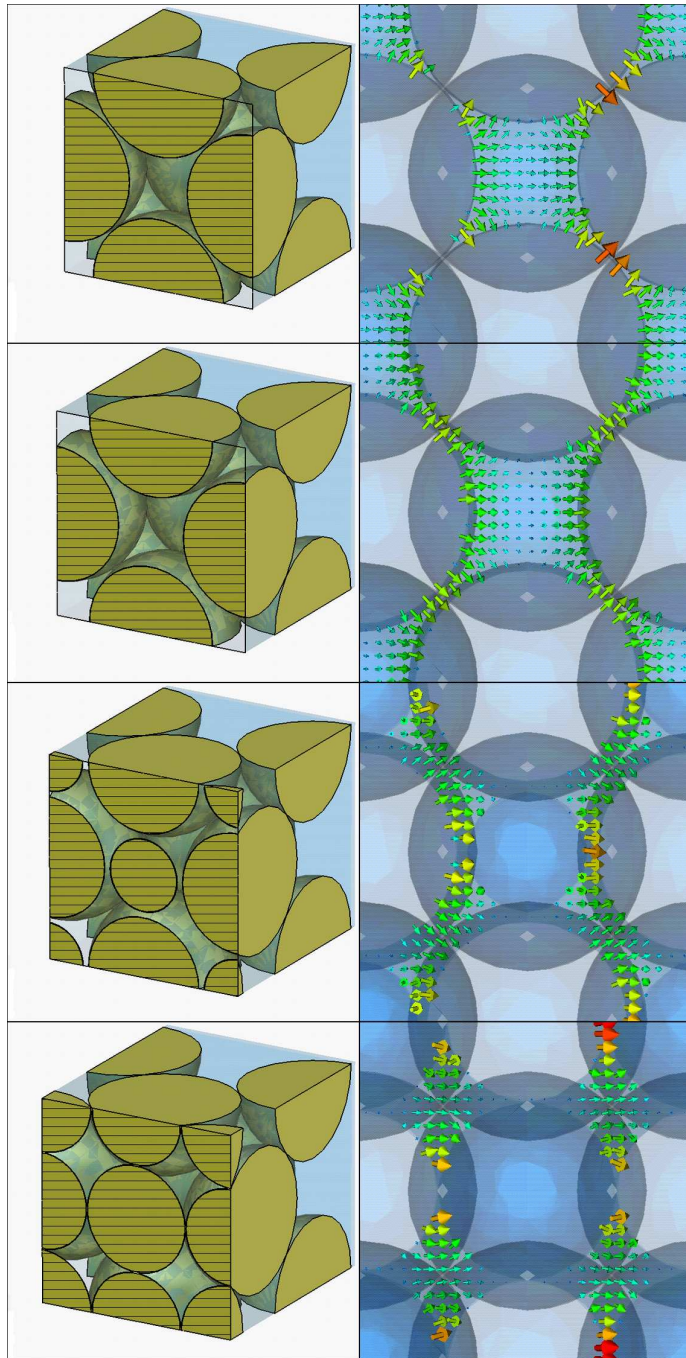


Figure 3.5: Cross-sectional plot through the  $z$ -planes of the model structure with  $2\ \mu\text{m}$  particles at different locations. Arrows indicate the strength of the electric field, logarithmic scales was used and red color indicates the strongest electric field, while yellow and green color represent moderate and weak electric field strength, respectively.

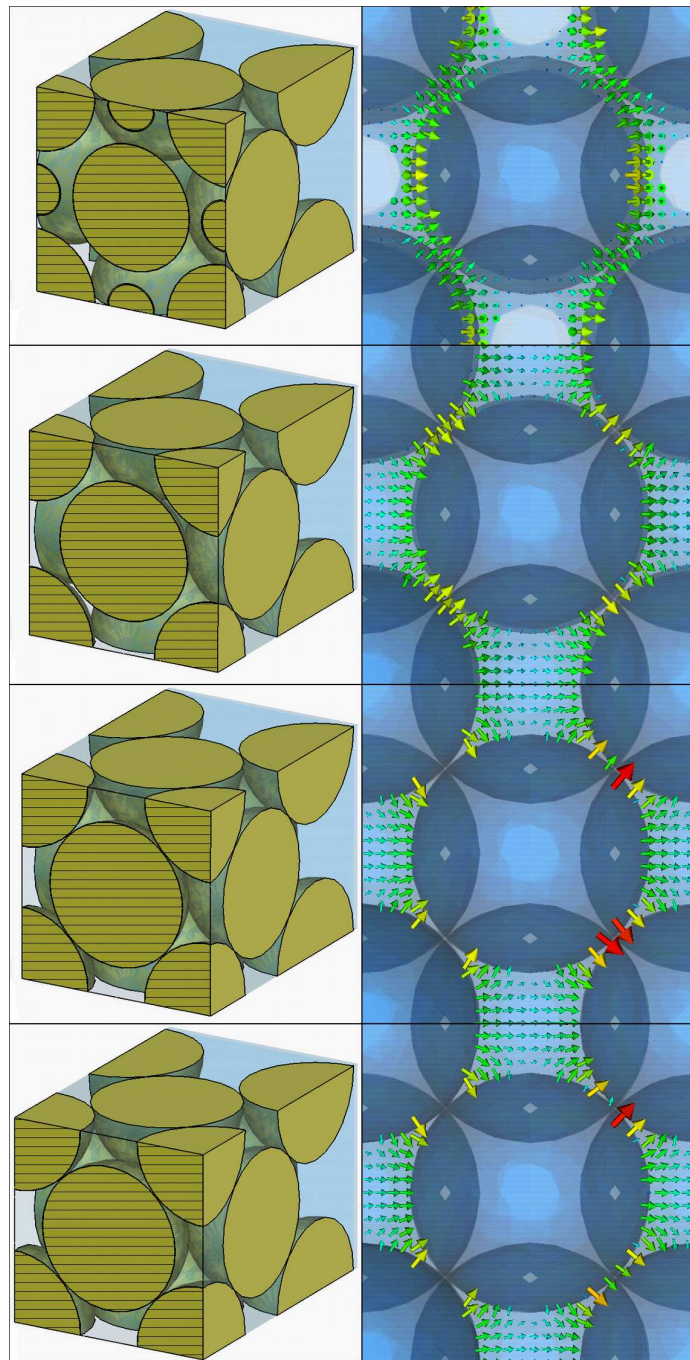


Figure 3.6: Cross-sectional plot through the  $z$ -planes of the model structure with  $2\ \mu\text{m}$  particles at different locations. Arrows indicate the strength of the electric field, logarithmic scales was used and red color indicates the strongest electric field, while yellow and green color represent moderate and weak electric field strength, respectively.

times larger than the peak value in free space. High electric field densities in regions where particles are very close to each other and where the oxide layer is located, give rise to relatively high dielectric losses. The high dielectric losses in the contact zones might lead to a quick formation of conductive contacts between the copper particles. This may explain the effect of the initial heating behavior of copper powder compacts heated in the electric field only. The temperature sharply peaks in the initial stage of the heating process and with the time the temperature drops and reaches equilibrium. This behavior is observed only during the first heating of the samples [76, 75, 77, 74].

As reported by Ma *et al.* [76], the conductivity of the 3  $\mu\text{m}$  copper powder compact after cold pressing is in the range of 0.01 - 1 S/m. Using the cavity perturbation methods Ma *et al.* [76] also measured values of  $\varepsilon''$  and  $\mu''$  for copper compacts. In the early stage of the microwave heating the reported values for  $\varepsilon''$  are in the range of 0.01 - 0.1 and values for  $\mu''$  in the range of 0.001 - 0.1. The values for  $\mu''$  obtained from the simulations are in a good agreement with experimental values. However the obtained numerical values for  $\varepsilon''$  are higher. This may be caused by overestimated  $\varepsilon'$  and  $\varepsilon''$  used in the simulations for the copper oxide, which are close to the value for the bulk copper oxide. The thickness of the native oxide layer in copper is in the range of few nm, and the exact dielectric properties are not known.

### 3.5 Mechanisms of Magnetic Losses

Experimentally it has been observed that the heating rate of copper powders, during heating in the magnetic field, resembles the behavior during the heating in the electric field. The temperature sharply peaks in the first few seconds, then drops and reaches a constant value [76, 75, 77]. This behavior was observed only during the initial heating. After cooling and reinserting the sample the sharp peak in the temperature profile does not occur [76].

As mentioned before, the magnetic losses occurring in non-magnetic, conductive materials are due to induced eddy currents. Figure 3.7 shows a cross-sectional plot of the current density at the peak value for the structure with 2  $\mu\text{m}$  particles at 2.45 GHz frequency. Simulations show that for an alternating magnetic field the eddy current density is strongest at the surface of the particles. A magnetic field of 200 A/m is chosen, which is comparable to the field value in the single mode cavity for an input power of 1800 W.

The eddy current density in the region close to the surface of the metallic particle can reach  $1.16 \cdot 10^8$  A/m<sup>2</sup> for the structure with 2  $\mu\text{m}$  particles, while



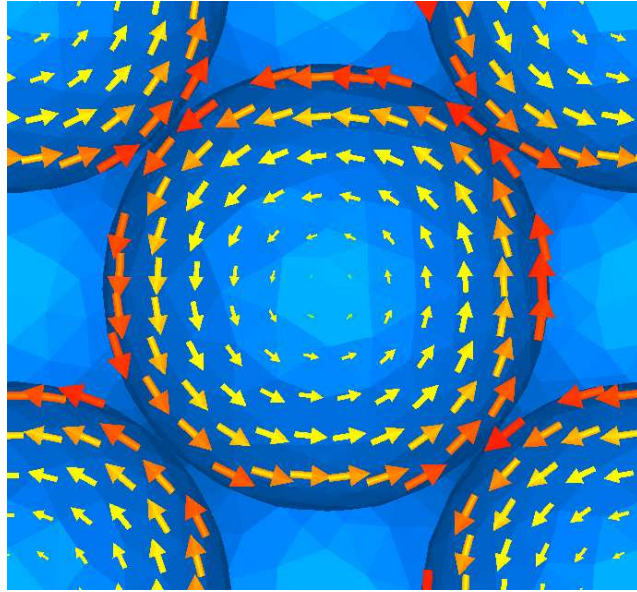
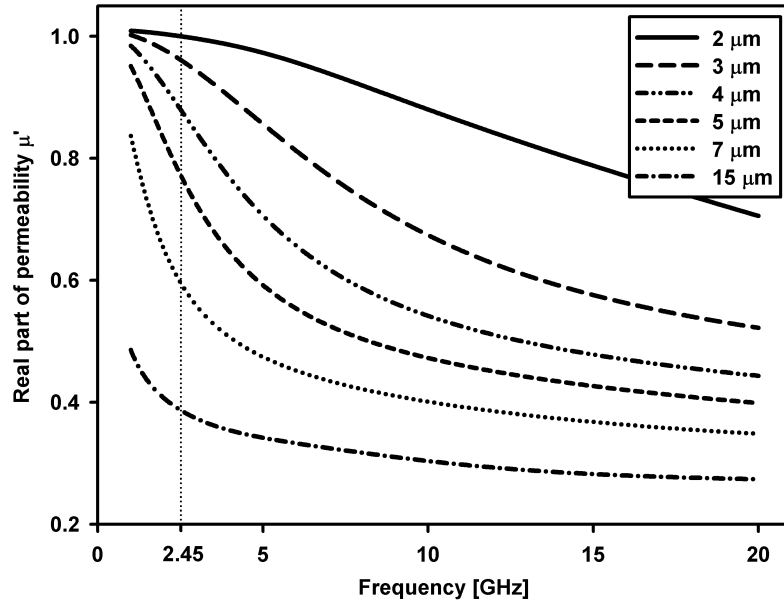


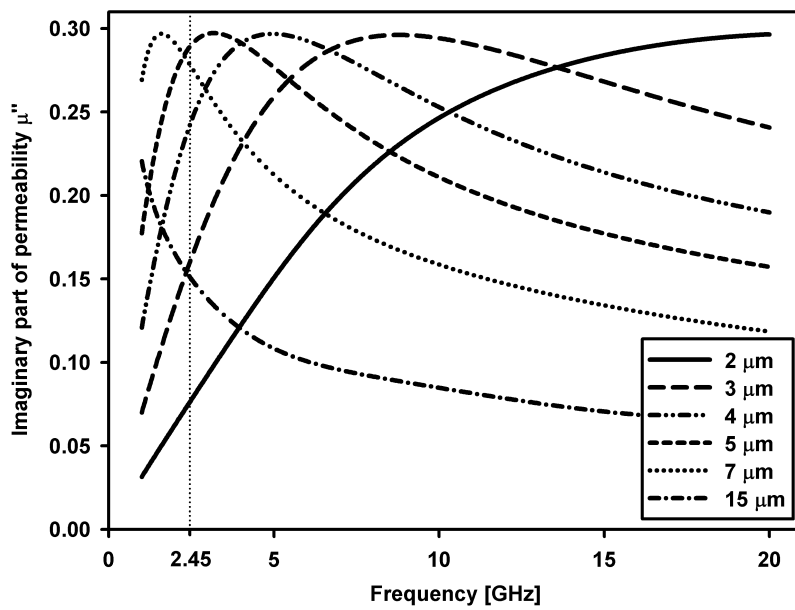
Figure 3.7: Cross-sectional plot of the current density, through the  $y$ -plane for the structure with  $2\ \mu\text{m}$  particles. The size of the arrows corresponds to the eddy currents density. The arrows size scale is  $\log_{100}$  for better visualization. Due to the fact that induced eddy currents are strongest on, and near to, the surface of a particle, the heating, and thus sintering, is very rapid.

the average value of the power density in the near surface region is  $7.35 \cdot 10^7\ \text{W}/\text{m}^3$  [92]. Extremely high heating rates explain quick formation of conductive contacts between particles. The heating of the copper powder compacts in the magnetic field is characterized by a sharp peak in the temperature at the early stage. This stage corresponds to the surface heating of particles which can be considered as non-interacting absorbers. After the initial high rate surface heating of the particles the conductive contacts are being formed and the particles cannot be considered as separate absorbers anymore. This leads to a dramatic decrease in the absorption of the microwaves and thus decreased heating rate. After the conductive contacts between particles are formed the heating rate relaxes and reaches a plateau [76, 75].

In order to study the effects of absorption of the magnetic field component, simulations were conducted for spherical particles with diameter 1 - 10, 15 and 25  $\mu\text{m}$ . The simulations were performed for a wide frequency range from 1 to 20 GHz. The complex values for  $\varepsilon$  and  $\mu$  were extracted for a single frequency of 2.45 GHz, and used in later simulations of the microwave heating of the copper powder compacts. Figures 3.8(a) and 3.8(b) show the real and imaginary part of the complex magnetic permeability, respectively. One can notice a clearly visible resonance behavior. The resonance frequency depends on the particle size and conductivity of



(a)



(b)

Figure 3.8: Simulated real (a) and imaginary (b) part of the magnetic permeability for copper powder compacts for selected particle diameters.

the material. For the sake of simplicity we only present the results for the copper particles. The dependence of the absorption coefficient ( $\mu''$ ) on the particle diameter implies different heating rates of the copper powder compacts composed of particles with different diameters [97, 98].

### 3.6 Microwave Heating in the Magnetic Field

The microwave heating simulations in the single mode ( $TE_{102}$ ) cavity were performed using COMSOL multiphysics FEM software. The simulation results are compared to the experimental values of the initial heating rate as presented in [76].

The setup of the model is similar to the one presented in [99]. Figure 3.9 shows the placement of the copper powder compact sample within the cavity with dimensions of 72 mm width, 36 mm height and 226.3 mm length. The sample is placed at the maximum of the magnetic energy density close to the cavity wall. The model of the cavity and the sample consists of around 50000 mesh elements. The coupled problem is solved in two steps. First, the stationary solution for the electromagnetic waves inside the cavity is obtained. The perfect electric conductor (PEC) boundary condition is set for all walls except the wall where the microwave port is located as shown in the figure 3.9. The solution is a standing wave with two anti nodes of the E-field component and the H-field rotating around the E-field anti nodes. The electromagnetic properties of the sample were taken from the extracted values of  $\varepsilon$  and  $\mu$  for the copper particles at 2.45 GHz frequency.

The second step is the transient solution of the heating process. The boundary condition for all the cavity walls was set to the constant ambient temperature 300 K. For the surface of the sample the selected boundary condition was a heat sink with radiation type surface-to-ambient. This type of boundary condition describes the surface radiosity according to the Stefan-Boltzmann law

$$J_0 = \varepsilon_s \sigma (T^4 - T_r^4), \quad (3.2)$$

where  $J_0$  is the total energy radiated per unit area per unit time,  $\varepsilon_s$  the surface emissivity,  $T$  the temperature in Kelvin,  $T_r$  the room temperature and  $\sigma$  the Stefan-Boltzmann constant. The value of the surface emissivity is the same as for the bulk copper  $\varepsilon_s = 0.7$  [99]. The heating time was set to 10 s, afterwards the heating rates were normalized for comparison with the experimental results [100].

The simulated heating rates are in a very good agreement with the experimental

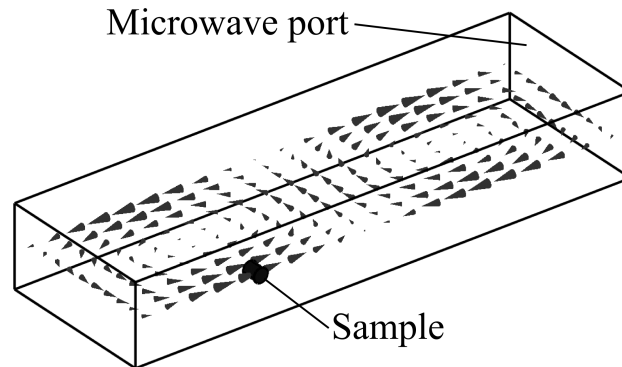


Figure 3.9: The single mode ( $TE_{102}$ ) cavity as used in simulations of the microwave heating in the magnetic field only. The arrows represent the magnetic field. The copper powder compact sample is placed close to the wall, where the magnetic field is strongest

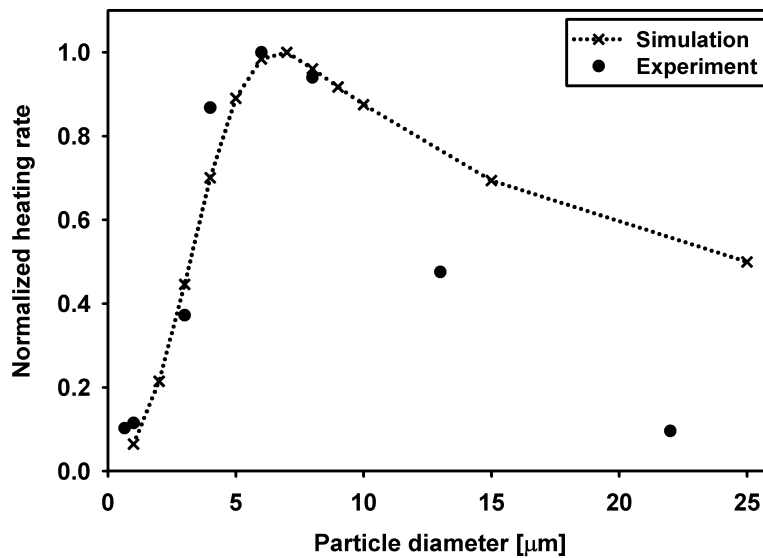


Figure 3.10: Initial heating rate of the copper powder compact. The results of the microwave heating simulations (dotted line with crosses) are compared to the experimental results (dots) taken from [100]

data taken from [100] up to the particle diameter of 8  $\mu\text{m}$  as shown in figure 3.10. In the further range the simulated heating rates are much bigger than experimentally found. As mentioned before in section 3.5 the bigger particles are more likely to create conductive contacts during the compaction procedure [76]. The simulation does not take this effect into account.

### 3.7 Resonance Frequency Dependance

As presented before in section 3.6 the effective magnetic permeability  $\mu$  of metallic powders shows resonant behavior. The resonance frequency, defined as the frequency at the maximum of the resonance peak in  $\mu''$  (3.8(b)), depends on the diameter  $d$  of the metallic particles [101, 102, 103]. The second parameter on which the resonance frequency depends is the conductivity  $\sigma$  of the metallic inclusions.

Four sets of simulations have been performed, to find the dependency of the resonance frequency on the diameter and the conductivity of particles  $f_{res}(d, \sigma)$ . The conductivity of annealed copper  $\sigma_c = 5.8e7$  S/m has been used for the reference set of simulations. Another three sets of simulations were performed for modified conductivities  $\sigma = \sigma_m \sigma_c$ , where  $\sigma_m$  is a modifier taking values 0.1, 0.01 and 0.001. Figure 3.11 shows the resonance frequency  $f_{res}(d, \sigma)$ , for four sets of simulations. The  $f_{res}(d, \sigma)$  follows a simple power law dependency

$$f_{res} = A_d d^{-B_d}, \quad (3.3)$$

where  $A_d$  and  $B_d$  are parameters obtained during the fitting process. The four curves for different conductivities share the same characteristics. The fit parameter  $B_d$  has been found to be alike for all four dependencies,  $B_d = 2$ , with an averaged margin error of 0.2%. The fit parameter  $A_d$  depends only on the conductivity, as shown in figure 3.12

$$A_d = A_\sigma \sigma^{-B_\sigma}. \quad (3.4)$$

The  $B_\sigma$  parameter has been found to be 0.966 with a margin error of 0.22%, and the  $A_\sigma$  parameter  $2.86 \cdot 10^9$  with a margin error of 2.35%. By replacing  $A_d$  in (3.3) with (3.4) one obtains the analytical formula for the resonance frequency function  $f_{res}(d, \sigma)$

$$f_{res} = \frac{A_\sigma}{\sigma^{0.966} d^2}, \quad (3.5)$$

where, for the sake of convenience,  $\sigma$  is in S/m,  $d$  in  $\mu\text{m}$ ,  $f_{res}$  in GHz.

The behavior of (3.5) can be used to predict the resonance frequency of

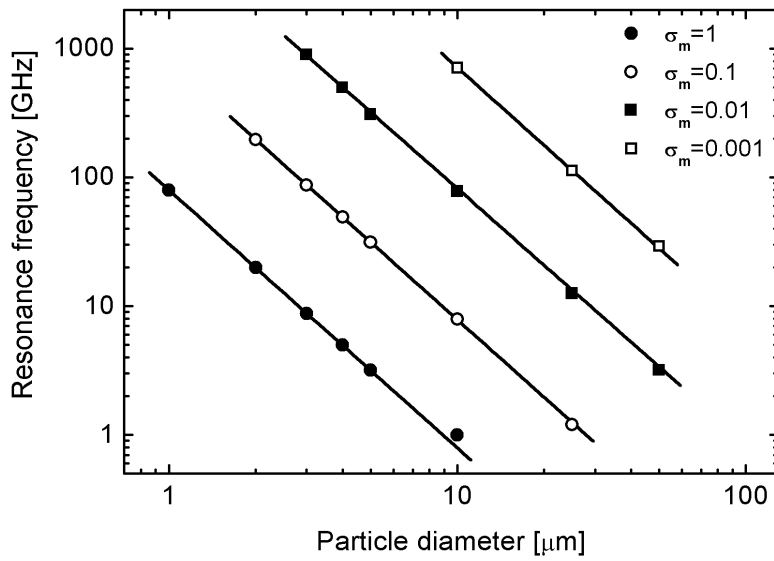


Figure 3.11: The dependence of the resonance frequency  $f_{res}$  on particle diameter, for four different conductivities:  $\sigma = \sigma_c$  (full circles),  $\sigma = 0.1 \cdot \sigma_c$  (empty circles),  $\sigma = 0.01 \cdot \sigma_c$  (full squares) and  $\sigma = 0.001 \cdot \sigma_c$  (empty squares). The solid line curves are fitted functions for all four cases, respectively.

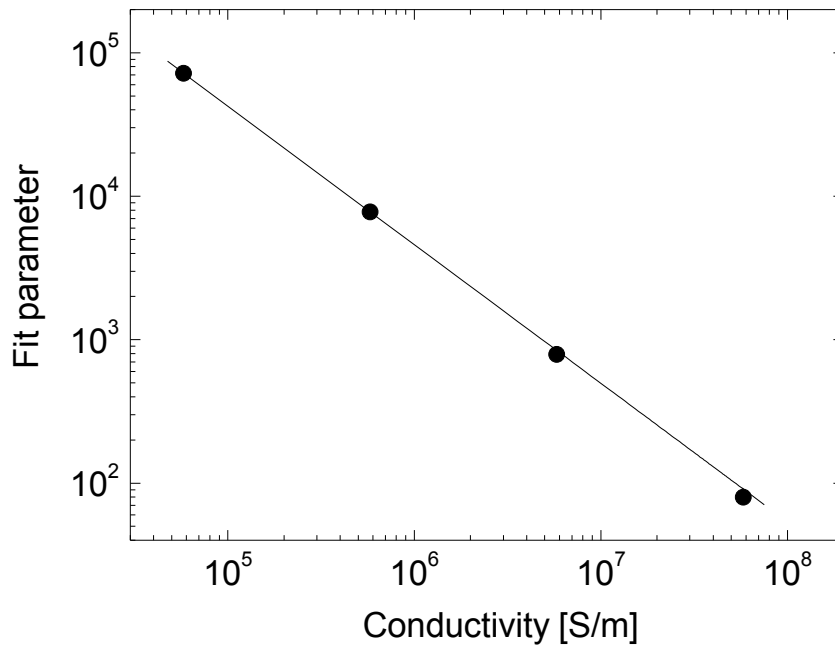


Figure 3.12: The fit parameter  $A_d$  depends only on conductivity, allowing us to use a simple analytical formula to express the dependency for the resonance frequency  $f_{res}$ .

processed metallic powders, or mixtures with dielectrics. The particle diameter dependency allows to heat specific particles, by choosing the correct frequency or the desired inclusion diameter. The resonance frequency is lower for bigger particles and for higher conductivities as well. That fact is important for high temperature, rapid microwave processing of new materials in a wide range of currently available industrial and laboratory furnaces.





# Chapter 4

## Summary

Application of microwave energy for materials processing is emerging as a novel and innovative technology with many advantages over conventional processing, such as reduction in processing cycle time resulting into substantial energy and cost savings, providing finer microstructure leading to improved mechanical properties. Microwave energy is highly versatile in its application to numerous diverse fields such as communication, microwave enhanced chemical reactions, food processing, rubber vulcanization, wood drying, etc. Application of microwave heating in ceramic powder processing was studied since early 1970's. However the microwave processing in powder metallurgy has only been under focus since the pioneering work of Roy and coworkers in 1999. After the discovery that metallic powders do not reflect microwaves like bulk metallic objects, but absorb and heat up in microwave field quite effectively, there has been growing interest in this topic.

A numerical approach for determining effective dielectric and magnetic properties of metallic powders was presented in this work. Similar to the calculation of effective properties of complicated structures of metamaterials, the combination of electromagnetic simulations using FIT and the extraction of effective properties can be used with success in the field of material science. The model of metallic powder consists of periodically arranged spherical conductive particles. The choice of copper as a representative of metals was due to availability of experimental data. The effective properties of the copper powders were simulated using FIT, which gives a general overview of the sample properties in way of scattering parameters. The frequency dependent scattering parameters yield information on effective electromagnetic properties of the investigated material or mixture. By adopting a mathematical formulation from an experimental reflection/transmission-free space measurement method, one can extract the effective dielectric permittivity and the effective magnetic permeability from the scattering parameters. A

numerical procedure has been developed in order to automatically extract the effective electromagnetic properties from the scattering parameters. The extraction procedure has been validated on known materials.

The simulation results are compared to the experimental data allowing to study and understand the basic mechanisms of microwave absorption as well as the sintering of metallic powders. The heating behavior of copper powders in either the electric or the magnetic field is similar however it is driven by different mechanisms. During the sintering in the electric field the microfocusing effect plays an important role. The electric field is much stronger in the contact zones between the particles leading to tremendous dielectric losses in the native oxide layer covering the copper particles. During the sintering in the magnetic field the conductive particles are heated by induced eddy currents. The absorption of the magnetic component depends on the conductivity and the particle size. The simulations over a wide range of frequency showed a resonant behavior in the effective magnetic permeability of copper powders. While the absorption of the electric component can only be explained qualitatively the absorption of the magnetic component of the microwaves is also quantitatively in a good agreement with the experiment results.

The simulations of microwave heating in the separated magnetic field of copper powders with different particle sizes were performed using FEM. The heating results are in very good agreement with the experimentally measured initial heating rates of copper compacts, simultaneously providing validation of the model of metallic powders. Furthermore, studies have been conducted on the influence of the particle size and the conductivity on the resonance frequency of the diamagnetic behavior of the effective magnetic permeability. It has been discovered that that the resonance frequency follows a simple empirical formula which can be effectively utilized.

The numerical modeling of metallic powders and interactions with microwaves is essential to understand the absorption mechanisms, as well as to identify micro and nanoscale microwave effects that lead to enhanced performance of the microwave sintering of powdered metals. It has been shown that the numerical modeling of effective electromagnetic properties of metallic powders can be used with success to analyze the electromagnetic properties and the behavior of such inhomogeneous materials.

# Appendix

## Extraction of the Effective Properties - Script Listing

```
1 clear; //clear variables
2 d=1e-3;//thickness of the slab [m]
3 dvac=1e-3;//thickness of additional free space [m]
4 //first part – files to load
5 //1=abs(S11),2=abs(S21),3=arg(S11),4=arg(S21)
6 INPUTFILE1      = '00_S11abs.txt';
7 INPUTFILE2      = '00_S21abs.txt';
8 INPUTFILE3      = '00_S11arg.txt';
9 INPUTFILE4      = '00_S21arg.txt';
10 OUTPUTFILE     = '00';//output file prefix
11
12 //second part (reference data) – files to load
13 //1=real(eps),2=imag(eps),3=real(mue),4=imag(mue)
14 INPUTFILE1x     = '00_eps1_lorentz_50GHz.txt';
15 INPUTFILE2x     = '00_eps2_lorentz_50GHz.txt';
16 INPUTFILE3x     = '00_mue1_lorentz_25GHz.txt';
17 INPUTFILE4x     = '00_mue2_lorentz_25GHz.txt';
18
19 //constants
20 EPS0=8.8541878176e-12;//permittivity of free space [F/m]
21 MUE0=4*%pi*1e-7;//permeability of free space [N*A^-2]
22 c0=1/sqrt(EPS0*MUE0);//speed of light in vacuum [m/s]
23 Z0=120*%pi;//wave impedance of free space [ohms]
24
25 ///FUNCTION DEFINITIONS START HERE///
26 //phase correction procedure
27 function [S11arg2,S21arg2]
28     =phase_correction(f,dvac,S11arg,S21arg);
29 S11arg2=S11arg+(2.*%pi.*(f.*1e9).*2.*dvac./c0);
```

```

30 S21arg2=S21arg+(2.*%pi.*(f.*1e9).*2.*dovac./c0);
31 S11arg2y=S11arg2;
32 S21arg2y=S21arg2;
33
34 T1=1;T2=1; //iterative shifting of phase (-pi,pi)
35 while T1==1 & T2==1
36     for i=1:1:size1
37         if S11arg2y(i)<-%pi then
38             n1(i)=floor(S11arg2y(i)/(-%pi));
39             S11arg2y(i)=S11arg2y(i)+n1(i)*2*%pi;
40         end
41         if S11arg2y(i)>%pi then
42             m1(i)=floor(S11arg2y(i)/(%pi));
43             S11arg2y(i)=S11arg2y(i)-m1(i)*2*%pi;
44         end
45         if S21arg2y(i)<-%pi then
46             n2(i)=floor(S21arg2y(i)/(-%pi));
47             S21arg2y(i)=S21arg2y(i)+n2(i)*2*%pi;
48         end
49         if S21arg2y(i)>%pi then
50             m2(i)=floor(S21arg2y(i)/(%pi));
51             S21arg2y(i)=S21arg2y(i)-m2(i)*2*%pi;
52         end
53         T1=0;T2=0;
54         if S11arg2y(i)<-%pi | S11arg2y(i)>%pi then
55             T1=1;
56         end
57         if S21arg2y(i)<-%pi | S21arg2y(i)>%pi then
58             T2=1;
59         end
60     end
61 end
62 S11arg2=S11arg2y;
63 S21arg2=S21arg2y;
64 endfunction
65
66 //calculate complex S-parameters
67 function [S11,S21]
68     =obt_S11_and_S21(S11abs,S21abs,S11arg,S21arg);
69 S11=S11abs.*exp(1.*%i.*S11arg);

```

```

70 S21=S21abs.*exp(1.*%i.*S21arg);
71 endfunction
72
73 //calculate reflection and transmission coefficients
74 function [R,T]
75     =obt_R_and_T(S11,S21);
76 K=(S11^2-S21^2+1)./(2.*S11);
77 R=K+sqrt(K^2-1);
78 T=(S11+S21-R)./(1-R.*(S11+S21));
79 endfunction
80
81 //calculate material properties
82 function [eps,mu,z,n,LAMBDA]
83     =obt00(f,S11,S21,d)
84 K=(S11^2-S21^2+1)./(2.*S11);
85 GAM1=K+sqrt(K.^2-1);
86 GAM2=K-sqrt(K.^2-1);
87 GAM=GAM2;
88 [i1,i2]=size(K);
89 for i=1:1:i1 do
90     if abs(GAM1(i))<1 & abs(GAM2(i))>1 then
91         GAM(i)=GAM1(i);
92     end
93     if abs(GAM1(i))>1 & abs(GAM2(i))<1 then
94         GAM(i)=GAM2(i);
95     end
96 end
97
98 z = (1 + GAM)./(1 - GAM);
99 R = (z - 1)./(z + 1);
100
101 lambda0=(c0.*ones(i1))./(f.*1e9);
102 gam0=(%i*%pi*2)./lambda0;
103
104 T=(S11+S21-GAM)./(1-GAM.*(S11+S21));
105 Tabs=abs(T);
106 Targ=atan(imag(T),real(T));
107
108 ni=0;
109 gam=log(ones(i1)./Tabs)./d+%i*(2*%pi*ni-Targ)./d;

```

```

110
111 eps=(gam./gam0).*((1-GAM)./(1+GAM));
112 mu=(gam./gam0).*((1+GAM)./(1-GAM));
113
114 n=sqrt(eps.*mu);
115 LAMBDA=c0./(1e9.*f.*real(n));
116
117 //higher n-branches, manual adjustment if needed
118 ni2=1;
119 for i=173:1:263 do
120     gam(i)=log(1./Tabs(i))./d+%i*(2.*%pi*ni2-Targ(i))./d;
121 end
122
123 ni2=0;
124 for i=264:1:i1 do
125     gam(i)=log(1./Tabs(i))./d+%i*(2.*%pi*ni2-Targ(i))./d;
126 end
127 //repeat if needed
128
129 eps=(gam./gam0).*((1-GAM)./(1+GAM)); //recalculate
130 mu=(gam./gam0).*((1+GAM)./(1-GAM));
131
132 n=sqrt(eps.*mu); //recalculate refractive index
133 LAMBDA=c0./(1e9.*f.*real(n)); //wavelength (material)
134 endfunction
135
136 //calculate ref. index and impedance (reference)
137 function [n,z]
138     =calc_ref_index_and_Z(EPS,MUE)
139 n=sqrt(EPS.*MUE);
140 z=sqrt(MUE./EPS);
141 endfunction
142
143 //calculate reflection and transmission (reference)
144 function [R,T]
145     =calc_R_and_T(f,z,n,d)
146 R=(z+1)./(z-1);
147 k0=(2.*%pi.*f.*1e9)./(c0);
148 T=exp(1.*%i.*k0.*n.*d);
149 endfunction

```

```

150
151 // calculate S-parameters (reference)
152 function [S11,S21,S11abs,S21abs,S11arg,S21arg]
153     =calc_S11_and_S21(R,T);
154 S11=(R.*(1-T.^2))./(1-R.^2.*T.^2);
155 S21=(T.*(1-R.^2))./(1-R.^2.*T.^2);
156 S11abs=sqrt(real(S11).^2+imag(S11).^2);
157 S21abs=sqrt(real(S21).^2+imag(S21).^2);
158 S11arg=atan(imag(S11),real(S11));
159 S21arg=atan(imag(S21),real(S21));
160 endfunction
161 ///FUNCTION DEFINITIONS END HERE///
162
163 // first part
164 //load files
165 N1=fscanfMat(INPUTFILE1);
166 N2=fscanfMat(INPUTFILE2);
167 N1arg=fscanfMat(INPUTFILE3);
168 N2arg=fscanfMat(INPUTFILE4);
169
170 [size1,size2]=size(N1);
171 clear size2;
172
173 //read vectors
174 x=N1(:,1);
175 S11abs=N1(:,2);
176 S21abs=N2(:,2);
177 S11arg=N1arg(:,2).*(1*%pi/180); //switch to radians
178 S21arg=N2arg(:,2).*(1*%pi/180);
179
180 v=x; f=x;
181
182 //apply phase correction if dvac is not equal 0
183 if dvac~=0 then
184     [S11arg,S21arg]=phase_correction(f,dvac,S11arg,S21arg);
185 end
186
187 // calculate complex Sxx parameters
188 [S11,S21]=obt_S11_and_S21(S11abs,S21abs,S11arg,S21arg);
189

```

```

190 //calculate reflection and transmission
191 [R,T]=obt_R_and_T(S11,S21);
192
193 //calculate material properties
194 [eps,mu,z,n,LAMBDA] = obt00(f,S11,S21,d);
195
196 //second part – reference data
197 //load files
198 N1x=fscanfMat(INPUTFILE1x);
199 N2x=fscanfMat(INPUTFILE2x);
200 N3x=fscanfMat(INPUTFILE3x);
201 N4x=fscanfMat(INPUTFILE4x);
202
203 vx=N1x(:,1); fx=vx;
204 [size1x,size2x]=size(N1x); clear size2x;
205
206 //read vectors
207 EPS1x=N1x(:,2);
208 EPS2x=N2x(:,2);
209 MUE1x=N3x(:,2);
210 MUE2x=N4x(:,2);
211
212 //reference material properties
213 EPSx=EPS1x-%i.*EPS2x;
214 MUEx=MUE1x-%i.*MUE2x;
215
216 //reference ref. index and impedance
217 [nx,zx]=calc_ref_index_and_Z(EPSx,MUEx);
218
219 dx=d; //slab thickness
220
221 //reference reflection and transmission coefficients
222 [Rx,Tx]=calc_R_and_T02(fx,EPSx,MUEx,dx);
223
224 //reference S-parameters
225 [S11x,S21x,S11xabs,S21xabs,S11xarg,S21xarg]
226 =calc_S11_and_S21(Rx,Tx);
227
228 //plot permittivity and permeability and reference data
229 subplot(121);

```



```
230 plot(v, real(eps), "b"); plot(vx, real(EPSx), "r");
231 plot(v, real(mu), "k"); plot(vx, real(MUEx), "g");
232 subplot(122);
233 plot(v, -1.*imag(eps), "b"); plot(vx, -1.*imag(EPSx), "r");
234 plot(v, -1.*imag(mu), "k"); plot(vx, -1.*imag(MUEx), "g");
235
236
237 //save to files
238 FINALMAT1=[v, real(z), imag(z), real(n), imag(n)];
239 fprintfMat(OUTPUTFILE+'.mat1', FINALMAT1, "%e");
240 FINALMAT2=[v, real(eps), imag(eps), real(mu), imag(mu)];
241 fprintfMat(OUTPUTFILE+'.mat2', FINALMAT2, "%e");
242 FINALMAT1x=[vx, real(zx), imag(zx), real(nx), imag(nx)];
243 fprintfMat(OUTPUTFILE+'.mat1x', FINALMAT1x, "%e");
244 FINALMAT2x=[vx, real(EPSx), imag(EPSx), real(MUEx), imag(MUEx)];
245 fprintfMat(OUTPUTFILE+'.mat2x', FINALMAT2x, "%e");
```



# Bibliography

- [1] H. Sobol and K. Tomiyasu. Milestones of microwaves. *Microwave Theory and Techniques, IEEE Transactions on*, 50(3): pp. 594–611, 2002. [cited at p. 1]
- [2] J. M. Osepchuk. A History of Microwave Heating Applications. *Microwave Theory and Techniques, IEEE Transactions on*, 32(9): pp. 1200–1224, 1984. [cited at p. 1]
- [3] J. M. Osepchuk. The history of the microwave oven: A critical review. In *Microwave Symposium Digest, 2009. MTT '09. IEEE MTT-S International*, pages pp. 1397–1400, 2009. [cited at p. 1]
- [4] N. E. Bengtsson and T. Ohlsson. Microwave heating in the food industry. *Proceedings of the IEEE*, 62(1): pp. 44–55, 1974. [cited at p. 1]
- [5] P. O. Risman and M. Celuch-Marcysiak. Electromagnetic modelling for microwave heating applications. In *Microwaves, Radar and Wireless Communications. 2000. MIKON-2000. 13th International Conference on*, volume 3, pages pp. 167–182 vol.3, 2000. [cited at p. 1]
- [6] T. Tsukagoshi. Study on microwave energy absorption in wedge type electromagnetic wave absorber and its application to microwave heating. In *Electromagnetic Compatibility, 1995. Symposium Record. 1995 IEEE International Symposium on*, pages pp. 568–572, 1995. [cited at p. 1]
- [7] Pat Hulls and Ralph Shute. Dielectric heating in industry application of radio frequency and microwaves. *Physical Science, Measurement and Instrumentation, Management and Education - Reviews, IEE Proceedings A*, 128(9): pp. 583–588, 1981. [cited at p. 2]
- [8] P. B. Kenington and D. W. Bennett. Living in harmony-industrial microwave heating and cellular radio. *Engineering Science and Education Journal*, 2(5): pp. 233–239, 1993. [cited at p. 2]

- [9] A. W. Fliflet, R. W. Bruce, A. K. Kinkead, R. P. Fischer, D. Lewis, III, R. Rayne, B. Bender, L. K. Kurihara, Gan-Moog Chow, and P. E. Schoen. Application of microwave heating to ceramic processing: Design and initial operation of a 2.45 GHz single-mode furnace. *Plasma Science, IEEE Transactions on*, 24(3): pp. 1041–1049, 1996. [cited at p. 2]
- [10] Youg Hee Lee. The industrial application of uniformly dispersing microwave and heating system. In *Microwave and Millimeter Wave Technology, 2002. Proceedings. ICMMT 2002. 2002 3rd International Conference on*, pages pp. 293–295, 2002. [cited at p. 2]
- [11] Yeongseob Kueon. The potential for material processing by microwave energy. In *Control, Automation and Systems, 2008. ICCAS 2008. International Conference on*, pages pp. 1966–1971, 2008. [cited at p. 2]
- [12] S. K. Shah and M. A. Joshi. Application of microwave heating in vacuum for bagasse drying. In *Recent Advances in Microwave Theory and Applications, 2008. MICROWAVE 2008. International Conference on*, pages pp. 477–479, 2008. [cited at p. 2]
- [13] A. Rosen and F. Sterzer. Applications of microwave heating in medicine. In *Microwave Symposium Digest, 1994., IEEE MTT-S International*, volume 3, pages pp. 1615–1618, 1994. [cited at p. 3]
- [14] Peter E. Glaser. Power from the Sun: Its Future. *Science*, 162(3856): pp. 857–861, 1968. [cited at p. 3]
- [15] R. L. Coble. Sintering Crystalline Solids. I. Intermediate and Final State Diffusion Models. *Journal of Applied Physics*, 32(5): pp. 787–792, 1961. [cited at p. 7]
- [16] Pei-Lin Chen and I-Wei Chen. Sintering of Fine Oxide Powders: II, Sintering Mechanisms. *Journal of the American Ceramic Society*, 80(3): pp. 637–645, 1997. [cited at p. 7]
- [17] I. Wei Chen and X. H. Wang. Sintering dense nanocrystalline ceramics without final-stage grain growth. *Nature*, 404(6774): pp. 168–171, 2000. [cited at p. 8]
- [18] D. Lynn Johnson and Ivan B. Cutler. Diffusion Sintering: I, Initial Stage Sintering Models and Their Application to Shrinkage of Powder Compacts.

- Journal of the American Ceramic Society*, 46(11): pp. 541–545, 1963.  
[cited at p. 8]
- [19] D. Lynn Johnson and Ivan B. Cutler. Diffusion Sintering: II, Initial Sintering Kinetics of Alumina. *Journal of the American Ceramic Society*, 46(11): pp. 545–550, 1963. [cited at p. 8]
- [20] R. M. German and Z. A. Munir. Surface Area Reduction During Isothermal Sintering. *Journal of the American Ceramic Society*, 59(9-10): pp. 379–383, 1976. [cited at p. 8]
- [21] N. Dolet, J. M. Heintz, L. Rabardel, M. Onillon, and J. P. Bonnet. Sintering mechanisms of 0.99 SnO<sub>2</sub>-0.01 CuO mixtures. *Journal of Materials Science*, 30: pp. 365–368, 1995. [cited at p. 8]
- [22] G. C. Kuczynski. Self-diffusion in sintering of metallic particles. *Trans. A.I.M.E.*, 185(2): pp. 169–178, 1949. [cited at p. 8]
- [23] B. Kanka and H. Schneider. Sintering mechanisms and microstructural development of coprecipitated mullite. *Journal of Materials Science*, 29: pp. 1239–1249, 1994. [cited at p. 8]
- [24] Robert E. Collin. *Foundations for Microwave Engineering*. Wiley-IEEE Press, 2 edition, 2000. [cited at p. 9]
- [25] John D. Jackson. *Classical Electrodynamics*. Wiley, third edition, 1998. [cited at p. 13]
- [26] Mário G. Silveirinha. Examining the validity of Kramers-Kronig relations for the magnetic permeability. *Phys. Rev. B*, 83: 165119, 2011. [cited at p. 13]
- [27] T. Weiland. A Discretization Method for the Solution of Maxwell's Equations for Six-Component Fields. *Electronics and Communications AEUE*, 31: pp. 116–120, 1977. [cited at p. 13]
- [28] T. Weiland. Time Domain Electromagnetic Field Computation with Finite Difference Methods. *International Journal of Numerical Modelling: Electronic Networks, Devices and Fields*, 9: pp. 295–319, 1996. [cited at p. 13]
- [29] CST Computer Simulation Technology AG, available at <http://www.cst.com>. [cited at p. 13]

- [30] Kane Yee. Numerical solution of initial boundary value problems involving Maxwell's equations in isotropic media. *Antennas and Propagation, IEEE Transactions on*, 14(3): pp. 302–307, 1966. [cited at p. 15]
- [31] T. Wieland. Rechnergestützte Methoden zur Berechnung von Feldern. Skriptum zum Vorlesung Feldtheorie II, 1998. [cited at p. 17]
- [32] U. van Rienen. *Numerical Methods in Computational Electrodynamics - Linear Systems in Practical Applications*. Springer, 2001. [cited at p. 17]
- [33] U. van Rienen. Vorlesungskript Theoretische Elektrotechnik, 2007. [cited at p. 17]
- [34] J. P. Berenger. A perfectly matched layer for the absorption of electromagnetic waves. *Journal of Computational Physics*, 114: pp. 185–200, 1994. [cited at p. 17]
- [35] Maria A. Stuchly and Stanislaw S. Stuchly. Coaxial Line Reflection Methods for Measuring Dielectric Properties of Biological Substances at Radio and Microwave Frequencies - A Review. *Instrumentation and Measurement, IEEE Transactions on*, 29(3): pp. 176–183, 1980. [cited at p. 23]
- [36] M. N. Afsar, J. R. Birch, R. N. Clarke, and G. W. Chantry. The measurement of the properties of materials. *Proceedings of the IEEE*, 74(1): pp. 183–199, 1986. [cited at p. 23]
- [37] A. P. Gregory and R. N. Clarke. A review of RF and microwave techniques for dielectric measurements on polar liquids. *Dielectrics and Electrical Insulation, IEEE Transactions on*, 13(4): pp. 727–743, 2006. [cited at p. 23]
- [38] Jyh Sheen. Comparisons of microwave dielectric property measurements by transmission/reflection techniques and resonance techniques. *Measurement Science and Technology*, 20(4): 042001, 2009. [cited at p. 23]
- [39] D. K. Ghodgaonkar, V. V. Varadan, and V. K. Varadan. A Free-Space Method for Measurement of Dielectric Constants and Loss Tangents at Microwave Frequencies. *IEEE Trans. Instrum. Meas.*, 37: pp. 789–793, 1989. [cited at p. 25]
- [40] D. K. Ghodgaonkar, V. V. Varadan, and V. K. Varadan. Free-space measurement of complex permittivity and complex permeability of magnetic materials at microwave frequencies. *Instrumentation and Measurement, IEEE Transactions on*, 39(2): pp. 387–394, 1990. [cited at p. 25, 27]

- [41] V. V. Varadan, R. D. Hollinger, D. K. Ghodgaonkar, and V. K. Varadan. Free-space, broadband measurements of high-temperature, complex dielectric properties at microwave frequencies. *Instrumentation and Measurement, IEEE Transactions on*, 40(5): pp. 842–846, 1991. [cited at p. 25]
- [42] S. Trabelsi, A. W. Kraszewski, and S. O. Nelson. A microwave method for on-line determination of bulk density and moisture content of particulate materials. *Instrumentation and Measurement, IEEE Transactions on*, 47(1): pp. 127–132, 1998. [cited at p. 25]
- [43] Samir Trabelsi and Stuart O Nelson. Free-space measurement of dielectric properties of cereal grain and oilseed at microwave frequencies. *Measurement Science and Technology*, 14(5): p. 589, 2003. [cited at p. 25]
- [44] T. Weiland, R. Schuhmann, R. B. Gregor, C. G. Parazzoli, A. M. Vetter, D. R. Smith, D. C. Vier, and S. Schultz. Ab initio numerical simulation of left-handed metamaterials: Comparison of calculations and experiments. *J. Appl. Phys.*, 90: pp. 5419–5424, 2001. [cited at p. 26]
- [45] D. R. Smith, S. Schultz, P. Markoš, and C. M. Soukoulis. Determination of effective permittivity and permeability of metamaterials from reflection and transmission coefficients. *Phys. Rev. B*, 65: 195104, 2002. [cited at p. 26]
- [46] M. Bayindir, K. Aydin, E. Ozbay, P. Markos, and C. M. Soukoulis. Transmission properties of composite metamaterials in free space. *Applied Physics Letters*, 81(1): pp. 120–122, 2002. [cited at p. 26]
- [47] Kin Li, S. J. McLean, R. B. Gregor, C. G. Parazzoli, and M. H. Tanielian. Free-space focused-beam characterization of left-handed materials. *Applied Physics Letters*, 82(15): pp. 2535–2537, 2003. [cited at p. 26]
- [48] P. Markoš and C. M. Soukoulis. Transmission properties and effective electromagnetic parameters of double negative metamaterials. *Opt. Express*, 11: pp. 649–661, 2003. [cited at p. 26]
- [49] Xudong Chen, Tomasz M. Grzegorzcyk, Bae-Ian Wu, Jr. Joe Pacheco, and Jin Au Kong. Robust method to retrieve the constitutive effective parameters of metamaterials. *Phys. Rev. E*, 70: 016608, 2004. [cited at p. 26]
- [50] Xudong Chen, Bae-Ian Wu, Jin Au Kong, and Tomasz M. Grzegorzcyk. Retrieval of the effective constitutive parameters of bianisotropic metamaterials. *Phys. Rev. E*, 71: 046610, 2005. [cited at p. 26]

- [51] G. Lubkowski, R. Schuhmann, and T. Weiland. Extraction of Effective Metamaterial Parameters by Parameter Fitting of Dispersive Models. *Microwave and Optical Technology Letters*, 49: pp. 285–288, 2007. [cited at p. 26]
- [52] G. Lubkowski. *Simulation of Electromagnetic Fields in Double Negative Metamaterials*. PhD thesis, Technische Universität Darmstadt, 2009. [cited at p. 26]
- [53] L. F. Chen, C. K. Ong, C. P. Neo, V. V. Varadan, and V. K. Varadan. *Microwave Electronics: Microwave Theory and Techniques for Materials Characterization*. John Wiley & Sons, Ltd, 2004. [cited at p. 27]
- [54] V. V. Varadan and R. Ro. Unique Retrieval of Complex Permittivity and Permeability of Dispersive Materials From Reflection and Transmitted Fields by Enforcing Causality. *Microwave Theory and Techniques, IEEE Transactions on*, 55(10): pp. 2224 –2230, 2007. [cited at p. 31]
- [55] U. C. Hasar and O. Simsek. A calibration-independent microwave method for position-insensitive and nonsingular dielectric measurements of solid materials. *Journal of Physics D: Applied Physics*, 42(7): 075403, 2009. [cited at p. 31]
- [56] Zsolt Szabó, Gi-Ho Park, Ravi Hedge, and Er-Ping Li. A Unique Extraction of Metamaterial Parameters Based on Kramers-Kronig Relationship. *Microwave Theory and Techniques, IEEE Transactions on*, 58(10): pp. 2646 –2653, 2010. [cited at p. 31]
- [57] U.C. Hasar. A Generalized Formulation for Permittivity Extraction of Low-to-High-Loss Materials From Transmission Measurement. *Microwave Theory and Techniques, IEEE Transactions on*, 58(2): pp. 411–418, 2010. [cited at p. 31]
- [58] Xing-Xiang Liu, David A. Powell, and Andrea Alù. Correcting the Fabry-Perot artifacts in metamaterial retrieval procedures. *Phys. Rev. B*, 84: 235106, 2011. [cited at p. 31]
- [59] Y. V. Bykov, K. I. Rybakov, and V. E. Semenov. High-temperature microwave processing of materials. *J. Phys. D: Appl. Phys.*, 34: pp. R55–R75, 2001. [cited at p. 37]



- [60] Yu. V. Bykov, S. V. Egorov, A. G. Ereemeev, K. I. Rybakov, V. E. Semenov, A. A. Sorokin, and S. A. Gusev. Evidence for microwave enhanced mass transport in the annealing of nanoporous alumina membranes. *Journal of Materials Science*, 36: pp. 131–136, 2001. [cited at p. 38]
- [61] D. Agrawal. Latest global developments in microwave materials processing. *Materials Research Innovations*, 14(1): pp. 3–8, 2010. [cited at p. 38, 42]
- [62] R. Roy, D. Agrawal, J. Cheng, and S. Gedevarishvili. Full sintering of powdered-metal bodies in a microwave field. *Nature*, 399: pp. 668–670, 1999. [cited at p. 38]
- [63] R. M. Anklekar, D. K. Agrawal, and R. Roy. Microwave sintering and mechanical properties of PM copper steel. *Powder Metallurgy*, 44: pp. 355–362, 2001. [cited at p. 39]
- [64] G. Sethi, A. Upadhyaya, and D. Agrawal. Microwave and conventional sintering of premixed and prealloyed Cu-12Sn bronze. *Science of Sintering*, 35(2): pp. 49–65, 2003. [cited at p. 39]
- [65] Tasnim Firdaus Ariff, Brian Gabbitas, and Deliang Zhang. The effect of powder sintering method on the densification and microstructure of pewter alloys. *IOP Conference Series: Materials Science and Engineering*, 4(1): 012023, 2009. [cited at p. 40]
- [66] C. Padmavathi, A. Upadhyaya, and D. Agrawal. Effect of microwave and conventional heating on sintering behavior and properties of Al-Mg-Si-Cu alloy. *Materials Chemistry and Physics*, 130: pp. 449–457, 2011. [cited at p. 40]
- [67] Chandran Padmavathi, Anish Upadhyaya, and Dinesh Agrawal. Microwave Assisted Sintering of Al-Cu-Mg-Si-Sn Alloy. *Journal of Microwave Power and Electromagnetic Energy*, 46(3): pp. 115–127, 2012. [cited at p. 40]
- [68] Avijit Mondal, Dinesh Agrawal, and Anish Upadhyaya. Microwave Sintering of Refractory Metals/alloys: W, Mo, Re, W-Cu, W-Ni-Cu and W-Ni-Fe Alloys. *Journal of Microwave Power and Electromagnetic Energy*, 44(1): pp. 28–44, 2010. [cited at p. 40]
- [69] K. Venkateswarlu, Suman Saurabh, V. Rajinikanth, Ranjan Sahu, and Ajoy Ray. Synthesis of TiN Reinforced Aluminium Metal Matrix Composites

- Through Microwave Sintering. *Journal of Materials Engineering and Performance*, 19: pp. 231–236, 2010. [cited at p. 41]
- [70] Wong Wai Leong Eugene and Manoj Gupta. Characteristics of Aluminum and Magnesium Based Nanocomposites Processed Using Hybrid Microwave Sintering. *Journal of Microwave Power and Electromagnetic Energy*, 44(1): pp. 14–27, 2010. [cited at p. 41]
- [71] A. Raja Annamalai, A. Upadhaya, and D. Agarwal. Effect of heating mode on sintering of ferrous compacts through powder metallurgy route. *International Heat Treatment & Surface Engineering*, 5(4): pp. 155–160, 2011. [cited at p. 42]
- [72] Keiichiro Kashimura, Motoyasu Sato, Masahiro Hotta, Dinesh Kumar Agrawal, Kazuhiro Nagata, Miyuki Hayashi, Tomohiko Mitani, and Naoki Shinohara. Iron production from  $\text{Fe}_3\text{O}_4$  and graphite by applying 915 MHz microwaves. *Materials Science and Engineering: A*, 556(0): pp. 977–979, 2012. [cited at p. 42]
- [73] Noboru Yoshikawa. Fundamentals and Applications of Microwave Heating of Metals. *Journal of Microwave Power and Electromagnetic Energy*, 44(1): pp. 4–13, 2010. [cited at p. 42]
- [74] Jiping Cheng, Rustum Roy, and Dinesh Agrawal. Experimental proof of major role of magnetic field losses in microwave heating of metal and metallic composites. *Journal of Materials Science Letters*, 20: pp. 1561–1563, 2001. [cited at p. 43, 60]
- [75] J. Cheng, R. Roy, and D. Agrawal. Radically different effects on materials by separated microwave electric and magnetic fields. *Mater. Res. Innov.*, 5: pp. 170–177, 2002. [cited at p. 44, 60, 61]
- [76] J. Ma, J. F. Diehl, E. J. Johnson, K. R. Martin, N. M. Miskovsky, C. T. Smith, G. J. Weisel, B. L. Weiss, and D. T. Zimmerman. Systematic study of microwave absorption, heating, and microstructure evolution of porous copper powder metal compacts. *J. Appl. Phys.*, 101: 074906, 2007. [cited at p. 45, 52, 54, 60, 61, 63, 65]
- [77] Rustum Roy, Ramesh Peelamedu, Larry Hurtt, Jiping Cheng, and Dinesh Agrawal. Definitive experimental evidence for Microwave Effects: radically new effects of separated E and H fields, such as decrystallization of

- oxides in seconds. *Materials Research Innovations*, 6: pp. 128–140, 2002. [cited at p. 45, 60]
- [78] M. Tanaka, H. Kono, and K. Maruyama. Selective Heating Mechanism of Magnetic Metal Oxides by Alternating Magnetic Field in Microwave Sintering Process. *ArXiv e-prints*, 2009. [cited at p. 45]
- [79] Tomotsugu Kato, Kosei Kobayashi, Noboru Yoshikawa, and Shoji Taniguchi. Microstructure Analysis of  $\text{Fe}_3\text{O}_4$  Heated by Microwaves in a  $\text{TE}_{10}$  Mode Cavity: Surface and Volume Characterization. *Journal of Microwave Power and Electromagnetic Energy*, 45(2): pp. 79–85, 2011. [cited at p. 45]
- [80] Jirun Luo, Christian Hunyar, Lambert Feher, Guido Link, Manfred Thumm, and Paolo Pozzo. Theory and experiments of electromagnetic loss mechanism for microwave heating of powdered metals. *Appl. Phys. Lett.*, 84: pp. 5076–5078, 2004. [cited at p. 46]
- [81] K. I. Rybakov, V. E. Semenov, S. V. Egorov, A. G. Ereemeev, I. V. Plotnikov, and Yu. V. Bykov. Microwave heating of conductive powder materials. *J. Appl. Phys.*, 99: 023506, 2006. [cited at p. 47]
- [82] P. Mishra, G. Sethi, and A. Upadhyaya. Modeling of Microwave Heating of Particulate Metals. *Metallurgical and Materials Transactions B*, 37b: pp. 839–845, 2006. [cited at p. 48]
- [83] V. D. Buchelnikov, D. V. Louzguine-Luzgin, G. Xie, S. Li, N. Yoshikawa, M. Sato, A. P. Anzulevich, I. V. Bychkov, and A. Inoue. Heating of metallic powders by microwaves: Experiment and theory. *Journal of Applied Physics*, 104(11): 113505, 2008. [cited at p. 49]
- [84] E. M. Kiley, V. V. Yakovlev, K. Ishizaki, and S. Vaucher. Applicability study of classical and contemporary models for effective complex permittivity of metal powders. *Journal of Microwave Power and Electromagnetic Energy*, 46(1): pp. 26–38, 2012. [cited at p. 49]
- [85] G. Veltl, F. Petzold, and P. A. Pueschner. Effect of microwaves on sintering process. In *Powder Metallurgy 2004 World Congress*, pages pp. 107–112, 2004. [cited at p. 50, 52, 55]
- [86] D. Demirskyi, D. Agrawal, and A. Ragulya. Neck growth kinetics during microwave sintering of copper. *Scripta Materialia*, 62(8): pp. 552–555, 2010. [cited at p. 50, 55]

- [87] D. Demirskyi, D. Agrawal, and A. Ragulya. Neck formation between copper spherical particles under single-mode and multimode microwave sintering. *Materials Science and Engineering: A*, 527: pp. 2142–2145, 2010. [cited at p. 50, 55]
- [88] D. Demirskyi, D. Agrawal, and A. Ragulya. Neck growth kinetics during microwave sintering of nickel powder. *Journal of Alloys and Compounds*, 509(5): pp. 1790–1795, 2011. [cited at p. 50, 55]
- [89] D. Demirskyi, D. Agrawal, and A. Ragulya. A scaling law study of the initial stage of microwave sintering of iron spheres. *Scripta Materialia*, 66(6): pp. 323–326, 2012. [cited at p. 50, 51, 55]
- [90] Dmytro Demirskyi, Hanna Borodianska, Dinesh Agrawal, Andrey Ragulya, Yoshio Sakka, and Oleg Vasylykiv. Peculiarities of the neck growth process during initial stage of spark-plasma, microwave and conventional sintering of WC spheres. *Journal of Alloys and Compounds*, 523: pp. 1–10, 2012. [cited at p. 51]
- [91] D. Gershon, J. P. Calame, and A. Birnboim. Complex permittivity measurements and mixing laws of alumina composites. *J. Appl. Phys.*, 89: pp. 8110–8116, 2001. [cited at p. 54]
- [92] T. Galek, K. Porath, E. Burkel, and U. van Rienen. Extraction of effective permittivity and permeability of metallic powders in the microwave range. *Modelling and Simulation in Materials Science and Engineering*, 18(2): 025015, 2010. [cited at p. 55, 61]
- [93] D. L. Johnson. Microwave Heating of Grain Boundaries in Ceramics. *J. Am. Ceram. Soc.*, 74: p. 849, 1991. [cited at p. 55]
- [94] K. I. Rybakov and V. E. Semenov. Mass transport in ionic crystals induced by the ponderomotive action of a high-frequency electric field. *Phys. Rev. B*, 52: 3030, 1995. [cited at p. 55]
- [95] A. Birnboim, J. P. Calame, and Y. Carmel. Microfocusing and polarization effects in spherical neck ceramic microstructures during microwave processing. *J. Appl. Phys.*, 85: pp. 478–482, 1999. [cited at p. 55]
- [96] T. T. Meek, R. D. Blake, J. D. Katz, J. R. Bradberry, and M. H. Brooks. Cation diffusion in glass heated using 2.45 GHz radiation. *J. Mater. Sci. Lett.*, 7: pp. 928–931, 1988. [cited at p. 55]

- [97] Maxim Ignatenko, Motohiko Tanaka, and Motoyasu Sato. Absorption of Microwave Energy by a Spherical Nonmagnetic Metal Particle. *Japanese Journal of Applied Physics*, 48(6): 067001, 2009. [cited at p. 63]
- [98] M. Ignatenko and M. Tanaka. Effective permittivity and permeability of coated metal powders at microwave frequency. *Physica B: Condensed Matter*, 405(1): pp. 352–358, 2010. [cited at p. 63]
- [99] J. Ma, C. T. Smith, G. J. Weisel, B. L. Weiss, N. M. Miskovsky, and D. T. Zimmerman. Single Mode Microwave Heating of Copper Powder Metal Compacts. *Excerpt from the Proceedings of the COMSOL Users Conference 2006 Boston*, 2006. [cited at p. 63]
- [100] J. Ma, J. F. Diehl, E. J. Johnson, K. R. Martin, N. M. Miskovsky, C. T. Smith, G. J. Weisel, B. L. Weiss, and D. T. Zimmerman. Erratum: “Systematic study of microwave absorption, heating, and microstructure evolution of porous copper powder metal compacts”. *J. Appl. Phys.*, 102: 109902, 2007. [cited at p. 63, 64, 65]
- [101] Avijit Mondal, Dinesh Agrawal, and Anish Upadhyaya. Microwave Heating of Pure Copper Powder with Varying Particle Size and Porosity. *Journal of Microwave Power and Electromagnetic Energy*, 43(1): pp. 5–10, 2009. [cited at p. 65]
- [102] A. K. Shukla, A. Mondal, and A. Upadhyaya. Numerical modeling of microwave heating. *Science of Sintering*, 42(1): pp. 99–124, 2010. [cited at p. 65]
- [103] A. Mondal, A. Shukla, A. Upadhyaya, and D. Agrawal. Effect of porosity and particle size on microwave heating of copper. *Science of Sintering*, 42(2): pp. 169–182, 2010. [cited at p. 65]



# Index

Dielectric losses, 60

Effective properties, 24, 26, 33, 39, 53

Kramers-Kronig relations, 13, 31

Magnetic losses, 39, 46, 54, 60

Maxwell's equations, 9, 13, 48

Microwave sintering, 37, 52

Permeability, 4, 10, 13, 24, 28, 34, 39,  
54, 65

Permittivity, 10, 18, 23, 25, 28, 35, 39,  
55

S-parameters, 27, 31, 35, 53

Sintering, 7, 37, 42, 50, 54





# Acknowledgments

This work was supported by the European Union through ADVATEC project (EU Marie Curie EST, 2005-2009, contract No MEST-CT-2005-020986) and CST GmbH.

Many people provided support during the whole time of my work on this PhD project. I would like to thank Prof. Dr. rer. nat. habil. Ursula van Rienen and Prof. Dr. rer. nat. habil. Eberhard Burkel for providing the opportunity to work on this topic in an excellent and friendly research environment.

I would like to thank my colleagues at the institute for fruitful discussions regarding my topic, especially Hans-Walter Glock, Carsten Potratz, Thomas Flisgen and Christian Bahls.

One more time I would like to thank Frau Prof. Ursula van Rienen for her patience, valuable discussions and help during writing this thesis.

Most of all I would like to thank my parents, Urszula and Leszek Galek, for all the support, willingness to help and most important of all, for being my parents.



# List of Contributions

## Conferences and Workshops

- T. Galek, *Microwave Assisted Sintering*, IPP Mini Workshop and ADVATEC Meeting II (22/06/2007), Rostock, Germany
- T. Galek, U. van Rienen, *Microwave Assisted Sintering*, 19th Workshop on Advances in Electromagnetic Research KWT 2007 (19-24/08/2007), Riezlern/Kleinwalsertal, Austria
- T. Galek, U. van Rienen, *Microwave Assisted Sintering*, 12th Symposium Maritime Elektrotechnik, Elektronik und Informationstechnik (8-10/10/2007), Rostock, Germany
- T. Galek, *Extraction of effective dielectric properties of inhomogeneous media*, Science and Engineering of New Materials Seminar (23/11/2007), Rostock, Germany
- T. Galek, U. van Rienen, E. Burkel, *Full 3D Electromagnetic Simulations of Microwave Heating of Ceramic and Metal Powders*, Advanced Processing of Novel Functional Materials APNFM2008 (23-25/01/2008), Dresden, Germany
- T. Galek, U. van Rienen, *Modeling of Magnetic and Dielectric Properties of Metallic and Ceramic Powders in the Microwave Range*, 9th International Workshop on Finite Elements for Microwave Engineering (8-9/05/2008), Bonn, Germany
- T. Galek, U. van Rienen, *Extraction of Effective Permittivity and Permeability of Metallic Powders in the Microwave Range*, Thirteenth Biennial IEEE Conference on Electromagnetic Field Computation (CEFC 2008) (11-15/05/2008), Athens, Greece

- T. Galek, U. van Rienen, *Modeling of Magnetic and Electric and Magnetic Properties of Inhomogeneous Media in the Microwave Range*, Methoden und Anwendungen der Feldsimulation and IPP Seminar (4/07/2008), Rostock, Germany
- T. Galek, U. van Rienen, *Modeling of Microwave Absorption Mechanisms of Metallic Powders*, 20th Workshop on Advances in Electromagnetic Research KWT 2008 (10-15/08/2008), Hardehausen, Germany
- T. Galek, U. van Rienen, *Modelling of Effective Dielectric Properties of Inhomogeneous Mixtures in the Microwave Range*, 15th International Symposium on Theoretical Electrical Engineering (ISTET 2009) (22-24/06/2009), Lübeck, Germany
- T. Galek, K. Porath, E. Burkel, U. van Rienen, *Simulations and Modeling of Relaxation Behavior in Magnetic Nanoparticles*, 21st Workshop on Advances in Electromagnetic Research KWT 2009 (22-28/08/2009), Riezlern/Kleinwalsertal, Austria
- T. Galek, U. van Rienen, *Magnetic Properties of Metallic Powders*, 22nd Workshop on Advances in Electromagnetic Research KWT 2010, (8-13/08/2010), Waren, Germany

## Journals

- T. Galek and U. van Rienen, *Microwave Assisted Sintering*, 12. Symposium Maritime Elektrotechnik, Elektronik und Informationstechnik.Hrsg.: Nils Damaschke, Universität Rostock, Fakultät für Informatik und Elektrotechnik (2007), Rostock
- T. Galek and van U. Rienen, *Modelling of Effective Dielectric Properties of Inhomogeneous Mixtures in the Microwave Range*, In proceedings of XV International Symposium on Theoretical Engineering (ISTET 2009)
- T. Galek, K. Porath, E. Burkel and U. van Rienen, *Extraction of Effective Permittivity and Permeability of Metallic Powders in the Microwave Range*, Modelling Simul. Mater. Sci. Eng. 18 (2010) 025015

# **Selbständigkeitserklärung**

Hiermit erkläre ich, dass ich die vorliegende Dissertation mit dem Titel "Modeling of Microwave Absorption Mechanisms in Metallic Powders" selbständig und ohne fremde Hilfe und nur unter Verwendung der von mir angegebenen Quellen und Hilfsmittel verfasst habe.

Rostock, 02. November 2012

Tomasz Galek